PASSIVATION KINETICS AT SEMICONDUCTOR INTERFACES

by

LIGIA GHEORGHITA

B.Eng., Polytechnic University of Bucharest, Romania, 1985
M.Sc., University of Guelph, 1993

A THESIS SUBMITTED IN PARTIAL FULFILLMENT OF
THE REQUIREMENTS FOR THE DEGREE OF

DOCTOR OF PHILOSOPHY

in

THE FACULTY OF GRADUATE STUDIES

Department of Chemistry

We accept this thesis as conforming
to the required standard

THE UNIVERSITY OF BRITISH COLUMBIA

June 1999

In presenting this thesis in partial fulfilment of the requirements for an advanced degree at the University of British Columbia, I agree that the Library shall make it freely available for reference and study. I further agree that permission for extensive copying of this thesis for scholarly purposes may be granted by the head of my department or by his or her representatives. It is understood that copying or publication of this thesis for financial gain shall not be allowed without my written permission.

Department of Chemistry

The University of British Columbia
Vancouver, Canada

Date 9 August, 1999

DE-6 (2/88)

Abstract

The interaction of atomic hydrogen with defects at a GaAs (100) surface was studied by continuously monitoring the photoluminescence of a GaAs wafer in a discharge-flow system at room temperature. It was found that there was an initial irreversible passivation of the surface in the presence of the hydrogen atoms, and this was followed by an improved (but reversible) passivation that occurred when the exposure to atomic hydrogen was discontinued. This reversible recovery of the passivation level was found to follow a non-exponential rate law.

A kinetic study of the interaction of atomic hydrogen with the defects at a Si/SiO_2 interface was undertaken at temperatures between 23°C and 330°C. The concentration of defects at the interface was monitored continuously, *in situ*, with a remote radio frequency (RF) probe, which measured the steady-state photogenerated carrier concentration. The results were similar to those obtained with GaAs. The kinetics of the hydrogen atom loss from both semiconductors have been analyzed in terms of a distribution of trapping sites. A comparison of the GaAs and Si/SiO_2 systems leads us to conclude that hydrogen atoms can be trapped at interstitial sites near these interfaces.

The reaction of molecular hydrogen with defects at the (111) Si/SiO_2 interface has been investigated in the 135°C to 300°C temperature range, using the RF-probe to continuously monitor the rate of removal of electrically active defects. The kinetic parameters calculated from these experiments are compared with earlier workers' electron paramagnetic resonance (EPR) studies of the so-called "P_b" defect. Our results confirm the non-exponential nature of the reaction reported by one of these studies, and are consistent with the rate constants obtained earlier at high temperatures. This process has an activation energy of 1.5 eV. However, the new results indicate that there are other interfacial defects, which could not be detected by EPR, that

react with H_2 in a process that has a much lower activation energy (0.5 eV). Similar experiments were conducted on intrinsic and p-type (100) Si/SiO_2 and the same non-exponential rate law was observed for the passivation of interfacial defects in the presence of H_2.

Table of Contents

List of Tables

List of Figures

List of Symbols

Symbol	Description	Units
A	pre-exponential factor	cm^3s^{-1}
D_{it}	interface trapped charge density	$cm^{-2}eV^{-1}$
E	energy	eV
E_a	activation energy	eV
E_a^o	mean activation energy	eV
E_A	acceptor energy level	eV
E_C	conduction band edge	eV
E_D	donor energy level	eV
E_d	defect energy level	eV
E_F	Fermi energy level	eV
E_{Fi}	Fermi energy level in an intrinsic semiconductor	eV
E_g	band gap energy	eV
E_V	valence band edge	eV
f(E)	Fermi-Dirac distribution function	
[H2]	molecular hydrogen concentration	cm^{-3}
h	Planck constant	J s
hν	photon energy	eV
k	first order rate constant	cm^3s^{-1}
k_B	Boltzmann constant	$J K^{-1}$
k_BT	thermal energy	eV
m	H_2 mass	kg
n	electron concentration	cm^{-3}
n_i	intrinsic electron concentration	cm^{-3}
N	doping concentration	cm^{-3}
N_A	acceptor impurity density	cm^{-3}
N_c	effective density of states in conduction band	cm^{-3}
N_D	donor impurity density	cm^{-3}
N_v	effective density of states in valence band	cm^{-3}
p	hole concentration	cm^{-3}
P	pressure	Torr or atm
P_b	Si/SiO_2 interfacial defect	
N_{it}	interface trap density	cm^{-2}
R	other electrically active Si/SiO_2 interfacial defect	cm^{-2}
R_c	interfacial or surface recombination centre	cm^{-2}
t	time	s or min
T	absolute temperature	K
V_T	threshold voltage	(V)
ε	binding energy for H_2 on a Si surface	eV
λ	wavelength	nm

ν	frequency of light	Hz
ρ	resistivity	Ω cm
σ	Gaussian spread	eV
τ	lifetime or decay time	s
Si≡Si•	Si atom with a half-filled orbital bonded to 3 other Si atoms in the crystal, i.e. a P_b defect	
–Si≡	P_b defect	
–O–Si≡	R defect	

Acknowledgements

First and foremost I would like to thank my supervisor, Professor Elmer Ogryzlo, for continued support, expert guidance, encouragement and never failing enthusiasm throughout this study. Many thanks are due to past students of the Ogryzlo laboratory, Dr. Hongjun Li and Lan Zheng, for useful discussions and comradeship.

I would like to thank Dr. Zheng-Hong Lu for supplying the oxynitrided silicon samples used in this work.

I appreciate the assistance of Dr. Tom Tiedje, for his valuable advice in interpreting some of my results. Many thanks are also due to his MBE Laboratory group for providing GaAs samples.

I am very grateful to several people at the Advanced Materials & Process Engineering Laboratory (AMPEL). Special thanks to Dr. Ruixing Liang in AMPEL, for kindly lending me the use of his furnace to grow silicon oxides.

The technical assistance of many proved invaluable. Without their help and resources this project would not have been completed. Sincere thanks are extended to all the members of the Chemistry Department Mechanical, Glass, and Electronics Shops, particularly Brian, Cedric, Ron, Steve, Brian, and Jason. Many thanks to everybody in the Chemistry Department Main Office, too. After such a long "graduate career" at UBC, I would like to say what a great pleasure it has been to work with so many knowledgeable, genuinely nice, and helpful people.

Finally, my gratitude and thanks go to my mother and father, to Jeremy, and to all my friends for their patience and encouragement over this long period of time.

1. INTRODUCTION AND LITERATURE REVIEW

1.1 Semiconductor Materials

Semiconductors are engineering materials that have had a major impact on contemporary society. These materials are the building blocks of transistors, solid state electronics and computers.

Silicon (Si) and germanium (Ge) are the most frequently used elemental semiconductors. Silicon is the most widespread semiconductor used for digital electronics principally because it is cheap, abundant, structurally robust, has a very stable oxide, and from an environmental point of view, is relatively harmless.[1] In nature, it is mainly found in the form of its oxides. These can be reduced in a furnace with carbon, at about 1450°C, to produce 98% pure metallurgical-grade silicon. As little as one part per million of an impurity in silicon has a profound effect on its electrical properties. A requirement for the starting material is typically less than one impurity atom per one billion silicon atoms. Consequently, electronic grade silicon requires considerable purification before use. For integrated circuit technology, it is also of great importance to produce dislocation free crystals. Dislocation-free crystals of silicon were first grown in the 1960's.[1]

The crystal must also have a defect-free surface or interface. In the case of an interface with a material that can have the same crystal structure, it is possible to decrease the number of such interfacial defects by growing a layer on the surface by the process known as epitaxy. In this technique, atoms are deposited on to the crystal surface such that each atom will find its

correct crystal lattice position where it forms bonds with the atoms in the solid surface. Epitaxial growth is an ideal starting point for the fabrication of diodes and transistors.

In addition to the elemental semiconductors, many alloys and compounds are semiconductors.[1] These may be formed from semiconducting or non-semiconducting elements. Copper oxide is the oldest semiconductor in commercial use, first appearing in copper-copper oxide rectifiers. The particular advantage of compound semiconductors is that they provide the device engineer with a wide range of energy gaps and mobilities, so that materials are available with properties that match specific requirements exactly. One of the most important groups of compound semiconductors are the III-V materials, so called because they are formed of elements from what used to be called Groups IIIA and VA of the old Periodic Table. Typical examples are InSb, AlP and GaAs.[1]

GaAs is one of the most versatile and useful semiconductors, being used in many devices including light-emitting diodes, lasers, and other optoelectronic devices. GaAs has a very important quality that Si does not have and that is the ability to emit light. In properties like average carrier velocity and breakdown field, GaAs is superior to Si. However, large-scale production of GaAs integrated circuits is more difficult than it is for Si. Table 1.1 lists some of the more important properties of Si, GaAs and SiO_2 at 300 K.[2]

1.2 Energy Bands in Semiconductors

Electrons in crystalline solids are restricted to certain bands of energy levels. The discrete energy levels of isolated atoms spread into bands of energy levels in the solid because in

Table 1.1 Properties of Si, GaAs and SiO_2 at 300 K. (From Mayer and Lau[2])

PROPERTY	Si	GaAs	SiO_2
Atoms/cm^3, molecules/ cm^3	5.0×10^{22}	4.42×10^{22}	2.27×10^{22} [a]
Crystal structure	diamond	zincblende	amorphous
Lattice constant (Å)	5.43	5.65	-
Atomic or molecular weight (g)	28.09	144.64	60.08
Density (g cm^{-3})	2.33	5.31	2.27[a]
Relative dielectric constant	11.9	13.1	3.9
Permittivity (F cm^{-1})	1.05×10^{-12}	1.16×10^{-12}	0.34×10^{-12}
Specific heat (J g^{-1} K^{-1})	0.7	0.35	1.0
Thermal conductivity (W cm^{-1} K^{-1})	1.48	0.46	0.014
Expansion coefficient (x 10^{-6} K^{-1})	2.6	6.86	0.5
Thermal diffusivity (cm^2 s^{-1})	0.9	0.44	0.006
Melting point (°C)	1415	1238	≈1700
Energy gap (eV)	1.12	1.424	≈9
Electron mobility (cm^2 V^{-1} s^{-1})	1500	8500	-
Hole mobility (cm^2 V^{-1} s^{-1})	450	400	-
Intrinsic carrier concentration (cm^{-3})	1.45×10^{10}	1.79×10^{6}	
Effective density of states (cm^{-3})			
conduction band	2.8×10^{19}	4.7×10^{17}	-
valence band	1.04×10^{19}	7×10^{18}	-
Electron effective mass	1.1 m_0[b]	0.067 m_0[b]	
Hole effective mass	0.56 m_0	0.48 m_0	
Resistivity (Ω cm)	10^3	10^8	10^{14}

[a] Formed under dry oxidation conditions.

[b] The free electron rest mass is m_0. These are average values for the effective mass.

solids the wave functions of electrons in neighbouring atoms overlap. Every solid has its own characteristic energy band structure. This is responsible for the wide range of electrical characteristics observed in various materials.

Semiconductor materials at 0 K have basically the same structure as insulators: a filled lower band, called the valence band, separated from an empty upper band, called the conduction band, by a band gap containing no allowed energy levels (Figure 1.1). However, the magnitude of the band gap E_g, also called the forbidden gap, is much smaller in semiconductors than in insulators.[3] The relatively small band gaps for semiconductors allow for the thermal excitations of electrons from the valence band to the conduction band. In other words, semiconductors have E_g within ~ 2 orders of magnitude of kT, while insulators have larger values for E_g. In metals the bands are only partially filled, so that the electrons can move more freely under the influence of an electric field. As expected from the metallic band structure of Figure 1.1, these materials have a high electrical conductivity.

The energy band diagrams of Figure 1.1 are simplified representations of a rather complex band structure. Figure 1.2 shows more complicated energy band diagrams for GaAs and Si in which the allowed values of energy are plotted against the so-called wave vector, k. The X-axis shows the magnitude of the wave vector k (which can be considered a quantum number for the electron momentum) along some important crystal directions. The curves above the band gap (E_g) are conduction bands, while the curves below E_g represent valence bands. For example, the band structure of GaAs has a minimum in the conduction band and a maximum in the valence band for the same k value (k = 0). Si, on the other hand, has its valence band maximum at a different value of k than its conduction band minimum.

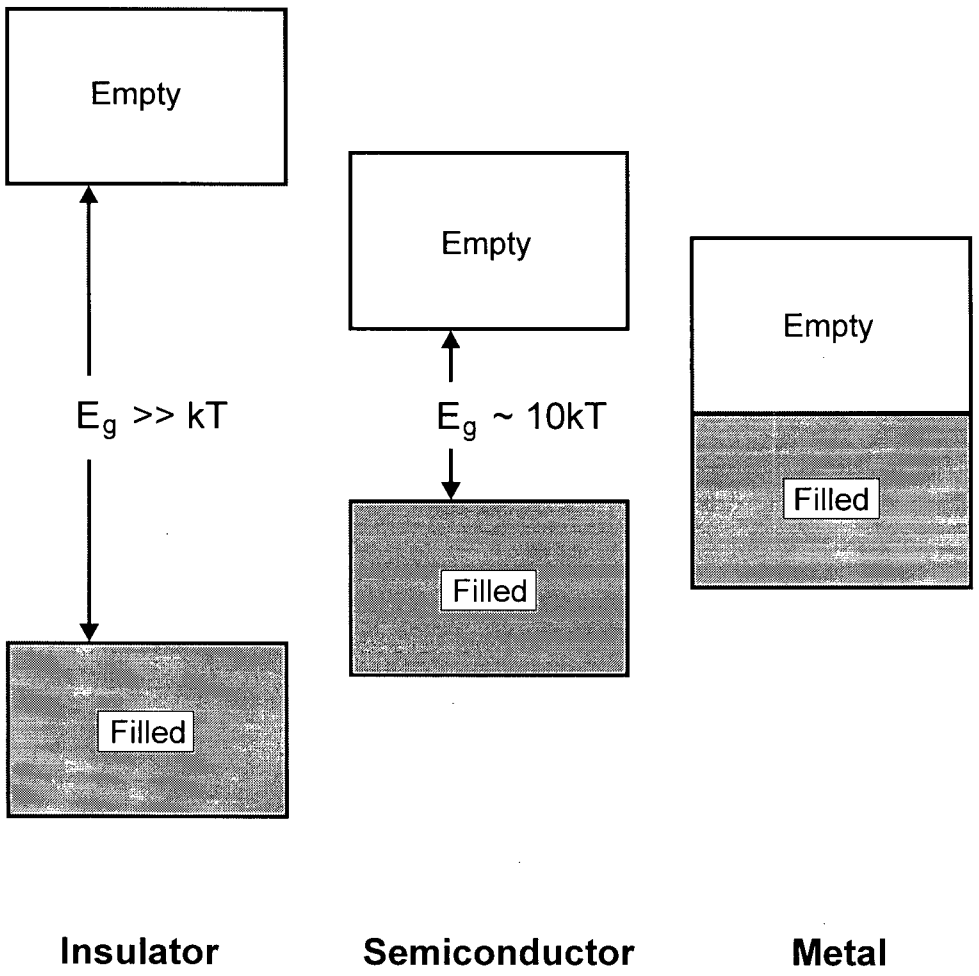

Figure 1.1 Typical band structure of insulators, semiconductors and metals at 0 K.

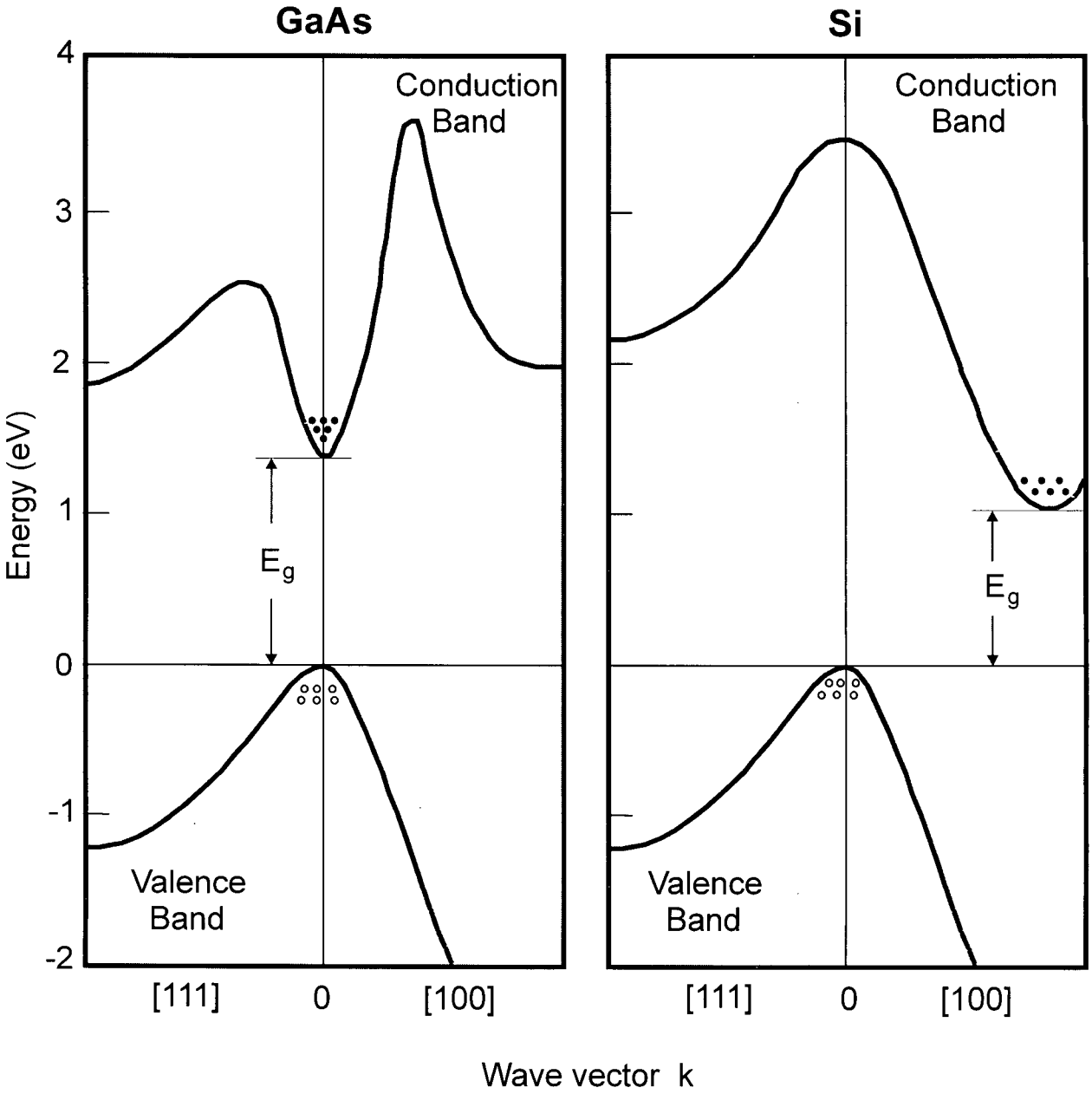

Figure 1.2 Band structure diagrams for GaAs and Si along the [100] and [111] crystal directions. Circles (o) indicate holes in the valence bands while dots (•) indicate electrons in the conduction band. (From Sze[4])

Electrons in the minimum of the conduction band can drop into the empty levels of the valence band in GaAs without a change in k value. A transition from the minimum point in the Si conduction band to the empty orbitals at the top of the valence band requires a change in k (or electron momentum). Thus there are two classes of semiconductors: direct and indirect band gap.

In a direct band gap semiconductor such as GaAs, an electron in the conduction band can fall to an empty state in the valence band, giving off the energy difference E_g as a photon of light. An electron in the conduction band minimum of an indirect semiconductor such as Si cannot fall directly into the empty orbitals near the valence band maximum without a large momentum change. This makes the emission of light a highly improbable process for silicon.

1.3 Electrons and Holes

As the temperature of a semiconductor is raised from 0 K, some electrons in the valence band receive enough thermal energy to be excited across the band gap to the conduction band. The result is a material with some electrons in an otherwise empty conduction band and some unoccupied levels, called holes, in an otherwise filled valence band. The conduction band electron and the hole created in the valence band are called an electron-hole pair (EHP).

After excitation to the conduction band, electrons are surrounded by a number of unoccupied energy levels. The equilibrium number of electron-hole pairs in pure silicon at room temperature is about 10^{10} EHP/cm^3, which is small compared to the Si atom density of $\approx 10^{22}$

atoms/cm^3. The few electrons in the conduction band are free to move about via many available empty levels in the conduction band.

Electrons in solids obey Fermi-Dirac statistics. The distribution of electrons over a range of allowed energy levels at thermal equilibrium is:[5]

$$f(E) = \frac{1}{1 + e^{(E-E_F)/k_B T}} \qquad [1.1]$$

where k_B is Boltzmann's constant. The Fermi-Dirac distribution function f(E), gives the probability that an available energy level at E will be occupied by an electron at any temperature T. The quantity E_F is called the Fermi level, and it represents an important quantity in the analysis of semiconductor behaviour. For an energy E equal to the Fermi level energy E_F, the occupation probability is ½. At 0 K f(E) = 0 for $E > E_F$ and f(E) = 1 for $E < E_F$, while at higher temperatures some probability exists for states above the Fermi level to be filled.

The Fermi distribution function can be used to calculate the concentrations of electrons and holes in a semiconductor, if the densities of available states in the conduction and valence bands are known. The concentration of electrons in the conduction band is:

$$n_0 = \int_{E_c}^{\infty} f(E)N(E)dE \qquad [1.2]$$

where N(E)d(E) is the density of states (DOS) in the range dE and n_0 is the equilibrium electron concentration. The number of electrons per unit volume in the energy range dE is the product of the density of states (cm^{-3}) and the probability of occupancy f(E). It has been shown that N(E) is proportional to $E^{1/2}$, so that DOS increases with electron energy. On the other hand, the Fermi function becomes very small for large energies. Thus the product f(E)N(E) decreases rapidly

above E_C, and very few electrons occupy levels far above the conduction band edge. Similarly, the probability of finding an empty level (hole) in the valence band [1-f(E)] decreases rapidly below E_V, and most holes occupy levels near the top of the valence band. This effect is demonstrated in Figure 1.3, which shows the density of available states, the Fermi function, and the resulting number of electrons and holes occupying available energy levels in the conduction and valence bands at thermal equilibrium (i.e., with no excitations except thermal energy).

1.4 Doping

A perfect semiconductor crystal with no impurities or lattice defects is called an intrinsic semiconductor. In such a material there are no charge carriers at 0 K, since the valence band is completely full, while the conduction band is empty. At higher temperatures electron-hole pairs are generated as valence band electrons are excited thermally across the band gap to the conduction band. These EHP's are the only charge carriers in intrinsic materials.

Since the electrons and holes are created in pairs, for an intrinsic semiconductor the number of electrons per unit volume in the conduction band (n) is equal to the number of holes per unit volume in the valence band (p):

$$n = p = n_i \qquad [1.3]$$

where n_i is the intrinsic carrier density. This relation between electrons and holes is depicted in carrier concentration graph of Figure 1.3 (a). The Fermi level lies in the middle of the band gap in intrinsic semiconductors.

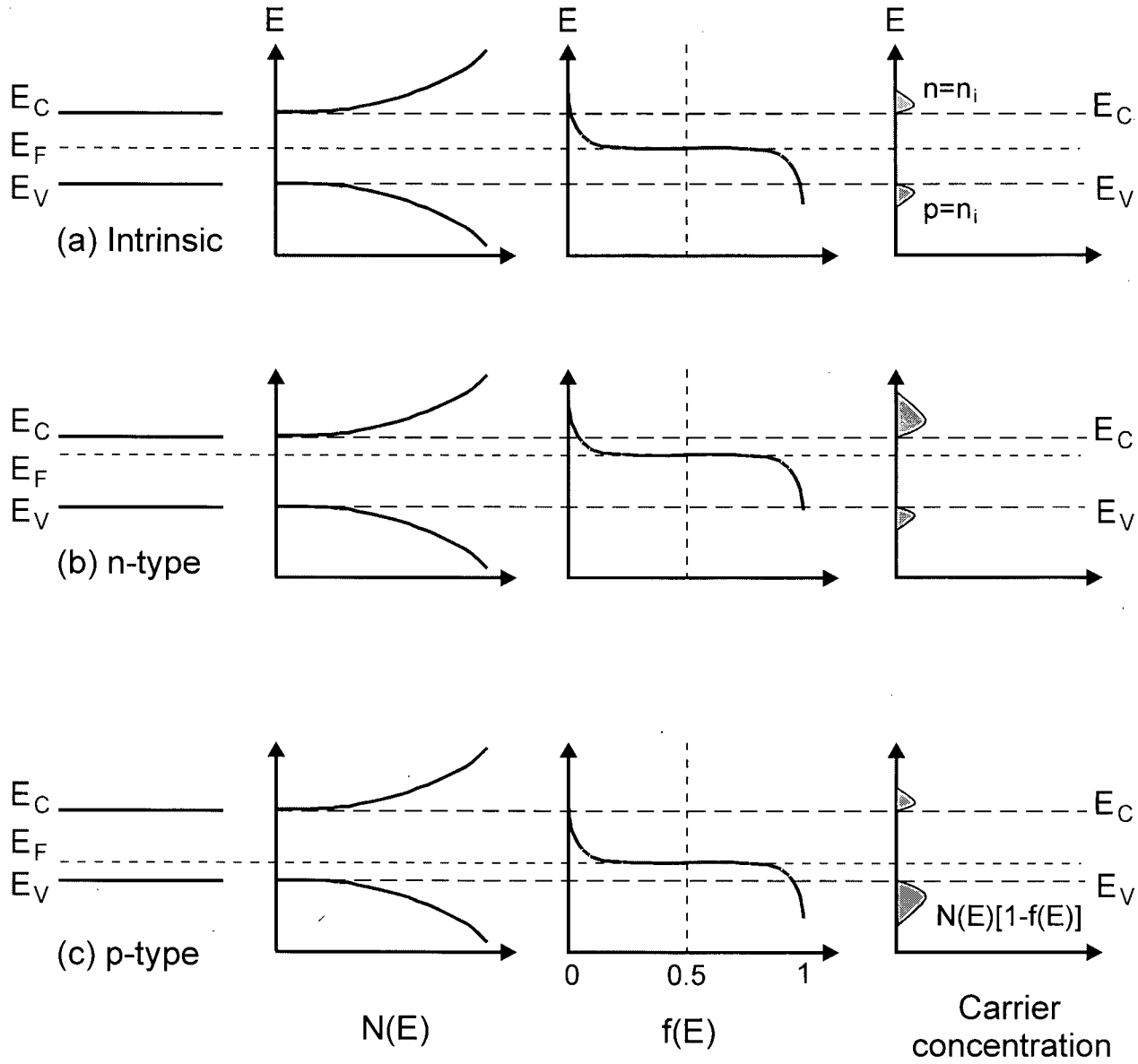

Figure 1.3 Schematic band diagram, density of states, Fermi-Dirac distribution, and the carrier concentrations for (a) intrinsic, (b) n-type, and (c) p-type semiconductors at thermal equilibrium. (From Streetman[5])

At a given temperature there is a fixed steady state concentration of electron-hole pairs that is determined by the fact that EHP's recombine at the same rate at which they are generated. Recombination occurs when an electron in the conduction band makes a transition (direct or indirect) to an empty level (hole) in the valence band, thus annihilating the pair.

In addition to the intrinsic carriers generated thermally, it is possible to create carriers in semiconductors by purposely introducing certain impurities into the crystal. This process, called doping, is the most common technique for varying the conductivity of semiconductors. By doping, a crystal can be altered so that it has a predominance of either electron or holes. Thus, there are two types of doped semiconductors: n-type (with an excess of electrons) and p-type (with an excess of holes). When a crystal is doped such that the equilibrium carrier concentrations n_0 and p_0 are different from the intrinsic carrier concentration n_i, the material is called extrinsic.

When impurities or lattice defects are introduced into an otherwise perfect crystal, additional levels are created in the energy band structure, usually within the band gap. For example, an impurity from Group V of the periodic table (P, As, and Sb) introduces an energy level E_D in the band gap, slightly below the bottom of the conduction band (E_C) in Si or Ge. Very little thermal energy is required to excite these electrons to the conduction band. At about 50-100 K virtually all of the electrons in the impurity level are "donated" to the conduction band, and such impurity levels are therefore called donor levels.

Atoms from Group III (B, Al, Ga and In) introduce impurity levels slightly above the valence band (E_V) of Si or Ge. These levels are empty at 0 K, but at low temperatures ($\approx$ 50 K), enough thermal energy is available to excite electrons from the valence band into the impurity

level, leaving behind holes. These types of impurity levels are called acceptor levels (E_A), since they "accept" electrons.

In an n-type material the Fermi level moves closer to the conduction band minimum (E_C), while in a p-type semiconductor it lies closer to the valence band maximum (E_V). This behaviour is illustrated in Figure 1.3 (b) and (c).

This simplified energy band picture with allowed states created by impurities is shown in Figure 1.4. Note that the intrinsic Fermi level is denoted here as E_{Fi}. Electrons in an n-type material or holes in a p-type material are called majority carriers, while holes in n-type and electrons in p-type are called minority carriers.

Impurities do not always serve as donors and acceptors in semiconductors. Some impurities (e.g. Au in Si) give rise to levels near the middle of the band gap and are called deep levels to distinguish them from the shallow impurity levels of dopants. Electrons that are originally in any energy level above the impurity level can drop into it, giving it, at least temporarily, a negative charge. Similarly, holes that are originally in levels below the deep impurity level can occupy the deep impurity level giving it, at least temporarily, a positive charge. We shall see that such processes can catalyze the recombination of electrons and holes.

1.5 The MOSFET

Transistors, which are made of several junctions between different semiconducting materials, form the building blocks of integrated circuits. A typical computer chip can contain several million transistors.

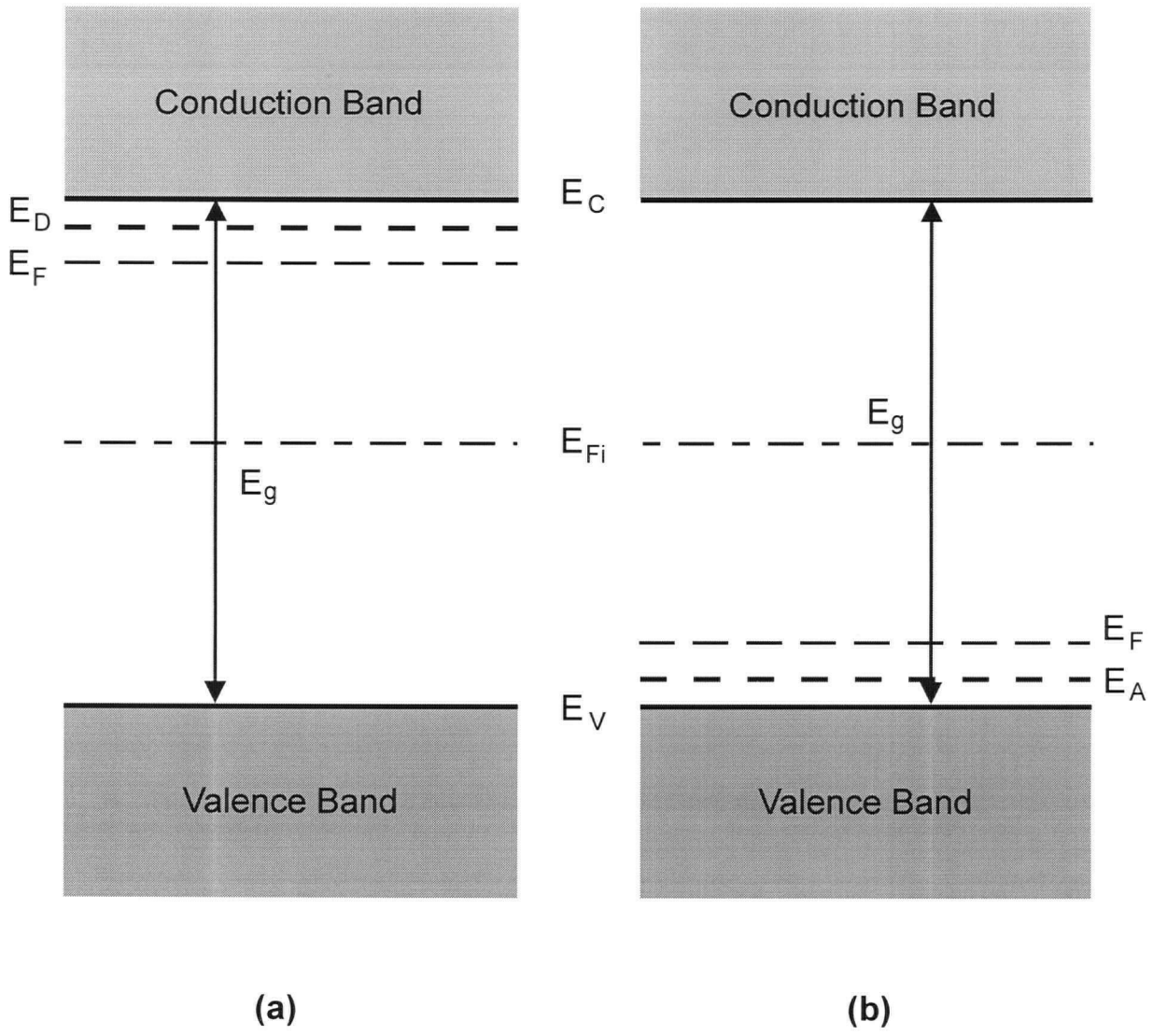

Figure 1.4 Band diagram showing the Fermi level E_F, and the intrinsic Fermi level, E_{Fi} in: (a) an n-type semiconductor, with a donor level E_D, and (b) a p-type semiconductor, with an acceptor level E_A.

The basic metal-oxide-semiconductor field-effect transistor (MOSFET) is illustrated in Figure 1.5 for the case of an n-type channel formed on a p-type Si substrate. The n^+ source and drain regions are diffused or implanted into a relatively lightly doped p-type substrate, and a thin oxide layer separates the Al metal gate from the Si surface. No current flows from drain to source without a conducting n channel between them.

When a positive voltage is applied to the gate relative to the substrate (which is connected to the source in this case), positive charges are deposited on the metal gate. In response, negative charges are induced in the underlying Si, by the formation of a depletion region and a thin surface region containing mobile electrons. These induced electrons form a conduction channel allowing current to flow from drain to source. An important parameter in MOSFETs is the threshold voltage V_T, which is the minimum gate voltage required to induce the conducting channel. Some n-channel devices already have a channel with zero gate voltage, and a negative voltage is required to turn the device off. Such a device is called a depletion-mode transistor, since a gate voltage is used to deplete a channel that exists at equilibrium. The more common MOSFET is normally off, with zero gate voltage, and operates in the enhancement mode by applying a gate voltage large enough to induce a conducting channel.

The MOSFET is particularly useful in digital circuits, in which it is switched from the "off" state (no conducting channel) to the "on" state. The magnitude of the source to drain current is controlled by the voltage on the gate electrode, which is insulated from the source and drain by the oxide.

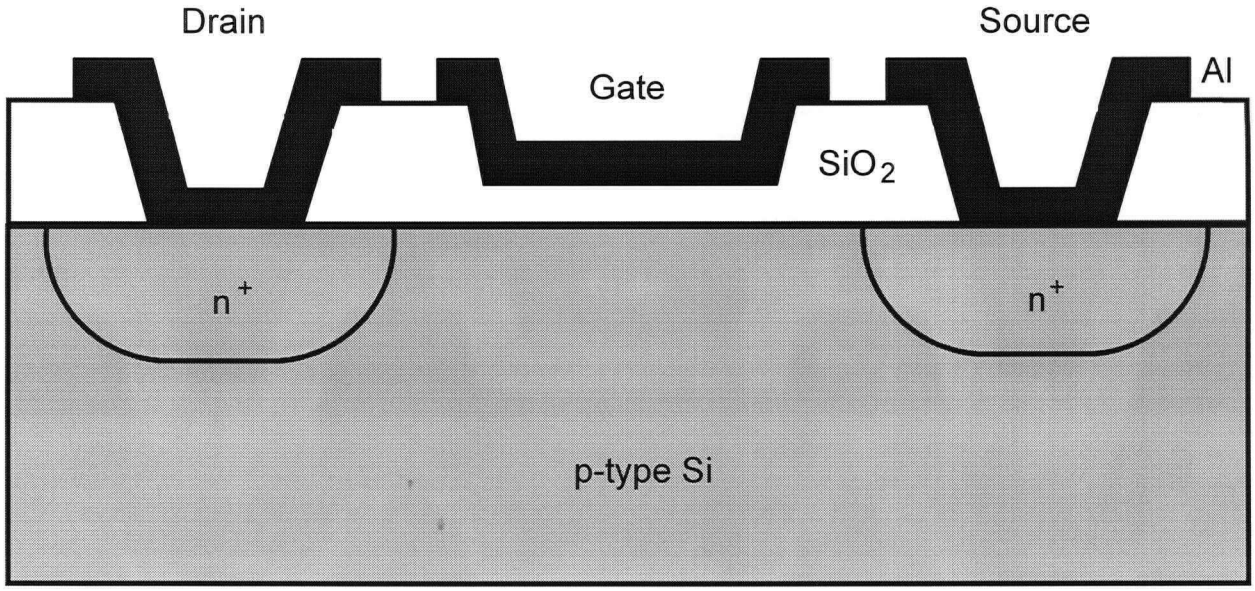

(a)

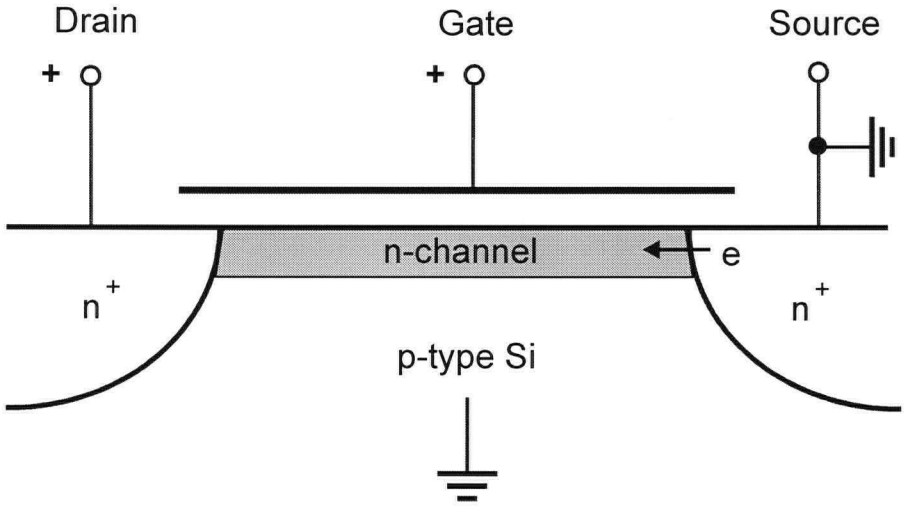

(b)

Figure 1.5 An enhancement-type (normally off) n-channel MOSFET: (a) cross section of the device, and (b) schematic illustration of the induced n-channel formed when applying a positive voltage to the gate. (From Streetman[5])

1.6 Electron - Hole Recombination

1.6.1 Radiative Recombination

The simplest example of light emission from a semiconductor occurs from direct excitation and recombination of an EHP. If the recombination occurs when an electron falls from an energy level in the conduction band into an empty level in the valence band, light can be given off in a process called radiative recombination. In silicon, for example, this process is described by the following equation:

$$e + h \xrightarrow{k_r} Si + h\nu \qquad [1.4]$$

where e is a free electron, h is a hole, hν is a photon and k_r is the radiative recombination rate constant.

The excess carriers in the semiconductor can be created either by using light, and the phenomenon is called photo-excitation, or by use of an electrical current and in this case the phenomenon is called electroluminescence. For steady state photo-excitation, the recombination of EHP's occurs at the same rate as generation, and in the absence of other carrier-loss processes one photon is emitted for each photon absorbed. Such a radiative recombination process is referred to as photoluminescence or fluorescence and is a characteristic of direct band gap semiconductors like GaAs.[6] Light emitting diodes and diode lasers are based on direct band gap materials.

The lifetimes of the excess carriers are determined by how rapidly the electrons and holes recombine. Radiative recombination in a direct band gap semiconductor is a fast process; the mean lifetime of the EHP is usually on the order of ns. For example, if the material is p-doped,

and the injection level is low, i.e., the photo-generated carrier concentrations Δn and Δp are much smaller than the dopant concentration, then we have the following approximations

$$p = p_0 + \Delta p \approx p_0 \qquad [1.5]$$

$$n = n_0 + \Delta n \approx \Delta n \qquad [1.6]$$

where n and p represent the electron and hole concentrations, respectively while n_0 and p_0 have the same significance at equilibrium. The rate of this recombination process is given by:

$$-\frac{dn}{dt} = k_r \Delta n \, p_0 \qquad [1.7]$$

This is a pseudo first order process because p_0 is essentially constant, and by solving this differential equation the radiative lifetime τ_r is obtained:

$$\tau_r = \frac{1}{k_r p_0} \qquad [1.8]$$

1.6.2 Direct Non-Radiative Recombination

Simple bimolecular non-radiative recombination of carriers in indirect band gap semiconductors such as Si is extremely slow because the energy released (equal to E_g) must be dissipated in lattice vibrations, as phonons. This process can be described by

$$e + h + \text{lattice} \xrightarrow{k_d} Si + \text{lattice}^* \qquad [1.9]$$

where k_d is the direct non-radiative recombination rate constant. Because direct non-radiative recombination is many orders of magnitude slower than other processes, we will ignore it.

1.6.3 Auger Recombination

Auger non-radiative recombination, which produces an energetic majority carrier, is also possible. In this process, which is quite rapid relative to simple bimolecular non-radiative recombination, the energy of the EHP is transformed into the kinetic energy of a free particle as described by either of the following equations

$$e + h + e \xrightarrow{k_A(n)} Si + e^* \qquad [1.10]$$

$$e + h + h \xrightarrow{k_A(p)} Si + h^* \qquad [1.11]$$

where e* and h* designate an electron and hole in a higher energy level, while $k_A(n)$ and $k_A(p)$ represent the Auger recombination rate constants for an n-type and p-type material, respectively. For a p-type material and using the same argument as before (equations [1.5] and [1.6]) the rate of change of electron concentration due to Auger recombination is given by

$$-\frac{dn}{dt} = k_A\, n p^2 = k_A\, \Delta n\, p_0^2 \qquad [1.12]$$

Using standard kinetic analysis, the Auger lifetime τ_A is then

$$\tau_A = \frac{1}{k_A p_0^2} \qquad [1.13]$$

Auger recombination events require the simultaneous presence in a small spatial volume of two electrons and a hole, or two holes and an electron, and are therefore more probable at high carrier concentrations. Values for the radiative and Auger recombination rate constants and lifetimes are given in Table 1.2 for p-type GaAs and Si. Note that the radiative lifetimes also

apply to n-type materials for a similar doping level (n_0). Radiative and Auger recombination are intrinsic to the material and thus are always present.

The total lifetime of a semiconductor τ_{total} is obtained by adding the reciprocal lifetimes

$$\frac{1}{\tau_{total}} = \frac{1}{\tau_r} + \frac{1}{\tau_A} \qquad [1.14]$$

since the total rate constant is also obtained by adding the pseudo first order rate constants:

$$k_{total} = k_r\, p_0 + k_A\, p_0^2 \qquad [1.15]$$

Table 1.2 Values of rate constants and lifetimes for radiative recombination and Auger processes in GaAs and Si. (From Ogryzlo[7])

SEMICONDUCTOR	k_r ($cm^3\ s^{-1}$)	τ_r (μs) (for $p_0=10^{15}$)	k_A ($cm^6\ s^{-1}$) n-type	k_A ($cm^6\ s^{-1}$) p-type	τ_A (s) (for $p_0=10^{15}$)
GaAs	2×10^{-10}	5	1.8×10^{-31}	4.0×10^{-30}	0.25
Si	10^{-14}	10^5	2.8×10^{-31}	1.0×10^{-31}	10

1.6.4 Defect Catalyzed Recombination

In most semiconductors the dominant loss of minority carriers occurs by defect catalyzed recombination, also called indirect recombination, which can occur in one of two two-step processes:

step 1: $$e + d \xrightarrow{k_d(n)} d^- \qquad [1.16]$$

step 2: $$d^- + h \xrightarrow{k_{d^-}(p)} d \qquad [1.17]$$

or

step 1: $$h + d \xrightarrow{k_d(p)} d^+ \qquad [1.18]$$

step 2: $$d^+ + e \xrightarrow{k_{d^+}(n)} d \qquad [1.19]$$

where d represents a deep level impurity or defect, also called a deep level recombination centre. Equations [1.16] and [1.17] dominate in n-type materials while equations [1.18] and [1.19] dominate in p-type materials. The lifetime of a semiconductor decreases with increasing deep level (mid gap) defect density.

As indicated above, the radiative recombination process in indirect band gap materials (e.g., Si or Ge) is very slow and thus may be detected only by very sensitive equipment. For these semiconductors the vast majority of recombination events occur via recombination levels within the band gap, and the resulting energy generated by recombining electrons is usually given up to the lattice as heat rather than by the emission of photons. Any impurity or lattice

defect can serve as a recombination centre if it is capable of receiving a carrier of one type and subsequently capturing the opposite type of carrier, thereby annihilating an EHP.

Deep level defects (i.e. mid gap impurities) in a semiconductor can act as non-radiative recombination centres through minority carrier capture. The recombination of EHP's at defect sites was first discussed by Shockley and Read (1952)[8] and by Hall (1952)[9]. The common mechanism is frequently called the Shockley, Read and Hall (SRH) recombination mechanism. Figure 1.6 shows the band gap of a semiconductor that has several types of impurity levels. Those near the mid gap position E_{Fi} are labelled recombination centres E_R. Also shown are levels that are designated as electron traps E_n and hole traps E_p. These lie near the conduction band and the valence band respectively. The SRH model states that a defect level may be either a trap or a recombination centre, depending on its energy E_d. The defect level is a trapping centre, or simply a trap, when the absolute value $|E_{Fi} - E_d|$ is large ($\sim E_g/2$) and the energy level E_d lies near either the conduction or the valence band. A captured electron or hole is thermally emitted back to the conduction or to the valence band, respectively. This process is also called temporary trapping. The demarcation between trapping and recombination centres is described in detail elsewhere.[10] If the energy level E_d lies near mid gap E_{Fi}, the SRH recombination rate becomes very large, and recombination is the most probable event. Thus, mid gap centres ($E_d \sim E_i$) are very effective recombination sites. An example of a very strong "lifetime killer" is atomic Au in Si. Au has energy levels very near mid gap in both n- and p-type Si.

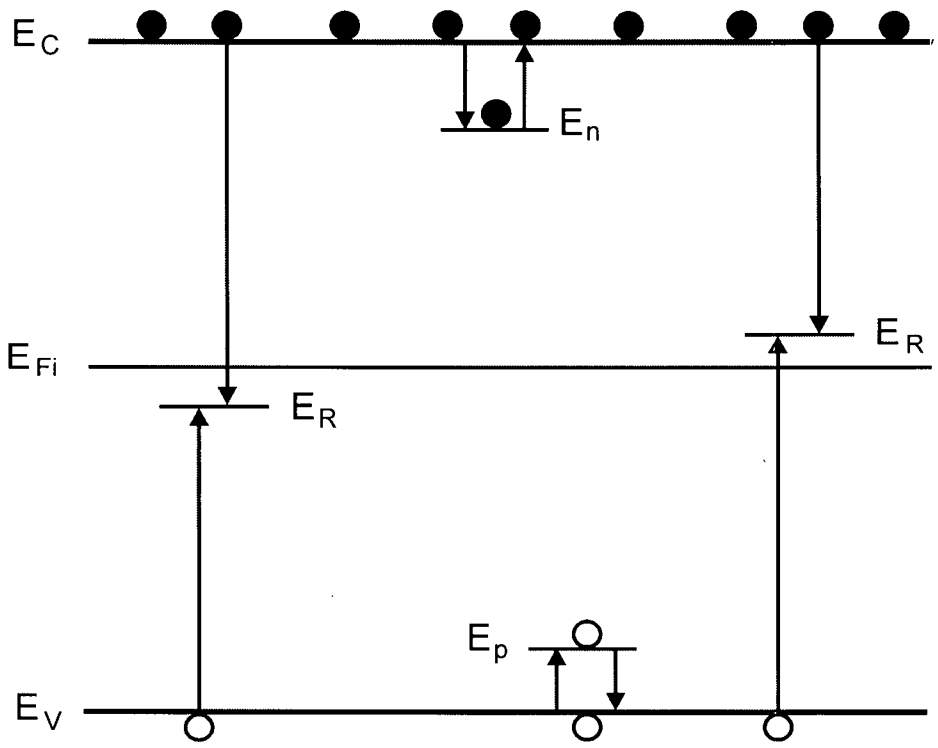

Figure 1.6 Schematic diagram of impurity related energy levels within the band gap of a semiconductor. The open circles indicate holes, while the solid black circles indicate electrons. Levels are labelled as to whether the defect is likely to be a trap or a recombination centre according to the SRH model. (From Ahrenkiel[16])

1.6.5 Surface or Interface Catalyzed Recombination

A much higher density of deep level defects often exists at the surface of semiconductors or at semiconductor/insulator or semiconductor/semiconductor interfaces. Such defects are called surface or interface defects. A classic case is the interface between silicon and its native oxide, SiO_2. Recombination at surface defects is usually found to obey the same rate laws as those found for bulk defects. They can be deep level defects or shallow level defects, with properties similar to those described in Figure 1.6 for bulk defects.

1.7 Measurement of Minority Carrier Lifetimes

As mentioned in the previous section, the radiative lifetime is intrinsic to the material and represents an upper limit to the measured lifetime. The non-radiative lifetime is normally dominated by defects and therefore increases as the material quality improves. Measurement of material quality is one of the principal reasons for doing lifetime measurements.

1.7.1 Techniques for Direct Band Gap Semiconductors

For strong light emitters such as GaAs and other direct band gap semiconductors photoluminescence (PL) decay is the standard technique for measuring the minority lifetime. Photoluminescence is induced with a very short laser pulse, of energy greater than the band gap. The minority carrier lifetime is measured by monitoring the PL intensity as a function of time. In general there are competitive non-radiative transitions and as a consequence the faster non-

radiative processes determine the measured lifetime. Some of the reasons why this technique is preferred for GaAs are because the lifetimes tend to be in the nanosecond range rather than in the microsecond range (i.e., Si), and trapping effects are generally much more severe in GaAs.

It is also possible to monitor changes in carrier lifetimes using a continuous laser intensity and measuring the steady-state photoluminescence intensity (PLI). Since the rate of excitation of EHP's remains constant, any change in luminescence is a direct measure of the changing minority carrier lifetime. The technique therefore provides information on the relative concentrations of surface defects if these dominate the carrier recombination rate.

In this case carriers are created near the surface of the sample. Surface states with energies that lie near middle of the band gap act as recombination centres, decreasing the steady-state carrier concentration. Such carrier traps present an opportunity for the carriers to recombine along an alternative pathway to that which gives rise to the luminescence at the band gap energy. In order to have a large effect the defect catalyzed recombination process must be competitive with the radiative recombination process. When the non-radiative process is faster than the radiative one, the recombination occurring at the surface traps reduces the PLI. In other words, a decrease in PLI signifies an increased number of carrier recombination sites (or centres), while an increase in PLI indicates a reduced number of such sites. If the surface defects that are responsible for the change in PLI can be identified, then monitoring the PLI can provide information about processes that are occurring at the surface of the sample. Thus photoluminescence can be used as an *in situ*, real time monitoring technique for the passivation of these materials.

1.7.2 Techniques for Indirect Band Gap Semiconductors

The effects of indirect recombination and trapping can also be measured by photoconductive decay experiments. A population of excess electrons and holes produced by short light pulses disappears with a decay constant characteristic of the particular recombination process. Recording the sample resistance (or conductivity) as a function of time can be used to monitor the time dependence of the carrier concentrations.

Another method uses the semiconductor interaction with microwaves to monitor the excess minority carrier density. Excess carriers are generated in the semiconductor with a continuous wave (CW) laser, and the sample is simultaneously irradiated with microwaves. The microwave reflection is measured and it increases as the conductivity of the sample increases. This is a very convenient method since, unlike photoconductive decay, it requires no contacts to the wafer.

Another contactless carrier decay technique was developed by Tiedje *et al.*[11], in which a radio frequency (RF) bridge circuit was capacitively coupled to the wafer. The photoconductivity produced by a short laser pulse, was measured by comparing the phases of the input RF signal and the reflected signal from the wafer. Li[12] modified Tiedje's technique so that it could be used to continuously monitor changes in surface states. This technique consists of an RF coil, inductively coupled to a silicon wafer and the same RF bridge used by Tiedje. A CW HeNe laser replaced the pulsed light source and its signal was chopped at a reference frequency in order to distinguish the laser-induced conductivity from the intrinsic conductivity of the semiconductor. The output of the lock-in amplifier is proportional to the minority carrier

concentration. Details about the circuit and the operation of the so-called RF-probe are given in the experimental chapter.

1.8 Passivation of Semiconductors

Early in the development of devices based on germanium and silicon, it was known that these materials contain dangling bonds (i.e. unsaturated valencies) which are potent minority carrier lifetime killers. These dangling bonds are responsible for states near the middle of the energy band gap which, depending on the applied bias, either remove the charge carriers needed for the operation of the device or generate unwanted charges. Dangling bonds occur primarily at the surface of the semiconductor, and also at lattice vacancies, dislocations, and are associated with certain impurities.

In order to achieve a low surface recombination rate (<10 cm/s) two different approaches may be used. The first approach involves surface passivation such that very few recombination centres exist in the surface. In the second approach the carriers are repelled from the surface by band bending, thus effectively reducing the flow of carriers to the surface states[13].

A well passivated surface may be achieved by attaching hydrogen atoms, for example, to the dangling bonds of a bare Si surface. This can result from simply dipping the sample in an HF solution. The surface stability of such a hydrogen-terminated surface in air depends on the conditions. Another surface passivation method involves the growth of a good quality oxide. The oxide covered Si surface is usually stable and has a relatively low interface state density, especially after annealing in hydrogen at about 400°C.[13]

The second approach, where carriers are repelled by band bending, can be achieved by: adding charges on the surface, by immersing the sample in a special electrolyte causing surface depletion, or by having a p-n junction at the surface.[13]

1.9 The Si/SiO_2 Interface and Defects

The technological thrust towards silicon ultra large scale integrated (ULSI) circuits with submicrometer elements has emphasized the need for a better structural model of the critical Si/SiO_2 interface in thermally oxidized wafers. The Si/SiO_2 structure is still a major component in current MOS devices. The so called "interface trapped charge" is represented by either positive or negative charges due to (i) structural, oxidation-induced defects, (ii) metal impurities, or (iii) other defects caused by radiation or similar bond breaking processes (e.g. hot electrons).[14] Much of the vulnerability of the MOSFET results from the interface region where defects are generated by interfacial stress. These defects, at room temperature, lead to electrically active interface states at energy levels distributed in the Si band gap. Much research has gone into the structural identification of these defects. Studies by several independent groups[15,16,17,18,19] indicate that a dominant role is played by interface defects in several technologically-relevant device-instabilities.

1.9.1 Historical Perspective of MOS Interface States

Surface states at intrinsic boundaries of pure semiconductor materials have been studied for more than 60 years.[20,21] One model that has been used to explain these states is the half filled orbital or "dangling bond". When a crystal such as silicon is cleaved, the surface plane has many exposed bonds that have just been broken in the process. If the split is homolytic the "dangling bonds" have only one electron each, and the state of the electron lies somewhere in the band gap of the semiconductor. Such unbonded orbitals are minimized on intrinsic Si surfaces, by a process of surface "reconstruction" which has been observed by several techniques, and especially by scanning tunnelling microscopy.[22] Extensive reconstruction of the Si surface does not occur at the well-bonded interface with SiO_2. Dangling bonds, very evident at such interfaces, were assumed to be a source of Si/SiO_2 interface states[23], long before they had been detected spectroscopically. Chemical, physical, and electrical studies of Si/SiO_2 interface states began in earnest when the MOSFET was first fabricated in the 1960's and they continue to the present day. A very suitable diagnostic technique that can reveal the nature of atomic-scale or point defects in semiconductors is electron paramagnetic resonance (EPR), also called electron spin resonance (ESR). EPR turned out to be a powerful tool to study the point defects at the surface and interface of silicon.[15]

Poindexter[16] has reviewed the history and physico-chemical perspective of MOS interface defects. The earlier studies were confined to (111) silicon wafers, owing to EPR sensitivity limitations. The most significant of these early studies was by Nishi[24], who detected three signals from (111) Si/SiO_2, termed P_a, P_b, and P_c centres. They were assigned by Nishi to trapped electrons in the oxide (P_a), trivalent silicon which has a nonbonding orbital electron in the oxide

near the interface (P_b), and trapped holes in the Si (P_c). Later the P_a centre was found to vary monotonically with the presence of phosphorus in the Si, and was assigned to loosely bound donor electrons.[25] The P_c signal was found to be large in Fe-enriched wafers, and was assigned to neutral atomic Fe in the Si bulk.[26] The most important centre, P_b, was deduced to be the entity $\bullet Si{\equiv}Si_3$ backbonded in the Si surface at the Si/SiO_2 interface on (111) wafers.[27,28] Only the orientation with the dangling bond perpendicular to the interface was found to be present in concentrations sufficiently high to be detected. Poindexter *et al.*[29] showed that the P_b centre cannot be identified with any other known defect in Si or SiO_2, in particular it is not like the E′ centre (paramagnetic oxygen deficient silicon sites in the oxide, with the structure $\bullet Si{\equiv}O_3$) and the non-bridging oxygen hole centre, the two most common defects in SiO_2.[30]

While it has been most intensively studied at the (111) Si/SiO_2 interface, the P_b defect has been observed for other surface orientations too, i.e., (100) and (110).[31] It has also been shown that the occurrence of P_b centres is not restricted to the Si/SiO_2 interface. For example, Stesmans and Van Gorp have found that the $\bullet Si{\equiv}Si_3$ defect is also the dominant defect at the (111) Si/SiN_4 interface.[32]

EPR studies have also been undertaken for the (100) face of silicon wafers, because of the importance of (100) Si in device applications. The measured P_b signal from a (100) wafer was found to be nearly an order of magnitude weaker than that from a (111) wafer. The observed ESR signal, previously assigned to the $\bullet Si{\equiv}Si_3$ dangling bond on the (111) surface, was found to have two components on (100) Si: (i) the P_{b0}, an $\bullet Si{\equiv}Si_3$ centre, and (ii) the P_{b1}, an unidentified centre tentatively assigned the $\bullet Si{\equiv}Si_2O$ structure, i.e. a partially oxidized P_b centre. Molecular orbital calculations[33] indicated that the $\bullet Si{\equiv}Si_2O$ structure might be incorrect, although oxygen

seemed to be involved. The assignment of P_{b0} as the (100) counterpart of P_b, was also questioned later.[34,35]

Several measurements of the population of paramagnetic P_b density versus Si/SiO_2 interface Fermi level provide approximate but clear information about the centre's electronic density of states.[36,37,38,39] Combined EPR, capacitance voltage (CV) measurements,[40,41,42,43,44] deep-level transient spectroscopy (DLTS),[45,46] and photoionization thresholds determinations[47] have revealed that P_b defects are interface states able to trap or lose an electron depending on the Si Fermi level position. Thus P_b centres are amphoteric and are found at ~ 0.55 eV above the valence band.

These studies showed that in a p-type material the P_b centre is a donor-like interface state defect that accepts a hole to form a positively charged site in a process that is described by the following equation:

$$P_b + h \rightarrow P_b^+ \qquad [1.20]$$

where h represents a hole. As the Fermi level moves upward towards the middle of the band gap, the positively charged P_b centre recovers an electron and becomes paramagnetic and neutral:

$$P_b^+ + e \rightarrow P_b \qquad [1.21]$$

where e represents an electron.

In an n-doped semiconductor, the P_b centre picks up another electron (i.e. behaves like an acceptor) becoming negatively charged and diamagnetic again.

$$P_b + e \rightarrow P_b^- \qquad [1.22]$$

The P_b centre is paramagnetic when the dangling bond has one unpaired electron; and it becomes diamagnetic by either accepting or donating an electron. The distribution of paramagnetic P_b centres is consistent with the distribution of the band gap density of states D_{it} (in eV^{-1} cm^{-2}) that is generally reported by CV measurements. This symbol (D_{it}) also serves to name the "interface states" or "interface traps". The P_b centres were found to account for 50-100% of the interface trap density, (N_{it}) measured electrically.[42]

The quantitative parameters for P_b centres and D_{it}, i.e. the P_b concentration, the P_b position in the band gap, and the interface trap density, obtained by different measurement techniques, are compiled in Table 1.3. The observed 1:2 ratio of $[P_b]$ to D_{it} integrated between E_v + 0.2 eV and E_v +0.9 eV was maintained for both (111) and (100) Si. Thus, the P_b dangling bonds were not established to be the source of all interface traps. It is also important to note that both the P_b concentration and the interface trap number density N_{it} on (100) were lower by about a factor of 3 compared to (111).

Poindexter *et al.* observed that $[P_b]$ and mid gap D_{it} correlated 1:1 quantitatively throughout a wide range of standard wafer processing regimes for both n- and p-type silicon: variable oxidation temperature; dry versus wet oxidation; cooling rate; effect of N_2 or Ar annealing, H_2 annealing, and post-metallization annealing.[25,30] The correlation was found to be independent of doping level. In samples with different oxide thicknesses, P_b and N_{it} did not vary significantly over the range 100-2000 Å, but P_b was smaller at 50 Å. On (100) Si, with native oxide etched off, it was observed that the P_{b0} signal reappeared promptly as the native oxide regrew, but P_{b1} did not reappear.[42] At that time the meaning of this result was still unclear. Deal[48] also observed a fairly good quantitative correlation between P_b concentration and mid gap interface state density N_{it}, after various processing treatments.

Table 1.3 Observed parameters for interface states and P_b centres in Si/SiO_2 structures. $[P_b]$ is the area concentration of P_b centres while the mid gap interface density N_{it}, is designated here as the area concentration of interface traps integrated between E_v + 0.2 eV and E_v + 0.9 eV. (From Poindexter[16])

PARAMETER	CV/DLTS	EPR
P_b on (111) Si		
$[P_b]$ (cm^{-2})	3.8×10^{12}	2.0×10^{12}
N_{it} (cm^{-2})	7.6×10^{12}	4.0×10^{12}
P_b position in band gap (eV)	0.57	0.49
P_{b0} and P_{b1} on (100) Si		
$[P_{b0}] + [P_{b1}]$ (cm^{-2})	1.3×10^{12}	0.7×10^{12}
N_{it} (cm^{-2})	2.7×10^{12}	1.4×10^{12}
P_{b0} position in band gap (eV)	indeterminate	0.56
P_{b1} position in band gap (eV)	indeterminate	0.34

1.9.2 Effect of Molecular Hydrogen on the Si/SiO_2 Interface

The dangling bond character of the P_b centre suggests that it should be chemically active. It was discovered in the 1970's that annealing of Si/SiO_2 interfaces in forming gas (10% H_2 and 90% N_2) at 400-500°C can greatly reduce the P_b defect density.[49] It was later shown that this effect is probably due to the presence of hydrogen near the interface, and hence can be attributed to passivation by H_2.

Brower[17] found that in the case of the (111) Si/SiO_2 interface, approximately 0.5% of the surface silicon sites are P_b centres. He proposed a model for the passivation kinetics of the P_b centres at the (111) Si/SiO_2 interface by using EPR.[50,51,52] In his study, dry thermal oxides approximately 500 Å thick were grown on (111) silicon substrates at 850°C. The intensity of the P_b resonance was measured as a function of the H_2 annealing time, pressure, and temperature. Brower found that H_2 passivated the P_b defects at a measurable rate between 230 and 260°C. From the EPR measurements he concluded that the rate equation for the P_b passivation was

$$-\frac{d[P_b]}{dt} = k[H_2][P_b] \qquad [1.23]$$

where k is the rate constant. Equation [1.23] indicates that the rate at which the interfacial density of P_b centres decreases due to the passivation process is proportional to the volume concentration of H_2 at the interface, $[H_2]$, the density of P_b centres, $[P_b]$, and the rate constant. If $[H_2]$ is constant at the interface, equation [1.23] describes a pseudo-first order process with a rate constant k', and its solution is:

$$\frac{[P_b]}{[P_b]_0} = e^{-k't} \qquad [1.24]$$

where $[P_b]_0$ is the initial interfacial density of P_b centres, and t is the annealing time.

The temperature dependence of k, was found to be described by the Arrhenius equation

$$k = A e^{-E_a / k_B T} \qquad [1.25]$$

where the activation energy for the passivation process was found to be E_a = 1.66 eV, the pre-exponential factor $A=1.94 \times 10^{-6}$ $cm^3 s^{-1}$, k_B is Boltzmann's constant, and T is the absolute temperature.

From his results, Brower inferred that the passivation process involves the binding of a hydrogen atom to the trivalent silicon atom, $\bullet Si{\equiv}Si_3$, resulting in the formation of a neutral, diamagnetic defect, symbolized as HP_b, according to the following chemical reaction:

$$P_b + H_2 \xrightarrow{k} HP_b + H \qquad [1.26]$$

The hydrogen-P_b centre interaction appeared fully reversible. Brower oxidized (111) silicon substrates in dry oxygen at 750°C to a thickness of 500 Å, passivated them with H_2 and D_2 at 300°C for 3-4 hours, and then annealed them in vacuum at temperatures ranging from 500 to 595°C.[53] Brower's results indicated that the high temperature return of the P_b centres is described by a first-order rate equation

$$-\frac{d[HP_b]}{dt} = k_d [HP_b] \qquad [1.27]$$

where k_d represents the dissociation rate constant, with a temperature dependence given by the Arrhenius equation

$$k_d = 1.2 \times 10^{12} e^{-2.56/k_B T} \qquad [1.28]$$

Brower ascribed his results to the chemical reaction

$$HP_b \xrightarrow{k_d} P_b + H \qquad [1.29]$$

Stathis, an IBM researcher, also studied the dissociation kinetics of hydrogen passivated (111) and (100) Si/SiO_2 interface defects and obtained an activation of 2.58 eV for the (111) interface, in excellent agreement with Brower's value.[54] He explained his slightly higher activation energy of 2.60 eV, for the (100) interface as a contamination problem.[55]

It is significant to note, as first indicated by Myers and Richards, that the sequence of the two chemical reactions describing the passivation process [1.26] and the dissociation process [1.29], is equivalent to the dissociation of the H_2 molecule[56]

$$H_2 \rightarrow H + H \qquad [1.30]$$

Brower and Myers showed that the P_b centre is in effect a catalyst in the H_2 dissociation process since it remains unchanged between the initial and final states of the chemical process.[57] The dissociation energy of the H_2 molecule in vacuum, $E_{H_2}^{vac}$, is known to be 4.52 eV.[58] However, according to the conservation of energy, the sum of the passivation reaction [1.26] and the dissociation reaction [1.29], Brower and Meyers concluded that the dissociation energy of the H_2 molecule in SiO_2 is approximately 4.22 eV. Comparison between this energy and 4.52 eV for the dissociation of the H_2 molecule in vacuum indicates that the reverse of the passivation reaction [1.26]:

$$H + HP_b \rightarrow P_b + H_2 \qquad [1.31]$$

and the reverse of the dissociation reaction [1.29]:

$$H + P_b \rightarrow HP_b \qquad [1.32]$$

occur with essentially no energy barrier and are controlled by the availability of atomic hydrogen.[57] These last three reactions are expected to play an important role in a radiation environment because of their exothermic nature and the availability of atomic hydrogen[59] (see next section).

In contrast to Brower's results, even though Stesmans[18] also used EPR, he found a non-exponential rate law in the passivation of P_{b0} and P_{b1} defects in (100) Si/SiO_2 (the oxide was grown at 176°C) with molecular H_2. He showed that if the decay is to be described by the same P_b-H_2 reaction limited kinetic model applying to interfacial P_b defects in (111) Si/SiO_2 (see Brower[50]), one has to assume a Gaussian distribution of activation energies around a mean value E_a, with a spread σ, and the integration limits (in eV) that span all possible E_{ai} values. Equation [1.25] then becomes

$$\frac{[P_{b0,1}]}{N_0} = \frac{1}{\sigma\sqrt{2\pi}} \int_0^{4.2} e^{-(E_{ai}-E_a)^2/2\sigma^2} \; e^{-t\,[H_2]\,A\exp(-E_{ai}/k_BT)} \; dE_{ai} \qquad [1.33]$$

where $[P_{b0,1}]$ represents the P_{b0} and P_{b1} density, N_0 is the initial defect density. By solving equation [1.33] simultaneously at all the working temperatures, Stesmans obtained the kinetic parameters: E_a=1.51 and 1.57 eV for P_{b0} and P_{b1}, respectively, σ = 0.15 eV, and a pre-exponential factor $A=1.43\times10^{-6}$ cm^3s^{-1}.[60]

Later, Stesmans also repeated Brower's study of the H_2 passivation of P_b defects in standard (111) Si/SiO_2 (thermal oxide grown at 870°C).[61] In contrast with Brower's results, he found that the $[P_b]$ removal by H_2 was also a non-exponential process. Stesmans argued that Brower did not observe this phenomenon because of an incorrect interpretation of the ESR data.

In contrast to Stesmans who monitored the P_b relative intensity through double numerical integration of the absorption derivative signal, Brower monitored the P_b densities by measuring the peak-to-peak height of the absorption derivative signal. As in the (100) Si/SiO_2 case, Stesmans found a Gaussian spread, but this time of a much lower value (σ = 0.06 eV), around the calculated mean activation energy E_a = 1.51 eV, as opposed to Brower's single-valued E_a = 1.66 eV. His calculated pre-exponential factor of 9.8×10^{-8} cm^3 s^{-1}, which is about a factor of 20 smaller than the one calculated by Brower, is identical to the expected value, approximated from geometric considerations:[62,63]

$$A \approx \frac{\nu_s}{V^{-1}} \qquad [1.34]$$

where the attempt frequency, ν_s for reaction [1.26] is of the order of magnitude of the vibrational frequency of H_2 (1.24×10^{14} Hz), and the density of accessible sites in vitreous SiO_2, V^{-1} corresponds to ~ 1.27×10^{21} interstices/cm^3.

Stesmans and Afanas'ev[64] reported a study of the generation of paramagnetic interfacial P_b defects in standard thermal (111) Si/SiO_2 by thermal processing in the range of 480-1135°C, at a pressure of $\leq 4 \times 10^{-7}$ Torr. The dissociation of HP_b (prominent from 460°C onward) was observed again. At the same time EPR revealed the existence of an irreversible P_b creation mechanism starting from ~640°C onward. The created P_b density increased with temperature, and showed no trend for levelling off up to 1135°C, where it was ~ 1.3×10^{12} cm^{-2}. The authors suggested that the crucial creation step for P_b interface defects was the post-oxidation thermal annealing in oxygen deficient ambient at temperatures above ~660°C.[65] The newly created P_b sites exhibited similar H-interaction kinetics as the natural ones. They could not be eliminated

by any subsequent thermal treatment in oxygen-free ambient at any temperature below the oxidation temperature. Oxidation was the only process found to eliminate the P_b centres. However, the interfacial degradation induced by post-oxidation annealing in vacuum was found to be much suppressed when annealing in He compared to other noble gases.[66,67,68]

Stathis[69] has published a comment on Stesmans' finding, drawing attention to his previous work[54] on the dissociation of HP_b's at temperatures up to 800°C, which showed no evidence of such a generation step. Stathis suggests that Stesmans' results may have resulted from either or both of two possibilities. Firstly, there could be a difference in the nature of the starting Si/SiO_2 sample because of carbon contamination from an acetone rinse in his work. A second difference might be the method of thermal treatment i.e., the lower pressure used by Stesmans ($4x10^{-7}$ Torr vs. $3x10^{-6}$-$5x10^{-5}$ Torr). He also found a discrepancy between Stesmans' reported P_b densities ($\approx 1x10^{13}$ cm^{-2}) and those observed by Brower and himself ($4\text{-}5x10^{12}$ cm^{-2}). Stathis attributes Stesmans ESR line shapes to dipolar interactions, not seen in other work, resulting from a very high concentration of P_b centres. In his reply to the Stathis comment, Stesmans totally disagrees with all the above mentioned arguments.[70]

Recently, other ESR experiments showed that the interface degradation induced in thermal (111) Si/SiO_2 by post-oxidation annealing in vacuum is strongly enhanced (by a factor of ~ 6) when performed in H_2 ambient.[71] It appeared that the standard H_2 post-oxidation annealing step used to passivate interface states, creates additional defects when it is conducted above ~ 550°C. This provides a good justification for the standard industrial practice of H_2 annealing at temperatures around 400°C.

Stesmans' most recent experiments suggested that P_{b0} and P_{b1} defects at the (100) Si/SiO_2 interface are chemically identical, i.e. both are $\bullet Si{\equiv}Si_3$ (P_{b1} is not a $\bullet Si{\equiv}Si_2O$ defect as initially proposed by Poindexter).[72] However, the P_{b0} and P_{b1} defects do differ physically. The P_{b0} defects are electrically active charge traps, while the P_{b1} defects are not.[73,74] It is inferred by Stesmans that, if half the P_b defects are not electrically active, this could be the fundamental reason why the (100) Si surface dominates device fabrication.

Stesmans found that annealing p-type (1$\bar{1}$1) Si/SiO_2 and (100) Si/SiO_2 interfaces in molecular hydrogen at temperatures in the range of 500-800°C introduced a considerable density (up to 10^{13} cm^{-2}) of positively charged centres.[75,76] He attributed the observed charged state to hydrogen bonding to a bridging oxygen atom at the interface (i.e. a threefold-coordinated oxygen), a structure resembling the hydronium ion, H_3O^+. This structure which has been proposed to have the structure $[Si_2{=}OH]^+$ is thought to be stabilized by the SiO_2 network rearrangement at the interface.[77] If this assignment is correct, the dissociation energy (2.4 eV) of this physically bonded hydrogen is comparable to that of an H-atom which is chemically bonded to a surface Si atom (2.6 eV).

1.9.3 Effect of Atomic Hydrogen on the Si/SiO_2 Interface

Cartier *et al.*[19,78] suggest that silicon dangling bonds, as detected by EPR, account for only a small fraction of the electrically detected interface states. They found that pre-existing silicon dangling bonds in Al-gate MOS capacitors on (111) silicon substrates were passivated during hot-electron stress, while defects (of an unidentified nature) were simultaneously generated.[79] This degradation is similar to the interface degradation caused by room temperature atomic

hydrogen supplied by a remote microwave plasma (2 GHz and 100 W) or by irradiation during device operation. Similarly, large numbers of interface states, which are not P_{b0} and P_{b1}, are produced at the (100) Si/SiO_2 interface by a remote hydrogen plasma. The interface state density was found to increase linearly with the H-atom dose over a wide range. The rate at which the interface states were created increased with decreasing oxide thickness and appeared to be thermally activated with an activation energy of ≈ 0.20 eV.[80] The (111) Si interface was found to degrade faster than the (100) Si interface.

In another study, Cartier *et al.* showed that atomic hydrogen exposure at room temperature also plays an important role in the formation of anomalous positive charge (APC) at the Si/SiO_2 interface.[81] The anomalous effect refers to an initial electron trapping followed by a build-up of positive charge in the oxide, and it was first observed in MOS structures subjected to electron injection. The charged state of the defect can be cycled between positive and neutral by the gate voltage (without injecting electrons and holes into the oxide). The APC exhibits charging/discharging times from fractions of seconds to hours.

The conclusion of the Cartier *et al.* studies is that silicon dangling bonds, as detected by EPR measurements, account for only a *small* (emphasized) fraction of the electrically detected interface states. Cartier *et al.* drew this conclusion after exposing the Si/SiO_2 structures to extremely high fluxes of atomic hydrogen ($\sim 10^{21}$ atoms/cm^2) to generate extremely high densities of interface states ($> 5\text{x}10^{12}$ /cm^2 eV). This constitutes the basis of Lenahan and Conley's criticisms in their 1998 review.[15] Firstly, they argued that the amount of hydrogen involved in the Cartier *et al.* experiments was many orders of magnitude greater than that present in the process they were attempting to model (a typical oxide of ~ 100 Å with ~ 0.1 % atomic

hydrogen would have about 10^{14} hydrogen atoms/cm^2). Secondly, they showed that since atomic hydrogen was not present during all the time involved (atomic hydrogen is dimerized in fractions of a second at room temperature[82]) in interface state generation (interface states exist for many seconds after a device is exposed to ionizing radiation[83]), atomic hydrogen by itself could not be responsible for most of the observation. Thirdly, since atomic hydrogen is very effective in passivating silicon dangling bonds[84], Lenahan and Conley did not consider testing a silicon dangling-bond-generation model with a process known to annihilate the dangling bonds an optimal approach. Fourthly, the authors argue that another problem with the Cartier *et al.* studies involved extremely high amounts of energy ($\approx 2\text{x}10^{27}$ eV/cm^3) which would be required to generate 10^{21} hydrogen atoms/cm^2. This amount of energy is ~ 10^6 times higher than the upper limit of technological relevance and would more than suffice to vaporize the ~ 100 Å SiO_2. The fifth and last point they brought into question was that the Cartier *et al.* study involved EPR measurements of P_b centres on ~ 100 Å thick oxides and CV measurements on ~ 500 Å thick oxides.[85] Since very large differences in interface state generation were consistently observed for different oxide thicknesses[86], it might not be surprising that Cartier *et al.* found very big differences in P_b and interface state densities.

Numerous studies[87,88] have demonstrated that improved resistance against hot electron degradation can be obtained by the nitridation and re-oxidation of SiO_2. Cartier *et al.*[89] used a remote H plasma to study the transport of atomic hydrogen, through this type of oxides. This so called "oxynitrided" SiO_2, was grown in dry O_2 at 1000°C, on p-type (100) Si, nitrided for 15 min in NH_3 at 1100°C, and re-oxidized in pure O_2 for ~ 200 min. Cartier *et al.* demonstrated that although atomic hydrogen is extremely reactive and produces large numbers of interface states,

its transport to the Si/SiO_2 interface is strongly suppressed in oxynitrided oxides. Thus, the suppression of the atomic hydrogen transport could be mainly responsible for the much lower degradation of reoxidized-nitrided oxides during high field, hot-electron stress as compared to thermal oxide.

Hess *et al.* reported the reduction of hot electron degradation effects in MOSFET's that had been thermally annealed in deuterium instead of hydrogen.[90] They observed transistor lifetime improvements by factors of 10-50, and suggested that the so-called "giant isotope effect" is due to the fact that deuterium is much more difficult to remove under the conditions used to desorb hydrogen. These researchers calculated the equilibrium concentrations of passivating adatoms in the crystalline Si/H_2 or D_2 system and showed that the substitution of D for H leads to a 1-1.5 orders of magnitude increase in the adatom concentration.[91]

1.10 Surface Characteristics of GaAs

An untreated III-V semiconductor surface has a great number of sites on which charge carriers can recombine. As in the case of silicon, such surface recombination is undesirable for electronic devices and a lot of effort has gone into passivating the surface with respect to the recombination of charge carriers.

Numerous descriptions of the carrier traps i.e., recombination centres, on the surfaces of III-V semiconducting materials have been proposed. As in the case of Si, it has been suggested that dangling bonds from the surface atoms may be responsible for the shortened carrier lifetimes

observed.[92] The following reaction has been proposed to be responsible for producing carrier traps on an oxidized GaAs surface:

$$2GaAs + As_2O_3 \rightarrow Ga_2O_3 + 4As \qquad [1.35]$$

Since reaction [1.35] is exothermic under normal conditions, the formation of atomic arsenic on the surface of GaAs is possible. It has been suggested that As could act as a carrier trap on oxidized III-V surfaces.[93]

Unlike silicon, which forms a natural oxide layer that acts as an effective dielectric material and eliminates the majority of the recombination centres on its surface, the oxides of the III-V materials are not effective in reducing the undesirable carrier-trapping surface-states. Therefore, other solutions have to be found to this problem. One of them is to deposit an additional epitaxial layer of a lattice matched semiconductor, with a larger band gap than the first semiconductor. This second layer acts as a barrier to the carriers, by preventing them from escaping to the surface, as they do not have sufficient energy to enter the larger band gap material. The limitations of this solution are especially obvious in optical applications such as lasers and MOSFET's, where an exposed surface or a metal-GaAs interface is necessary.

Wet surface passivation techniques are also used but have a short lasting effectiveness and are rather difficult to control.

As a consequence of these problems, effective dry passivation techniques, more compatible with other dry processing steps of semiconductors, have been sought. Gottscho *et al.* have studied the passivation of GaAs by hydrogen.[94,95,96,97] Although hydrogen does not appear to provide permanent passivation, an understanding of this process would be instrumental in developing techniques using more permanent elements such as sulphur.

1.11 Thesis Goals and Objectives

It has been known for many years that hydrogen has a passivating effect on silicon surfaces and interfaces. It is a common industrial practice to subject silicon wafers to a high temperature (> 400°C) annealing in H_2. However, the effect of hydrogen incorporated during the annealing process is somewhat uncertain, and device degradation during operation has been linked to the presence of hydrogen.

The objective of the present research was a systematic study on the effect of molecular and atomic hydrogen on both the (100) and the (111) Si/SiO_2 interface at a series of temperatures, using an *in situ* technique for monitoring interfacial recombination centres during exposure to H_2, H and when the reactant is removed.

Earlier studies of interfacial defects in non luminescent semiconductors have been done principally with CV or EPR measurements. Neither technique is capable of monitoring the defect concentration continuously, *in situ*, and in real time.

Traditionally, only one interfacial defect in Si/SiO_2 (the P_b centre), and its passivation by H_2 has been probed by EPR. Although EPR is a very sensitive diagnostic tool, it needs special experimental conditions such as: the stacking of many samples together to enhance the effective signal, a very low (4.3 K) working temperature, and several tedious procedures for heating up the sample for exposure to H_2 followed by cooling down before each measurement. Our "contactless" analytical technique, the RF probe, responds to defects in integrated circuit materials, and could be of considerable help in developing better processing methods. By using the *in situ* RF probe we aim to study the recombination centre concentrations which occur while

the Si/SiO_2 interface is interacting with H_2 or H-atoms. With this technique we are able to measure all the electrically active defects at the Si/SiO_2 interface, and it will be interesting to compare our results with those obtained by EPR.

We also undertook the study of interactions of H-atoms with GaAs, with the idea that a comparison of the same reaction with Si might shed light on the processes occurring in both systems. For the GaAs study the steady-state photoluminescence provided a probe of the surface processes as they were occurring.

2. EXPERIMENTAL

2.1 Materials

2.1.1 Gallium Arsenide Samples

The GaAs samples were cut from single crystal, semi-insulating (100) wafers (carrier concentration, $n \approx 10^{14}$ cm^{-3}) grown by molecular beam epitaxy (MBE) in the Physics Department at the University of British Columbia. Other GaAs wafers were supplied by EG&G Optoelectronics Canada (Vaudreuil, Quebec). Figure 2.1 (a) and (b), respectively, show the typical structure of these samples. This configuration, with a layer of wider band gap AlGaAs below the GaAs, was chosen in order to keep the carriers confined to the GaAs layer and thus to maximize the sensitivity of the PLI to the changes on the exposed surface. The samples were undoped or only modestly doped, in order to reduce the carrier loss by radiative recombination in the bulk.

Figure 2.1 Schematic diagram of GaAs sample structure: (a) UBC samples, and (b) EG&G samples.

2.1.2 Silicon Samples

The Institute for Microstructural Sciences (NRC, Ottawa) provided some of the silicon samples used for this project. 1800 Å of intrinsic Si (i-Si) was grown on top of either n or p-type (100) Czochralski silicon substrates (resistivity ≈ 15 Ωcm) by chemical vapour deposition. This sample structure is listed in the first line of Table 2.1.

The Institute for Microstructural Sciences also provided other silicon samples used in this work. These samples were p-type (100) Si/SiO_2 structures, with a resistivity of ~ 50 Ωcm. The thermal oxide films were in some cases subjected to rapid thermal annealing at high temperatures in N_2O, a process that is called oxynitridation. Some of the oxynitrides were re-oxidized. These (100) Si/SiO_2 structures are also listed in Table 2.1 (lines 2 and 3).

The third type of silicon sample used in this work was purchased either from Monsanto Co. (Electronics Division, Palo Alto, CA) or from ZITI Inc. (Monterey, CA). These single crystal wafers were boron-doped, with a (111) surface orientation. The Monsanto (M) samples were Czochralski grown 3" silicon wafers, with a resistivity of 5-10 Ωcm. The resistivity of the ZITI (Z) 3" Czochralski wafers was about 5-30 Ωcm. The last two lines in Table 2.1 summarize the information on the ZITI and Monsanto samples.

2.1.3 Chemicals

Hydrofluoric acid (Aldrich, A.C.S. reagent grade) with an assay of 48.0-51.0% was used. Deionized water with a resistivity of 18 MΩcm was supplied by the Advanced Materials and Process Engineering Laboratory (AMPEL) at the University of British Columbia.

Table 2.1 Types of (100), (111) p-Si/SiO_2, and (100) i-Si samples used in this work.

Sample ID	Sample Orientation	Oxidation	Nitridation	Re-oxidation	SiO_2 Thickness (nm)
#I2	(100)	[a]Thermal/900°C [a]O-plasma/200°C	No	No	>20 <2
#8	(100)	[b]Thermal	N_2O @1050°C	No	<10
#7	(100)	[b]Thermal	N_2O @950°C	No	<10
#Z1	(111)	[a]Thermal/850°C	No	No	>20
#M1	(111)	[a]Thermal/850°C	No	No	>20

[a] Oxide grown in our laboratory.
[b] Oxide grown at the Institute for Microstructural Sciences (NRC, Ottawa).

2.1.4 Gases

The gases used were hydrogen, deuterium, argon, oxygen, helium, nitrogen, hydrogen sulphide and nitrogen dioxide. The hydrogen, oxygen, argon, and helium were all ultra high purity gases from Praxair. The prepurified nitrogen and the CP grade deuterium were Linde products. The quoted purity of hydrogen, argon and helium was 99.999%, while that of oxygen was 99.993% with maximum moisture of 5 ppm. Nitrogen and deuterium had a maximum purity of 99.998% (5 ppm maximum moisture) and 99.5%, respectively. The CP grade hydrogen sulphide, with a minimum purity of 99.6% (liquid phase) was supplied by Matheson. Nitrogen dioxide, with a purity of 99.5 mole % in liquid phase, supplied by Matheson was used to titrate hydrogen and oxygen atoms.

2.2 Reactor and Experimental Setup for Gallium Arsenide

A schematic diagram of the reactor and the experimental setup is shown in Figure 2.2. Although the discharge-flow system resembled that used for silicon, the detection system was optical rather than electronic.

The reactor was constructed from Pyrex, with an outer diameter (OD) of 38 mm, an inner diameter (ID) of 35 mm, and a length of 180 mm. The 160 mm long discharge tube was made of quartz with OD=12 mm, and ID=10 mm. A light trap was added at the end of the discharge region to keep the UV radiation, originating from the plasma, from impinging on the sample. The Pyrex reactor was separated from the rotary pump (Sargent-Welch Model No. 1402, 160 liters/min pumping speed) by a butterfly valve. A short, thick rubber tube connected the pump to

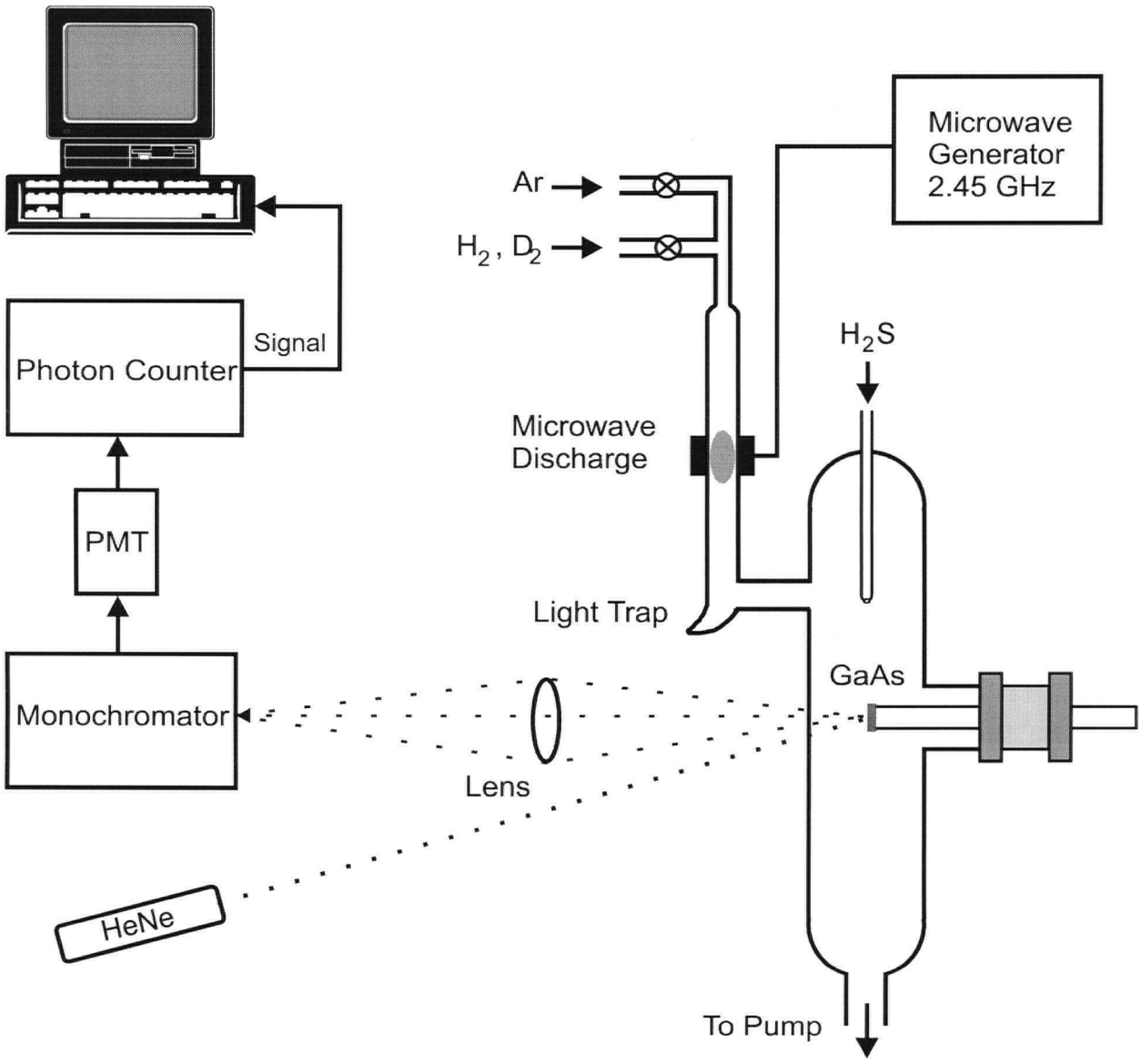

Figure 2.2 Schematic diagram of the reactor and experimental setup for GaAs.

the valve, in order to minimize vibrations from the pump. The system base pressure was typically a few milliTorr. The sample holder was a 10 mm diameter glass tube, attached with concentric, Cajon type, Delrin® (Cadillac Plastic) fittings. The sample was attached vertically to the end of the tube with the aid of a drop of silicone high vacuum grease (Edwards).

Usually the experiments were conducted at room temperature. However, when it was necessary to monitor the temperature, a 1 mm diameter flexible K-type temperature probe (Cole-Parmer H-08514-96, 1100 °C maximum temperature) was inserted into the sample holder. The temperature was displayed on a digital readout (Omega Model 115 KC). A heating wire wrapped around the reactor in the sample region was used to heat the sample.

The gases (hydrogen, deuterium, and argon) were introduced into the system through ¼ inch copper tubing and a Cajon reducing union placed at the end of the discharge tube. Polyethylene tubing, a Cajon fitting and a 6 mm diameter glass tube with a very small opening at the end were used for introducing a small flow of hydrogen sulphide into the reactor just above the sample. Fine control of the hydrogen and deuterium flow rates was obtained by using variable leak valves (Granville-Philips series 203). The argon flow rate was controlled with a bellows sealed metering needle valve (Nupro SS-4BMG), while the hydrogen sulphide flow was controlled with a micro-metering valve (Whitey SS-21RS4). Plug valves (Nupro B-4P4T and Nupro SS-4P4T) were used to shut the gas lines off completely. Gas pressures were measured using a pressure transducer (MKS Baratron Type 122A) with a range of 10^{-3}-10 Torr.

Periodic cleaning of the reactor and especially the discharge region was done by washing in a 10% HF solution and rinsing well in deionized water.

An E.M.S. Microtron 200 microwave power generator (2.45 GHz), attached to a quarter wave cavity was used to create the hydrogen or deuterium plasma inside the quartz discharge tube. The discharge region was cooled with compressed air to prevent overheating and to reduce H and D-atom recombination on hot walls. The microwave was operated in the range of 40 to 100 W.

2.3 Photoluminescence Detection

Gallium arsenide is a direct band gap semiconductor, therefore photoluminescence could be used to measure the changes in carrier concentrations occurring at the surface. The GaAs band gap (≈865 nm at room temperature) fluorescence was excited, by a 10 mW red (632.8 nm) HeNe laser. The luminescence was collected by a 60 mm diameter lens (focal length of 130 mm) and focused onto a 2 mm aperture entrance slit of a 0.3 m scanning monochromator (GCA/McPherson Model 218), dispersed and detected by an infrared sensitive (RCA-7102) photomultiplier tube (PMT). The PMT signal measured by a photon counter (Quantum Photometer Model 9511) operated at 1200 V, was then collected by a computer (IBM 486DX33). Thus the GaAs *in situ* relative photoluminescence intensity (PLI) measured as a function of real time could be plotted and analyzed using the Microcal Origin program.

A highly doped ($n = 10^{18}$ cm^{-3}) GaAs sample was used for optimizing the optical alignment and calibrating the monochromator. This type of sample had a very high PLI that was easy to measure. After putting the sample into place on the holder and aligning it with the focusing lens and the entrance slit, the monochromator was scanned from 780 nm to about 920

nm, with a speed of 1000 nm/min. The peak in the PLI was observed at a wavelength λ_{max}= 865 nm. Using this procedure, the emission band could be checked for any of the samples, but the wavelength of the maximum was always found to be the same.

By keeping the monochromator wavelength set at 865 nm, the signal was maximized, by adjusting the alignment. A band-pass filter (750-900 nm) at the back of the monochromator entrance slit was used to minimize the contribution to the PLI from stray light. In order to further minimize such interference, all the experiments were performed in complete darkness.

2.4 Reactor and Experimental Setup for Silicon

A schematic diagram of the reactor and the experimental setup is shown in Figure 2.3. The main part of the apparatus consisted of a reaction chamber, a microwave cavity for creating a remote plasma, and a mass spectrometer for monitoring gaseous species.

The Pyrex reactor had an outer diameter (OD) of 28 mm, and inner diameter (ID) of 25 mm. The 180 mm long discharge tube was made of quartz with OD = 12 mm, and ID=10 mm. A light trap between the discharge region and the reaction region kept the UV radiation from reaching the sample. The Pyrex reactor was integrated into the vacuum system with the aid of a glass-to-metal adapter.

The plasma was created in the discharge tube with a quarter wave cavity attached to an E.M.S. Microtron 200 microwave power generator operated at 2.45 GHz, with an incident power of 0-200 W. The working power was typically between 40-100 W. The compressed air flowing around the cavity helped to cool down the hot plasma region when the plasma was on.

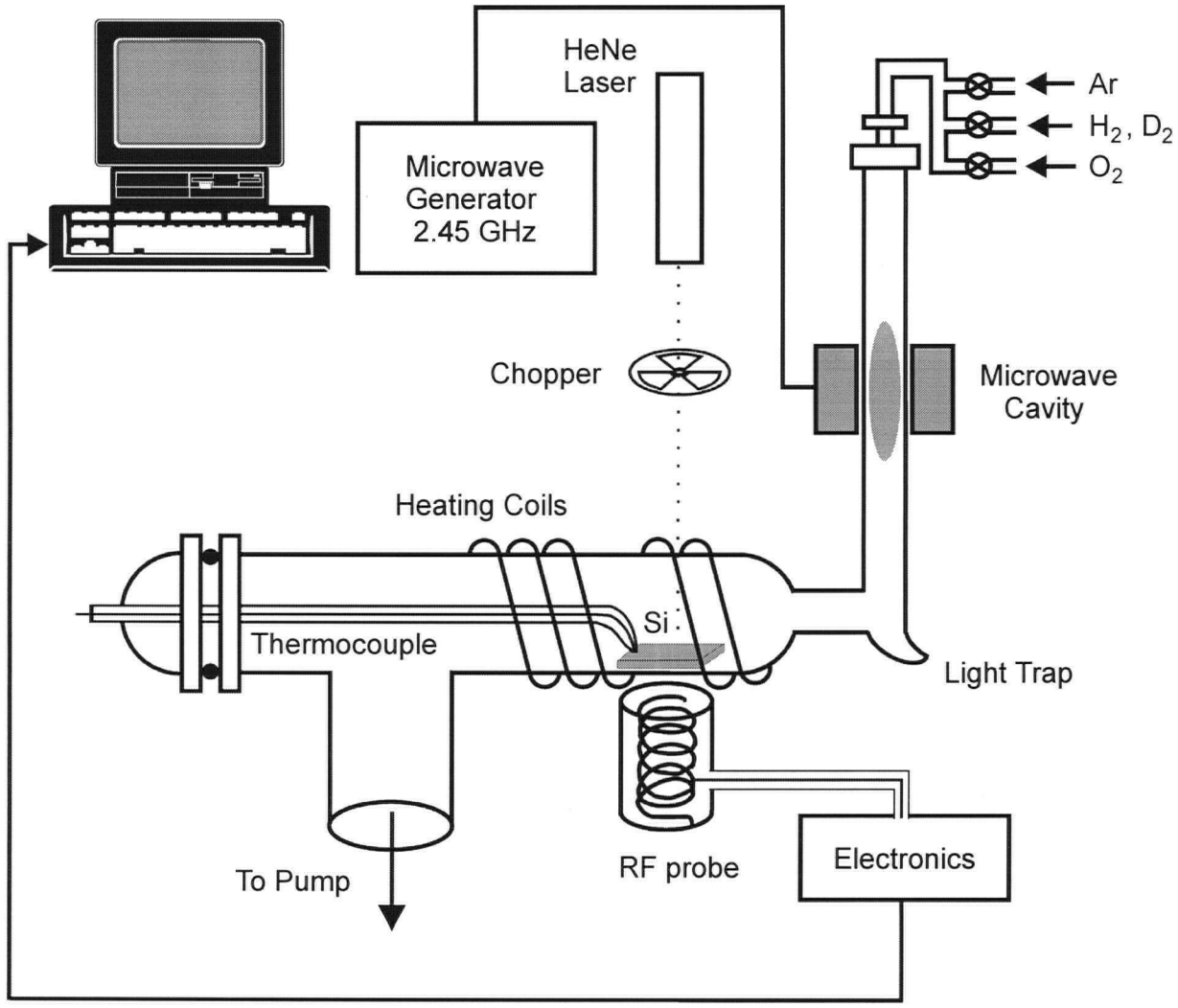

Figure 2.3 Schematic diagram of the reactor and experimental setup for silicon passivation.

The gases (hydrogen, deuterium, argon and oxygen) were introduced into the system through ¼ inch copper tubing and a Cajon reducing union placed at the end of the discharge tube. Fine control of the hydrogen and deuterium flow rates was obtained by using a variable leak valve (Granville-Philips series 203). The argon and oxygen flow rates were controlled with bellows sealed metering needle valves (Nupro SS-4BMG). Diaphragm valves (Nupro SS-DLS4) and plug valves (Nupro B-4P4T) were used to shut the gas lines off completely. The gas pressures were measured by a capacitance manometer (Edwards Barocel Series 600) with a pressure range of 10^{-3}-10 Torr. A cold cathode pressure gauge (HP Model 421) was used to measure the pressure in the range of 10^{-2}-10^{-10} Torr.

Special precautions were taken in order to avoid the introduction of air or moisture into the system. For this purpose, a small flow of argon provided a positive pressure while loading and unloading samples. Either argon or oxygen was used to bring the system up to atmospheric pressure after completing an experiment.

The flow system was pumped by a molecular drag pump (Alcatel MDP 5010, pumping speed of 7.5 liters/second nitrogen) backed by a rotary pump (Sargent-Welch Model No.1376, pumping speed of 300 liters/minute). Using the two pumps permitted work with a gas pressure of about 50-75 mTorr, while the base pressure of the system was about 10^{-6} Torr. The molecular drag pump has a high pumping speed and therefore a fast flow rate in the discharge flow system. This allows a smaller decay of the atomic species produced in the discharge region, thus assuring a higher concentration of atoms in the sample region. However, higher working pressures (0.1-0.3 Torr) were also used. For these experiments the molecular drag pump was bypassed leaving only the rotary pump on.

Periodic maintenance was necessary for the reaction chamber in order to obtain a high concentration of atomic species and to maintain reproducibility. For this purpose, the reaction chamber was disconnected from the system; the Pyrex and quartz parts were washed in 10% HF solution and rinsed well in deionized water (DIW).

The silicon sample was placed flat on the bottom of the Pyrex reactor. A heating wire wrapped around the reactor in the sample region was used to heat the sample. A 6-mm diameter hollow Pyrex tube was bent at the tip to touch and hold down the sample. The glass at the tip was thinned, so that when a 1-mm diameter flexible K-type temperature probe (Cole-Parmer H-08514-96, 1100°C maximum temperature) was inserted into the tube it made contact with the flattened end of the tube, and hence measured the sample temperature. A high performance (0.01°C resolution, 0.2°C accuracy) digital indicator (Omega Model DP41-TC-A) displayed the temperature. The analog output (0-5 V in the temperature range of 0-500°C) of this indicator was collected by a computer (IBM 486DX33).

2.5 The RF-Probe

A radio frequency (RF) probe, shown schematically in Figure 2.4, provided a "contactless" technique for monitoring the steady-state carrier concentration of the silicon samples. In order to maximize the sensitivity of the probe to the changes in the silicon conductivity, it was pressed against the outer wall of the Pyrex reactor underneath the sample.

The RF-probe consisted of a helical resonator made of a copper coil, which was inductively coupled to the sample. Li and Ogryzlo[98,99] describe the operation of the RF-probe in

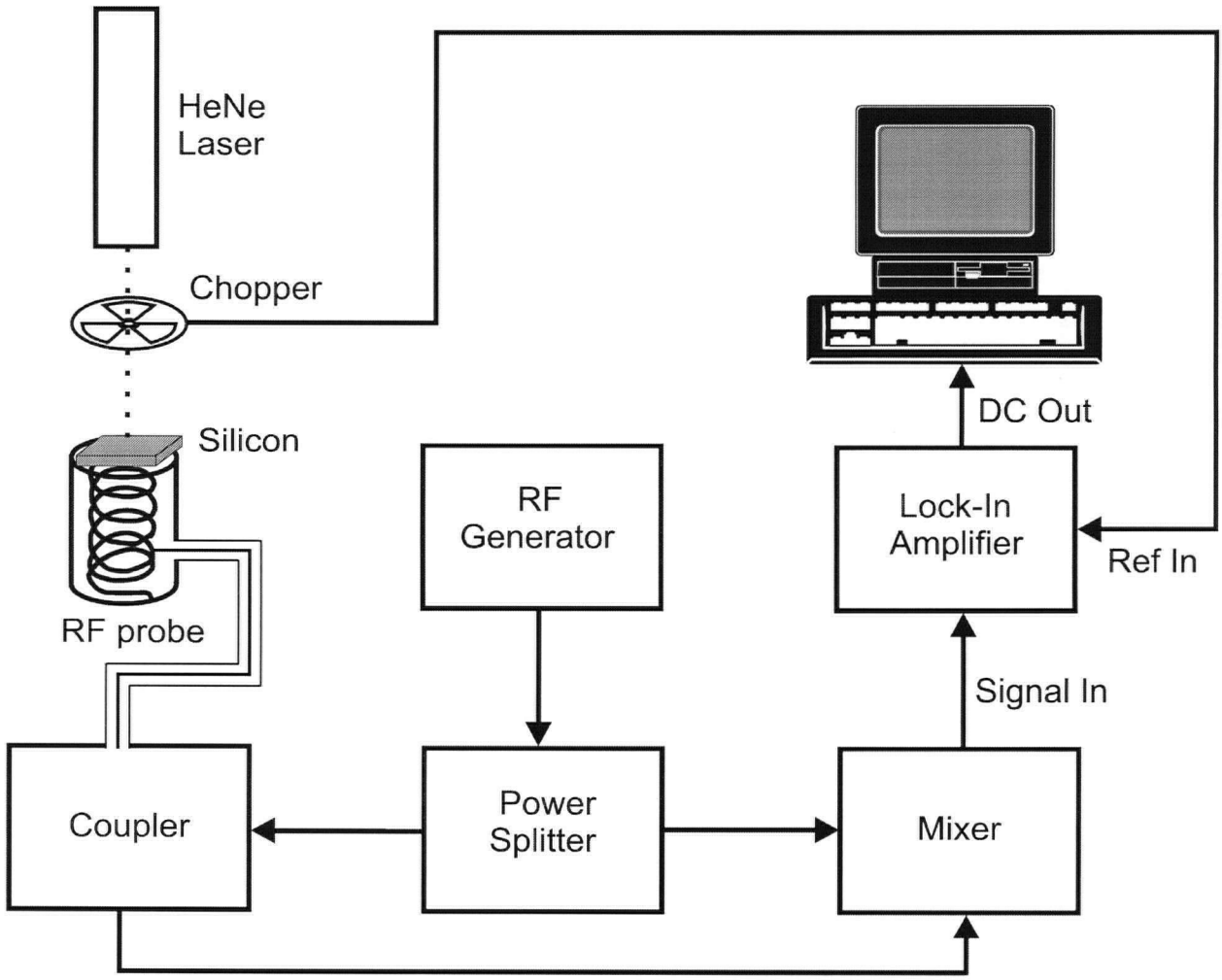

Figure 2.4 Schematic diagram of the "contactless" measuring system for silicon.

detail. The RF-circuit contains a splitter, a coupler, and a mixer connected as shown in Figure 2.4. The RF generator (HP Model 3200B VHF oscillator, frequency range 10-500 MHz, RF output power > 150 mW in the band 130-260 MHz) provided a signal that was split in two by the splitter (Mini Circuits ZFSC-2-1). One of the signals went into the coupler (Mini Circuits ZFDC-10-2), and then into the helical resonator. The Cu coil reflected the signal with an altered magnitude and phase into the mixer (Mini Circuits ZFM-2H). The other signal coming from the splitter went directly into the mixer and acted as a reference. Earlier work[99] has shown us that the magnitude of the change in this signal is proportional to the change in conductivity of the sample, which, in turn is proportional to the change in concentration of the minority carriers. The signal from the mixer was detected by a lock-in amplifier (EG&G Princeton Applied Research Model 5102). The analog output was collected by a computer (IBM 486DX33) used for the data acquisition. The sampling rates ranged from 1 data point/s to 1 data point/min, depending on the monitored process.

The beam from a 10 mW, 633 nm HeNe laser, chopped at 400 Hz reference frequency by a chopper (Grubb Parsons), was directed at the silicon sample. The photon energy of the laser is larger than the silicon band gap (≈1100 nm) and free electron-hole pairs are formed. The chopping frequency was high enough so that it could accurately measure changes occurring in less than a second, but low enough to be at least two orders of magnitude slower than the longest carrier lifetime. The lock-in amplifier measured only the carriers generated by the chopped laser beam and its output voltage was collected by the computer for further analysis. The RF-probe signal is very sensitive to temperature changes. Therefore, the previously mentioned collection

of the analog temperature signal was very important in determining whether the signal increase or decrease was due to chemical treatment applied to the sample or to the temperature variations.

Previous experiments by Li[12], who varied the laser intensity, have shown that the output from the lock-in amplifier is proportional to the steady-state charge-carrier concentration. If the laser intensity is constant the steady state photo-generated carrier concentration is inversely proportional to the surface or interface defect density, since carrier losses at the surface or interface are several orders of magnitude greater than in the bulk of the semiconductor. Therefore, although the recorded signal from the lock-in amplifier was the steady-state carrier concentration, the data analysis was conducted on the reciprocal of this quantity. The collected data were plotted and analyzed with the Microcal Origin curve-fitting program.

2.5.1 The Effect of Temperature on the RF-Probe Signal

A change in temperature was found to have a very significant effect on the RF-probe signal. In other words, the resonance frequency of the RF-probe shifted for different working temperatures.

A silicon sample with a resistivity > 50 Ωcm was required to produce a strong, noise free signal from the mixer. The resonance frequency of the RF-probe was near 245 MHz, and therefore it was operated at resonance frequencies ranging from 240 to 250 MHz. The change in signal with temperature was measured in order to correct for any drift in the sample temperature during the course of the experiment. The lock-in amplifier signal, and thus the mixer output signal, are shown as a function of temperature in Figure 2.5. Here an H_2 annealed p-Si(111)/SiO_2 (#M1) sample was used for the calibration. The signal increased with temperature, went through

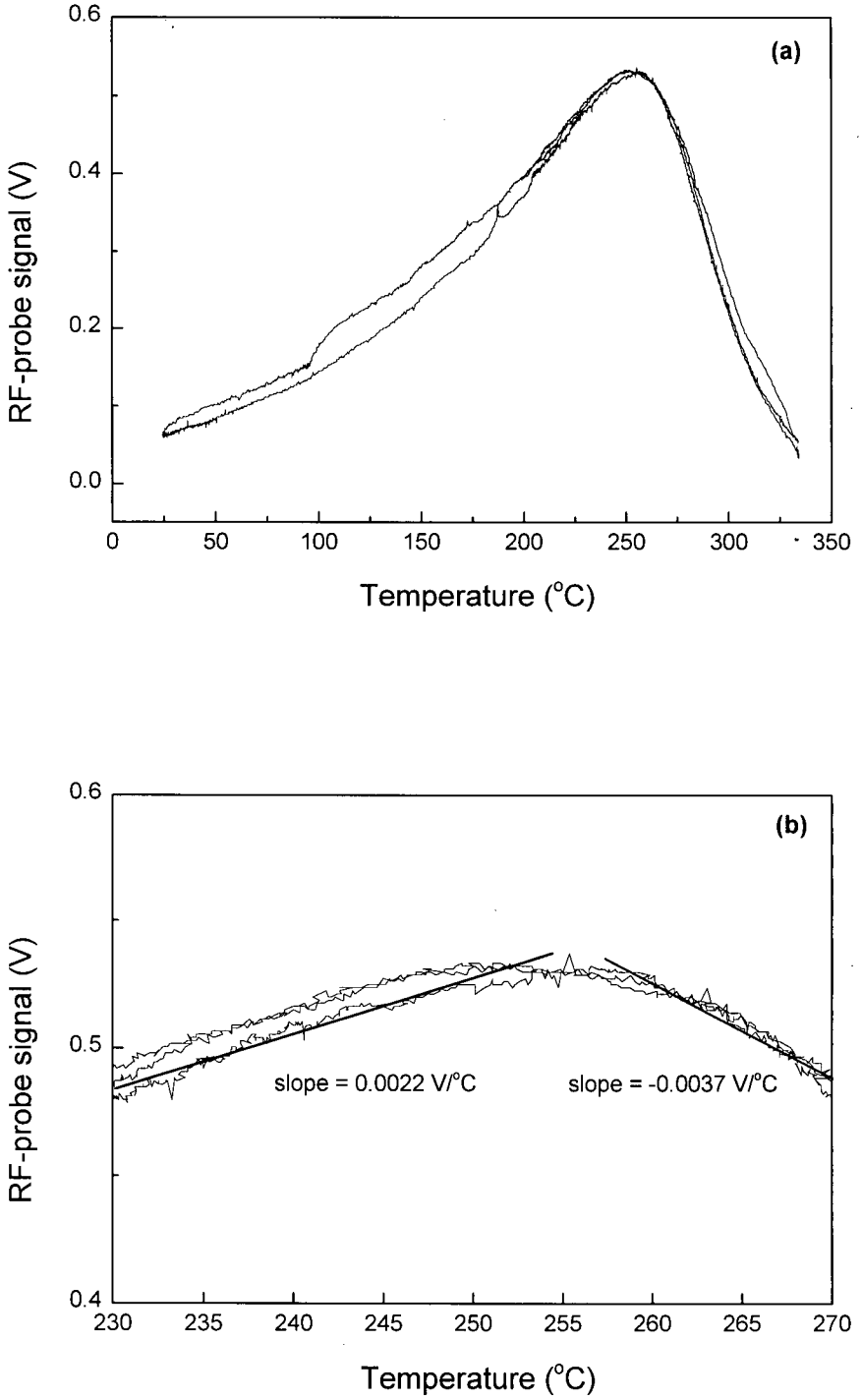

Figure 2.5 Temperature calibration of the RF-probe signal for 248 MHz resonance frequency where (a) and (b) represent different temperature ranges.

a peak and then decreased again rather rapidly at temperatures higher than approximately 275°C. From the Figure 2.5(a) it is clear that the maximum signal was obtained at about 255°C, but it did not change significantly over the 230-270°C temperature range as illustrated in Figure 2.5(b). The slope of about 0.002-0.004 V/°C in that range was used to correct for the temperature variations of the signal.

2.6 Mass Spectrometer

The schematic diagram of the stainless steel mass spectrometer (MS) vacuum chamber is shown in Figure 2.6.

The system was pumped down to ~10^{-7} Torr with a turbo-molecular pump (Edwards EXT70, pumping speed of 52 liters/second nitrogen) backed by a rotary pump (Sargent-Welch Model No. 1402, pumping speed of 160 liters/minute). A pneumatic valve (Kurt J. Lester Model SA0075PVTE) located between the turbo pump and the rotary pump was used to prevent back streaming of hydrocarbon vapours from the rotary pump oil in case of power failure. Dry nitrogen could be admitted into the system with a solenoid vent valve (Edwards TAV5) attached to the vent port of the turbo-molecular pump, which functioned as an extra power failure protection.

A gate valve (MDC electro-pneumatic, Model GV-1500V-P) connected to the MS chamber to the reaction chamber. The "differential" gasket between the gate valve and the flange on the reactor side was a copper plate with an approximately 100 μm diameter pinhole in its centre. It served to leak small amounts of gases from the reaction chamber into the MS chamber.

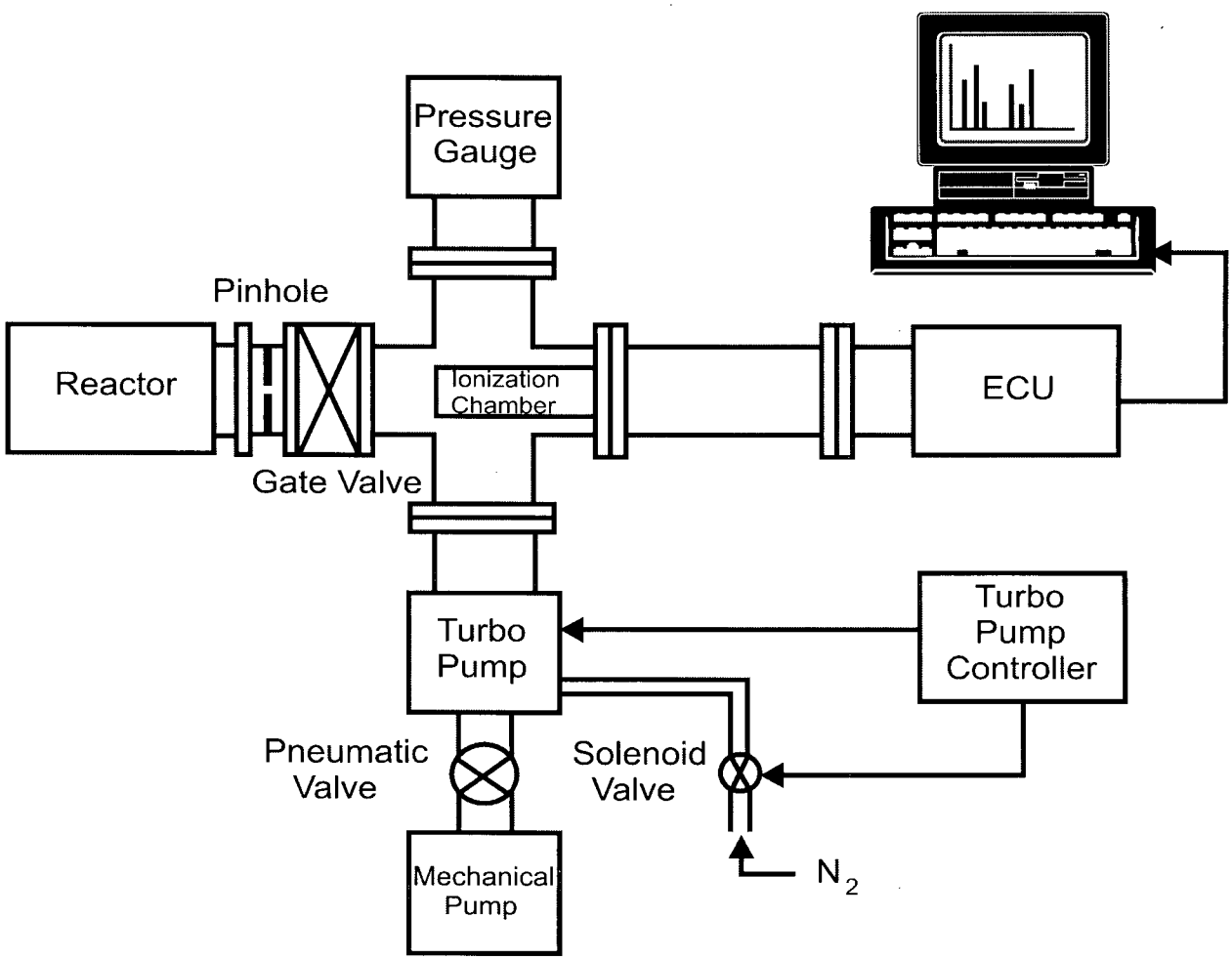

Figure 2.6 Experimental setup for the mass spectrometer.

Diffusion and sampling on the low-pressure side were rapid because of the low pressure in the MS chamber.

The mass spectrometer was a quadrupole mass analyzer MKS partial pressure transducer (PPT) residual gas analyzer with a mass range of 1 to 200 atomic units. It consisted of a compact ion source quadrupole sensor, an electronic control unit (ECU), and an interactive PPT software connected to a PC (IBM 486DX33) to control and monitor the mass spectrometry.

The maximum operating pressure of the sensor was $1x10^{-4}$ Torr. The total pressure of the system was measured with an ionization gauge (Leybold-Heraeus Combitron CM330). The quadrupole mass sensor also displayed the pressure of the quadrupole chamber in the range of $1x10^{-4}$ to $2x10^{-9}$ Torr.

2.7 Experimental Procedure

2.7.1 Wafer Preparation

The 5x5 mm GaAs samples cut from the wafer were dipped in a 10% HF solution for about 60 seconds, and rinsed in deionized water. They were quickly inserted into the reactor and dried under a flow of argon.

The etching of GaAs in HF gets rid of the arsenic oxides (As_2O_3 and As_5O_5) on the surface[100], but XPS measurements have shown that the surface is left gallium rich, with Ga_2O_3 still present.[94]

A 1:10 HF solution in deionized water was used for cleaning the Si wafers. Samples with dimensions of about 5x10 mm were first cut from the wafer and then dipped in the HF solution for about 60-90 seconds, then rinsed in deionized water, and quickly introduced in the reactor.

The HF etched away the native silicon oxide and left the surface hydrogen atom terminated. The stability in air of these surfaces is quite good, i.e. a few hours in air.

2.7.2 Atomic Hydrogen and Deuterium Exposure of GaAs

A GaAs sample was first loaded in the reactor, positioned on the sample holder, and aligned with the monochromator entrance slit. The system was then pumped down to a pressure of about 5 mTorr, using the rotary pump.

Hydrogen or deuterium atoms were generated in a microwave discharge. Molecular hydrogen (0.1 Torr) diluted with up to 0.3 Torr of argon flowed through the quartz discharge tube about 10 cm (or 10 ms) upstream from the sample. The microwave generator was operated in the range of 50 to 100 W. The plasma was ignited with a Tesla coil. The GaAs wafer was then exposed to the atomic hydrogen for various periods of time (from a few seconds up to 5 minutes). At the end of these periods, the hydrogen plasma was switched off, and the H_2/Ar gas mixture continued to flow over the sample.

2.7.3 Atomic Sulphur Exposure of GaAs

Sulphur atoms were produced *in situ* from the two step reaction of hydrogen sulphide with atomic hydrogen:

$$H_2S + H \rightarrow HS + H_2 \qquad [2.1]$$

$$HS + H \rightarrow S + H_2 \qquad [2.2]$$

Reactions [2.1] and [2.2] are very rapid, and yield one S-atom for every two H-atoms consumed.

The technique involves adding a very small amount of H_2S (1-2%) to a stream of H-atoms.[101] The reactor was heated to a temperature of about 80°C, to avoid the condensation of sulphur on the cold walls. Hydrogen atoms were generated using the procedure described in section 2.7.2. Then the H_2S valve was opened letting in a small amount of gas which reacted with the H-atoms according to the above reactions. The experiment was terminated by switching off the H plasma, and then shutting off the H_2S flow.

2.7.4 Oxidation of Silicon

The thermal oxidation of silicon was performed in a Lindberg tubular furnace (Type 55342) in AMPEL at the University of British Columbia. The silicon wafers were placed on a quartz boat and transferred into a quartz tube inside the furnace for thermal oxidation. A temperature control panel was used to program the "ramping up" and to monitor the temperature inside the furnace. Nitrogen was flushed through the tube before the heating started, during the heating up process, and during the cooling down period. This ensured that no extra oxidation could occur at lower temperatures and no impurities could reach the sample. Dry oxygen (1 atm), passed through a tube immersed in liquid nitrogen to get rid of any moisture, was flowed over the sample when the temperature reached the desired value for the oxidation process. The majority of silicon samples were oxidized at 850-900°C for 0.5-1 h. Some samples were oxidized at a lower temperature of ~200°C for 2.5 hours. After the oxidation period the samples were allowed to cool down to room temperature under a flow of N_2. The oxide thickness was of ~ 200 Å, and ~ 20 Å, for the high temperature and the low temperature oxidation, respectively.

A silicon dioxide layer was also obtained by exposing a silicon surface to atomic oxygen at 200°C. Li[102] and Zheng[103] have shown that higher or lower temperatures than 200°C do not produce a significant increase in the oxide thickness. The maximum thickness obtained was of about 20 Å, as determined from XPS measurements. Oxygen atoms were produced in the microwave discharge operated at 100 W and located upstream from the reaction chamber. Molecular oxygen at a pressure of 0.5 Torr was passed directly through the discharge without inert gas dilution. This pressure was chosen in order to maximize the oxygen atom (O-atom) concentration and to minimize their recombination on the quartz walls.

2.7.5 Atomic Hydrogen and Deuterium Exposure of Si/SiO_2

A silicon sample was first loaded in the reactor and positioned on top of the RF probe. The system was then pumped down to a pressure of about 5 mTorr, using the mechanical pump only. The reactor, and the sample within, was heated by the heating coils when the experiments were conducted at ~200°C.

Atomic hydrogen or atomic deuterium were generated in a microwave discharge in the same manner as that used for GaAs. In this case, the microwave generator was operated at 40 W. The silicon wafer was then exposed to the atomic hydrogen for various periods of time (from a few seconds up to 15 minutes).

To avoid sample overheating from the recombination of H-atoms, the hydrogen atom concentration was kept low by diluting with argon and operating the microwave discharge at low powers. When lower atomic hydrogen concentrations were desired the molecular drag pump was

used in addition to the rotary pump. A higher vacuum (<10^{-5} Torr) was attained in this case, and 5 mTorr of H_2 in 50 mTorr of Ar were used.

2.7.6 Passivation of Si/SiO_2 by Molecular Hydrogen and Deuterium

Some of the Si/SiO2 samples were treated with H_2 or D_2, as used in the standard industrial H_2 annealing, before exposure to atomic H. The substrates were heated up to about 450°C under a flow of Ar (≈30 sccm) at atmospheric pressure, with the mechanical pump off. When the temperature reached the desired setting the Ar flow was shut off while H_2 (or D_2), at a pressure of 760 Torr (flow of about 30 sccm), was let in. The samples were kept under H_2 (or D_2) for 30 minutes, then the heating was stopped and they were cooled back to room temperature under Ar.

2.7.7 Vacuum Annealing of Si/SiO_2

We found that small amounts of hydrogen are always present during the thermal oxidation step. Therefore the Si/SiO_2 samples that had either been unintentionally exposed to hydrogenic impurities or that had been previously treated with H_2 were vacuum annealed at 700-730°C for 75 min. This process was performed in a small tubular Lindberg furnace (Type 167). The silicon wafers were placed into a quartz tube inside the furnace for thermal annealing. The quartz tube was pumped down using a turbo-molecular pump (Edwards EXT70, pumping speed of 52 liters/second nitrogen) backed by a rotary pump (Sargent-Welch Model No. 1402, pumping speed of 160 liters/minute). When the pressure reached 2-4x10^{-6} Torr, the Lindberg furnace was

heated up to the desired temperature. After the annealing period, the samples were cooled down to room temperature still under vacuum. The vacuum annealing was performed in order to drive away the hydrogen out of the silicon sample and and enable the study of the passivation kinetics of defects by H_2.

2.7.8 Passivation Kinetics of Si/SiO_2 by Molecular Hydrogen

Molecular hydrogen reactivity was studied at temperatures in the range of 100-300°C, in order to measure the passivation rate of interface defects (i.e. recombination centres) by H_2. The Si/SiO_2 samples were introduced in a heated quartz reactor and exposed to a flow of He (~20 sccm, 760 Torr) used as a blank (to make sure that no passivation occurred in the absence of H_2) for periods of time ranging between 30 min to 2-3 hours. Then the He flow was shut off while H_2 at a pressure of 760 Torr was let in. The substrates were kept under a small flow of hydrogen (~20 sccm) for up to 24 hours at the desired temperature. The RF-probe signal (i.e. carrier density), as well as the temperature were monitored continuously during this entire period.

2.7.9 Titration of Oxygen Atoms

The technique, which we used for oxygen atom detection, involves the "titration" of oxygen atoms with nitrogen dioxide:

$$O + NO_2 \rightarrow NO + O_2 \qquad [2.3]$$

This reaction is very rapid so that no NO_2 remains downstream when less than an equivalent of NO_2 has been added to the stream of oxygen. When an excess of NO_2 has been added downstream, then:

$$[NO_2] = [NO_2]_0 - [O] \qquad [2.4]$$

where $[NO_2]_0$ is the nitrogen dioxide concentration in the absence of oxygen.

Reaction [2.3] is very fast; therefore O atoms are rapidly consumed by NO_2. It is difficult to monitor NO (mass=30) with the mass spectrometer since it is also the product of NO_2 dissociation. We therefore monitored NO_2 (mass=46).

Alternatively one can observe the titration endpoint with the following chemiluminescence reaction:

$$O + NO \rightarrow NO^* \rightarrow NO_2 + h\nu \qquad [2.5]$$

Reaction [2.5] is very slow and its greenish chemiluminescence can be seen in the dark. Therefore, the end point of the titration can be taken by choosing from two possibilities. The first case is the point at which the light intensity reaches its maximum, i.e. the concentrations of O and NO are equal and half the O atoms have been titrated by NO_2. In the second case we can observe the extinction of light because all the O-atoms have been removed by reaction [2.5], i.e. the concentration of the O atoms equals the NO_2 concentration.

We used a combination of both the above techniques to determine the NO_2. We introduced 0.600 Torr of oxygen in the reactor. At the maximum emission end point (i.e. when the NO_2 is first detected by the MS), we noted the pressure of NO_2 introduced in the system (0.024 Torr). This indicated that the pressure of oxygen atoms was 0.048 Torr. By taking the

ratio of the two pressures (0.048/0.600) and assuming an ideal behaviour for O and NO_2, we determined that 4% of the O_2 was dissociated at room temperature.

2.7.10 Titration of Hydrogen Atoms

Hydrogen atoms also react with nitrogen dioxide:

$$H + NO_2 \rightarrow NO + HO \qquad [2.6]$$

Reaction [2.6] is not followed by a chemiluminescence reaction so we had to monitor the disappearance of NO_2 by using the mass spectrometer. For a pressure of 0.600 Torr of H_2, we measured a pressure of 0.030 Torr of NO_2 consumed in reaction [2.6]. Therefore, by following the same reasoning as in the case of O atom titration, a 2.5% dissociation of H_2 occurred at room temperature.

3. RESULTS AND DISCUSSION (I): Interaction of Atomic Hydrogen with the GaAs Surface

3.1 Interaction of Hydrogen Atoms with (100) GaAs Surfaces

The GaAs samples were exposed to atomic hydrogen or deuterium for various periods of time (from a few seconds up to 2 minutes) at room temperature. Indistinguishable results were obtained with D-atoms, and therefore only the H-atom results are presented.

The changes in the 865 nm PLI of two GaAs samples (i.e. UBC samples from different MBE growth batches) exposed to hydrogen atoms are shown in the two graphs of Figure 3.1. The PLI of both samples increased by about a factor of 3 when the discharge was turned on. When the discharge was shut off, the PLI increased even further. It reached a plateau that was up to 10 times higher than the initial PLI (for the first sample) and up to 100 times higher than the initial PLI (for the second sample). When the H-atoms were switched on again the PLI decreased to the level obtained by the initial increase. When the H-atoms were switched off again the PLI increased to the previous plateau level. This last process (i.e. decrease and increase of the PLI) could be repeated almost indefinitely as long as the exposures to H-atoms were kept short. Typical exposure times ranged between 30-60 s. The slight decrease in the PLI (last plateau in both graphs on the R.H.S. of Figure 3.1) is due to a longer H-atom exposure. The preferential removal of As from the surface and the resulting Ga rich layer could account for the observed decrease in the PLI. If Ga is in its metallic form, it could be a very effective carrier recombination catalyst. The initial process, in which the PLI increased when the H-atoms were switched on, could be observed again if the GaAs samples were re-etched in HF.

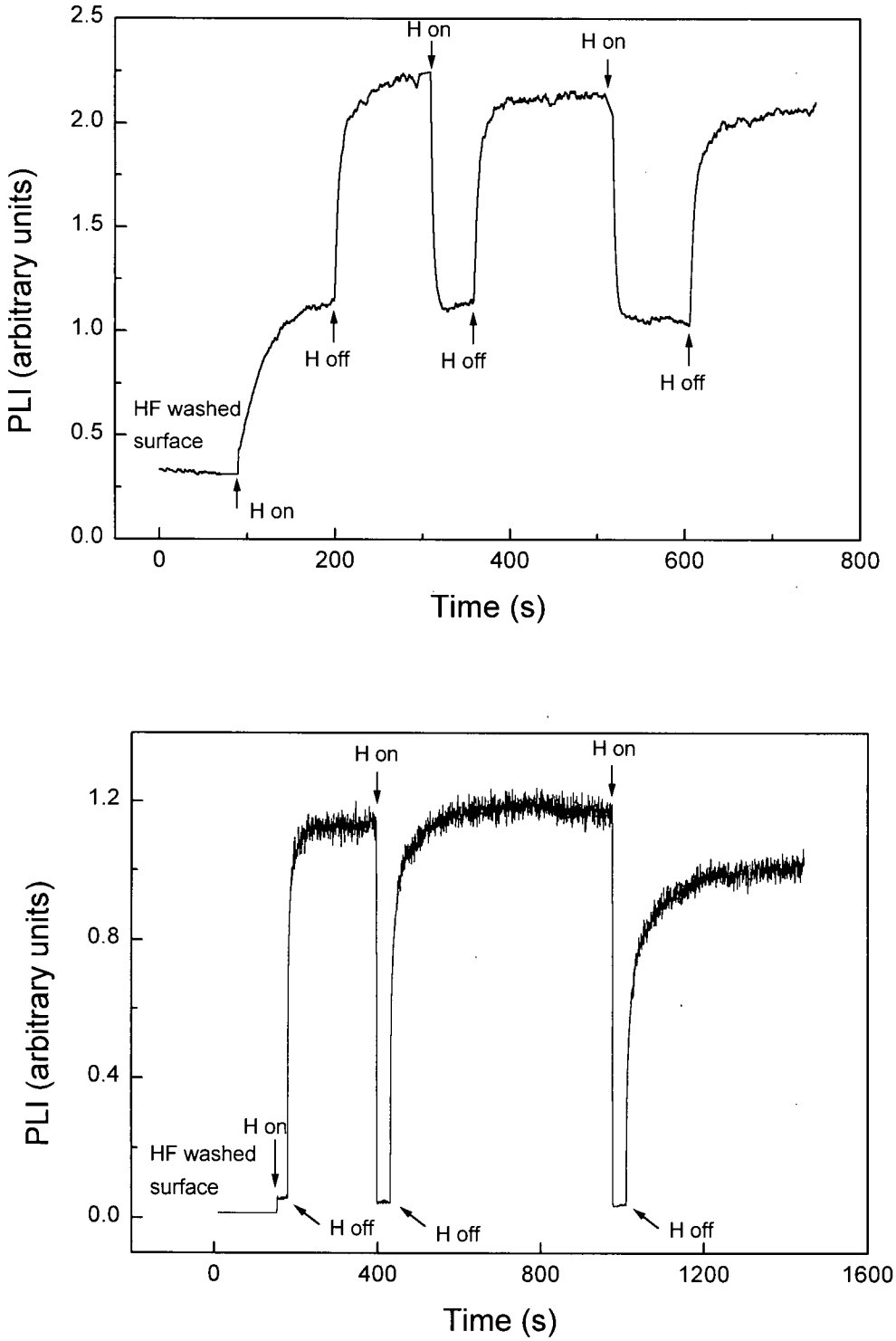

Figure 3.1 Plot of the PLI as a function of time showing the effect of H-atom exposures on (100) GaAs surfaces (two different samples) at room temperature.

Changes in the surface recombination centre (R_c) density (i.e. the inverse of the 865 nm PLI signal), of the two GaAs samples exposed to hydrogen atoms are shown in Figure 3.2. These plots were used for the kinetic analysis. We call the initial decrease in recombination centre density, $[R_c]$, the irreversible process. The further decrease followed by an increase in $[R_c]$, when the H-atoms are switched on and off, is termed a reversible process. We will now take a separate look at the irreversible and reversible processes observed for the first sample in Figures 3.1 and 3.2.

Figure 3.3 illustrates the semi-logarithmic plot of the normalized, relative recombination centre density as a function of time for the irreversible process. This plot is a reasonably straight line, as can be seen from the solid line obtained by least-squares fitting of the data points. A simple exponential decay fits the $[R_c]$ versus time curve for the irreversible process in GaAs. The software program performed the fitting according to the following equation:

$$[R_c] = b + a_1 e^{-t/\tau} \qquad [3.1]$$

where $[R_c]$ is the recombination centre density, b is a baseline correction representing the recombination centre density at infinite reaction time, a_1 is a normalization constant, and τ represents the recombination centre lifetime. Therefore this process follows a first order kinetic rate law. This initial removal of recombination centres could be due to (i) increased termination of dangling bonds by H-atoms, (ii) surface reconstruction, (iii) the etching away of surface oxides, and/or removal of As[104].

The reversible disappearance of recombination sites seen after GaAs has been repeatedly exposed to H-atoms cannot be described by a single exponential decay. Figure 3.4, where the logarithm of the relative recombination centre density is plotted as a function of time, illustrates

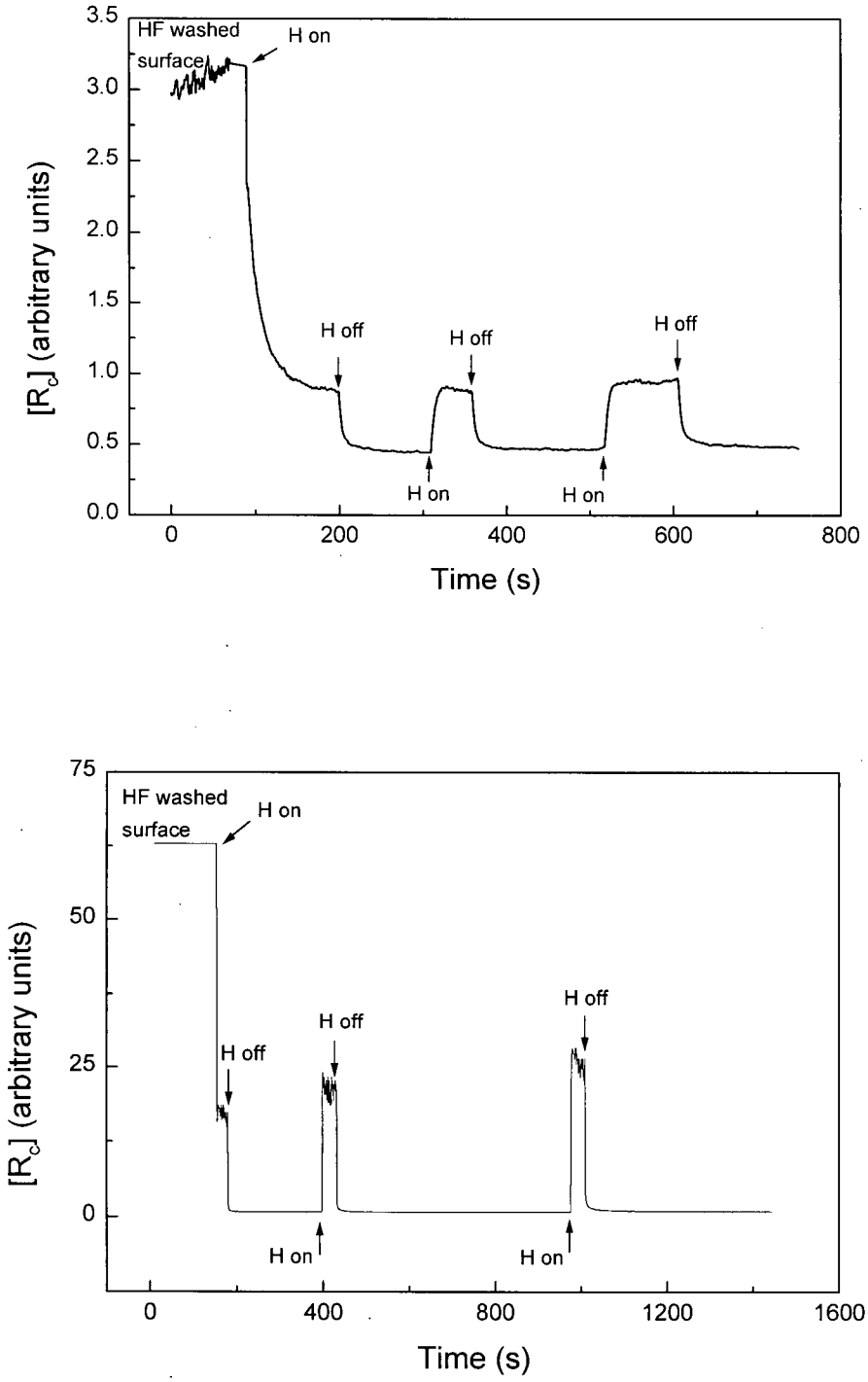

Figure 3.2 Plot of the recombination centre density as a function of time showing the effect of H-atom exposures on (100) GaAs surfaces (two different UBC samples) at room temperature.

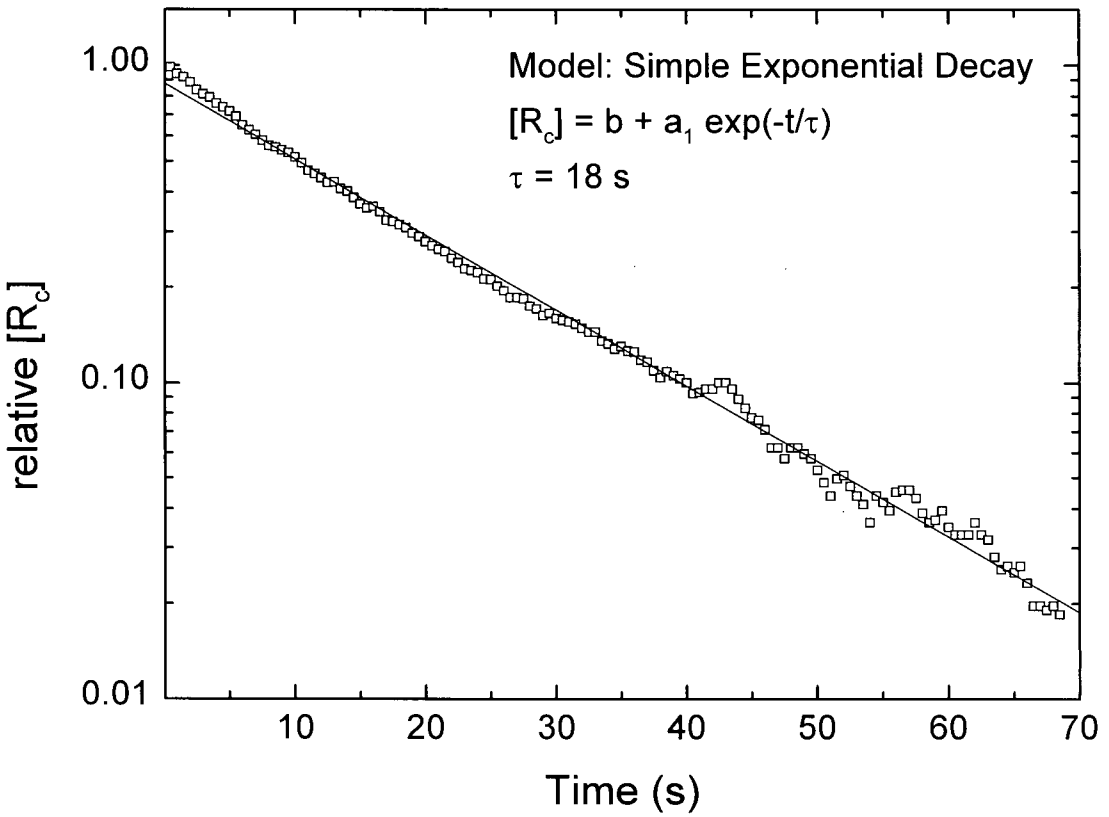

Figure 3.3 Effect of atomic H on a (100) GaAs surface at room temperature. This effect was observed after exposure of a freshly washed surface to H-atoms and it represents the irreversible process. The solid line represents the least-squares fitting line for a simple exponential process.

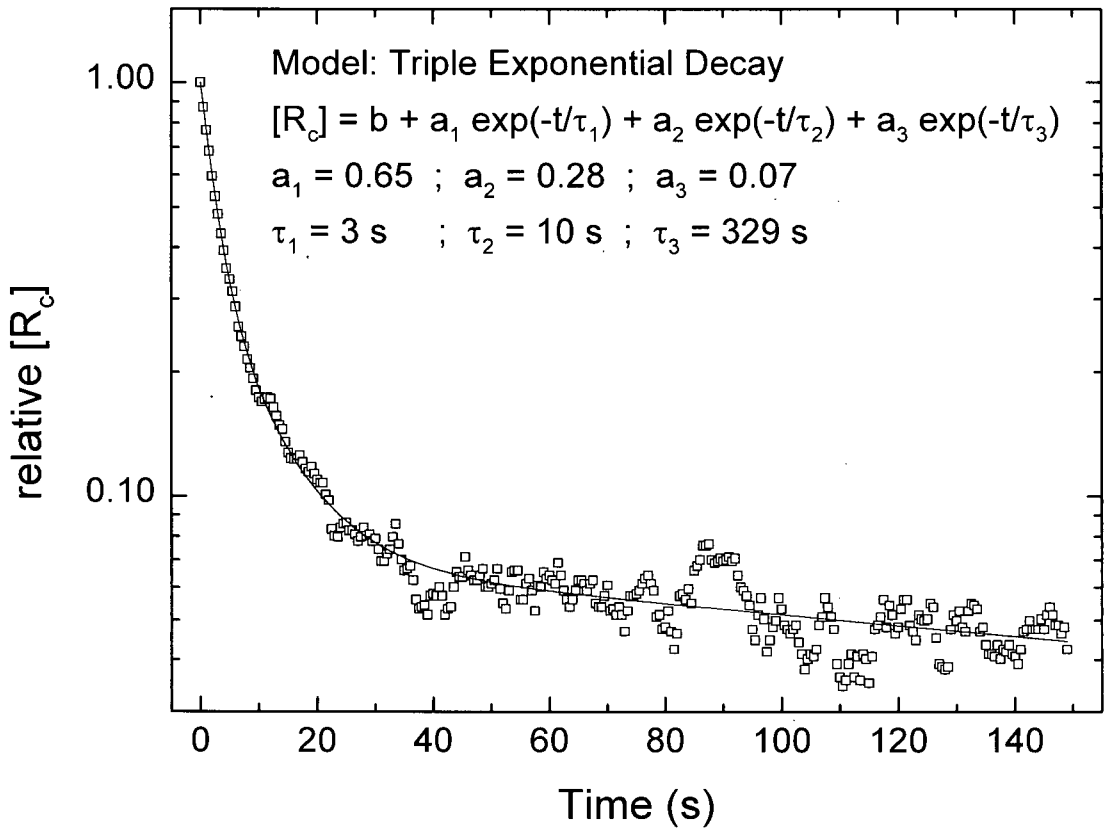

Figure 3.4 Effect of atomic H on a (100) GaAs surface at room temperature. This effect was observed after repeated H-atom exposures and it represents the reversible process. The solid line is the triple exponential decay best fit.[a]

[a] The fitting curve was obtained by using the Microcal Origin program. Note that at long times, the lifetimes (especially τ_3) are more affected by drift, therefore the value is not very significant.

the non-exponential decay of the process. However, this process can be fitted quite well with a triple exponential in the form:

$$[R_c] = b + a_1 e^{-t/\tau_1} + a_2 e^{-t/\tau_2} + a_3 e^{-t/\tau_3} \qquad [3.2]$$

where $[R_c]$ and b have the same significance as in the previous equation, the normalization constants a_1, a_2, a_3 represent the relative contributions of three different recombination centres, and τ_1, τ_2, τ_3 represent their lifetimes (i.e. the inverse of the rate constants) governing their individual decay rates. The solid curve shown in Figure 3.4 represents the triple exponential fitted curve, and suggests that there are at least three kinds of recombination centres with lifetimes ranging from a few seconds to a few minutes at room temperature.

There are a number of possible explanations for this disappearance of recombination sites when the H-atoms are shut off. Gottscho[94] initially proposed that this could be due to the accumulation of electrons on the surface because this phenomenon was observed in a plasma. However, since the phenomenon is also observed downstream from the plasma, Gottscho later interpreted the phenomenon as a physical adsorption of H-atoms, which serve as recombination centres. If these readily desorb, then the decay, which is observed when the H-atom source is removed, could be explained.

Ogryzlo *et al.*[105] suggested an alternative explanation in terms of surface reconstruction. They proposed that the presence of gaseous H-atoms could destroy the stable (2x1) surface structure that eliminates a large fraction of the dangling bonds. When the atoms are no longer attacking the surface, the (2x1) structure with its reduced dangling bonds could re-form.

As described in the following chapter we have been able to observe a very similar behaviour at the Si/SiO_2 interface. Since surface reconstruction is not a possible explanation

there, we conclude that the phenomenon is most probably due to H-atoms (recombination centres) absorbed near the surface or interface in both GaAs and Si.

3.2 Effect of the Microwave Generator Power on a (100) GaAs Surface

The effect of the microwave generator power on GaAs Samples was also studied. For this purpose, the upstream microwave discharge used to obtain H-atoms was operated at different power levels.

The plot of the recombination centre density for a (100) GaAs surface (EG&G sample) exposed to H-atoms obtained in a 75 and 50 W upstream plasma is illustrated in Figure 3.5. The $[R_c]$ increased by almost 2 orders of magnitude when a hydrogen-passivated surface was exposed to H-atoms obtained by using a microwave power of 75 W. When the H-atoms were switched off the $[R_c]$ decreased to the original level. Afterwards, the sample was exposed to H-atoms obtained by using a microwave power of 50 W. This produced an increase in the $[R_c]$ of only about a factor of 25 (i.e. ~3 times less than the previous increase). When the H-atoms were shut off, the $[R_c]$ decreased to the original level again. We already know that the H-atoms create temporary recombination sites in the GaAs samples. It is therefore clear that operating the discharge at a higher power level produces a much larger number of H-atoms, which in turn create more traps in GaAs. This effect is linear, since a 30% decrease in the power level produced a decrease of about 30% in the recombination centre density.

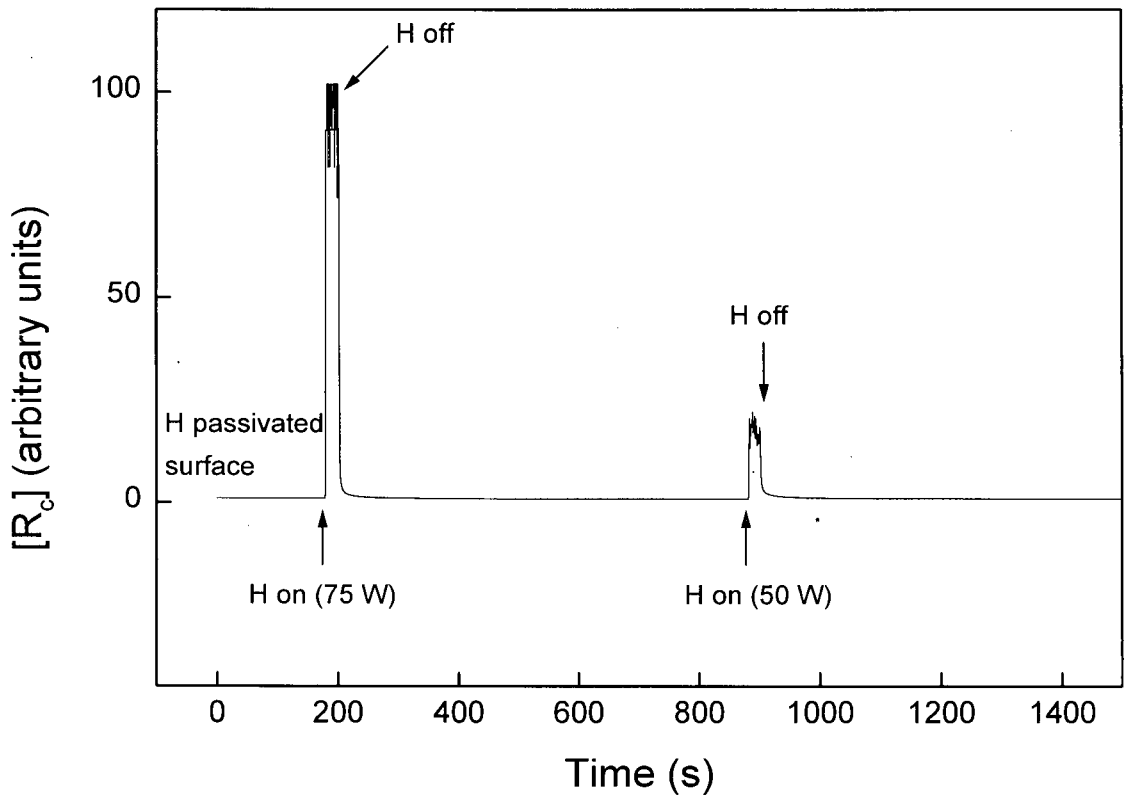

Figure 3.5 Effect of microwave generator power on a (100) GaAs surface exposed to atomic H at room temperature.

3.3 Interaction of Sulphur Atoms with (100) GaAs Surfaces

Sulphur atoms were produced *in situ* at 80°C with the two step rapid reaction of hydrogen sulphide with atomic hydrogen, yielding one S-atom for two H-atoms consumed. The treatment of GaAs surfaces with sulphur atoms produced only a small increase in the PLI, but with a much greater stability in air.

Figure 3.6 illustrates the behaviour of a GaAs sample that had been previously passivated by atomic hydrogen, and that was further exposed to H-atoms. This exposure produced an increase in $[R_c]$ by less than a factor of 2. When the H_2S gas was let in to "titrate" the H-atoms and form S-atoms, a sudden decrease in the $[R_c]$ was observed. This was followed by a slow increase in $[R_c]$ approximately to the passivation level obtained by H-atoms. When the discharge was switched off, the recombination centre density decreased by less than a factor of 2 compared to the H-atom passivated surface. Sulphur condensation on the reactor walls led to a very slight increase in the $[R_c]$ of the S passivated surface.

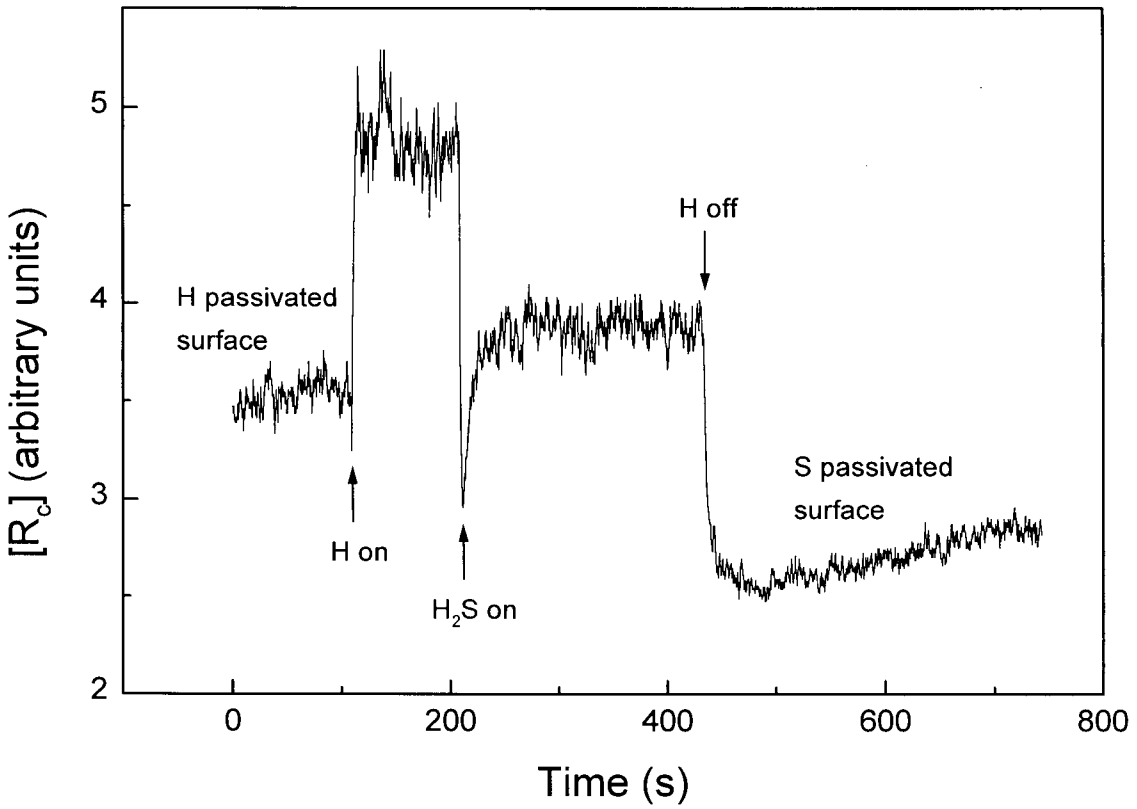

Figure 3.6 Plot of the recombination centre density as function of time, showing the effect of S-atoms exposure on a (100) GaAs surface at 80°C.

4. RESULTS AND DISCUSSION (II): Interaction of Atomic Hydrogen with the Si/SiO_2 Interface

4.1 Intrinsic (100) Si/SiO_2 Interfaces

A 20 Å layer of SiO_2 was grown at 200°C on intrinsic silicon (i-Si) by exposing a clean, HF washed surface to atomic oxygen, as described in the experimental chapter. Because silicon luminescence is extremely weak, its PLI could not be used. We therefore measured the changing surface carrier recombination sites by continuously monitoring the laser induced (633 nm HeNe laser) conductivity of an SiO_2 covered Si wafer with an RF-probe (see page 56 in the experimental chapter) during the exposure to H or D-atoms. The RF-probe signal measures the steady state carrier concentration that is inversely proportional to the concentration of interface states.

The Si/SiO_2 samples were exposed to atomic hydrogen or deuterium, for various periods of time (from a few seconds up to 2 minutes). Most of the Si/SiO_2 exposures to atomic hydrogen or deuterium were performed at high temperatures (at or above 200°C). As in the case of GaAs, indistinguishable results were obtained with D-atoms, and therefore only the H-atom results are presented.

The observed changes in the carrier density (i.e. the RF-probe signal) of an i-(100) Si/SiO_2 sample while it is being exposed to atomic hydrogen intermittently are illustrated in Figure 4.1. As in the case of GaAs (see previous chapter), when the discharge was first switched on the carrier density increased. The carrier density increased even further when the discharge

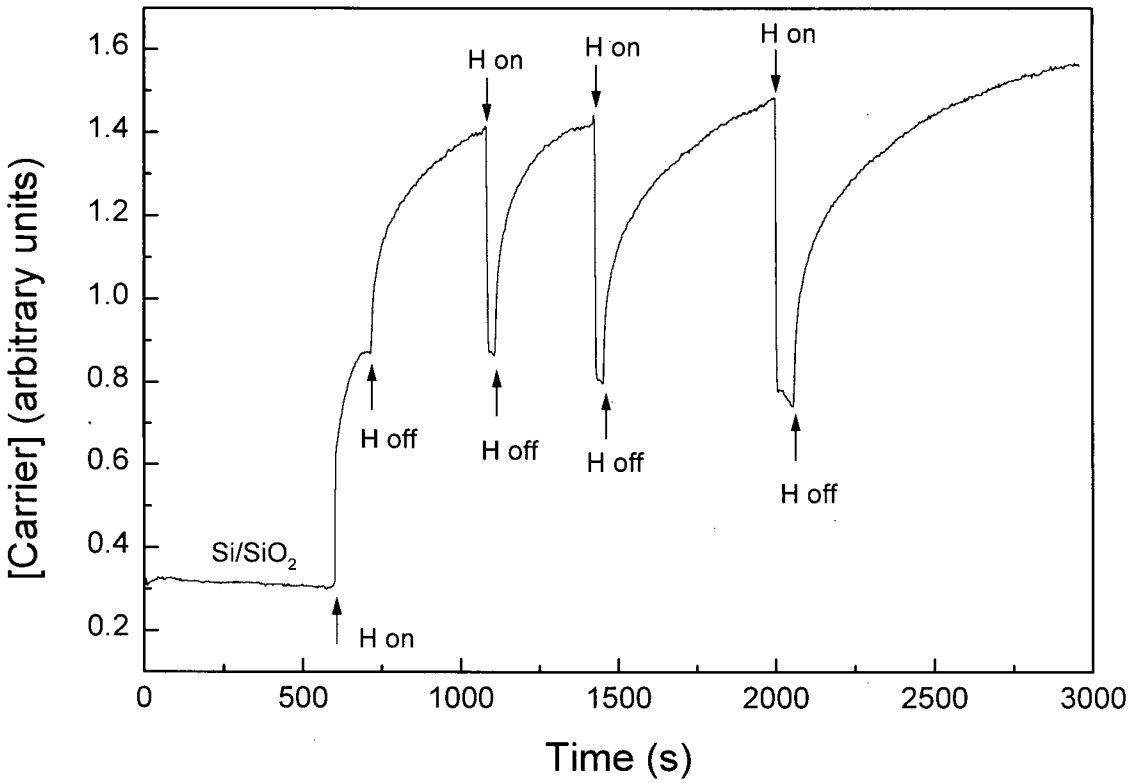

Figure 4.1 Plot of the carrier density (RF-probe signal) as a function of time. Effect H-atom exposures on an intrinsic (100) Si/SiO_2 interface at 200°C.

was shut off. When the H-atoms were switched on again, the carrier density decreased. This was followed by an increase in carrier density when the H-atoms were switched off. This last process could be repeated almost indefinitely as long as the exposure to H-atoms was kept short (typical exposure times ranged between 30-60 s). It will be recalled that we observed very similar phenomena in GaAs exposed to H-atoms.

As in the case of the GaAs measurements, in order to perform a kinetic analysis of the changing interfacial defect density, we must convert these plots to defect densities by taking the inverse of the carrier densities. Figure 4.2 illustrates these changes in the interface recombination centre density, $[R_c]$, as a function of time. This figure mirrors the changes observed in Figure 4.1. We see the initial fast drop in $[R_c]$ when the discharge was turned on, followed by a further decrease in $[R_c]$, when the discharge is turned off. As in the case of GaAs the first process is irreversible, and this is followed by a reversible process cycling between the two passivation levels.

4.1.1 The Irreversible Process

Figure 4.3 illustrates the irreversible processes for the intrinsic Si/SiO_2 interface. It can be seen that the beginning of this process is too fast for our detection system to follow. This initial drop (first 2 data points in Figure 4.3) represents a very large change in recombination centre density and appears to be about 85% of the total $[R_c]$. It seems quite likely that this change in $[R_c]$ could be due to the initial passivation of interfacial defects, which we refer to as R_c (P_b centres, which account for a fraction of the total number of defects[106], and other defects), by atomic hydrogen according to the reaction:

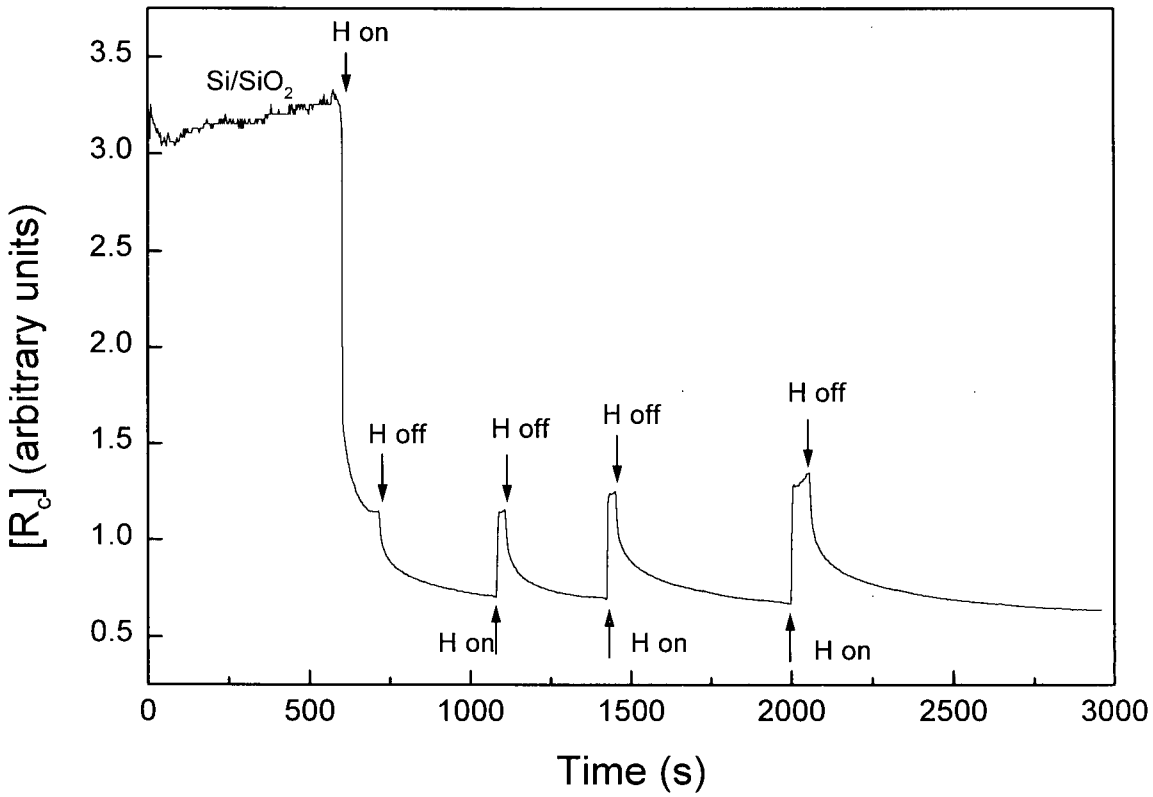

Figure 4.2 Plot of the recombination centre density as a function of time. Effect of H-atom exposures on an intrinsic (100) Si/SiO_2 interface at 200°C.

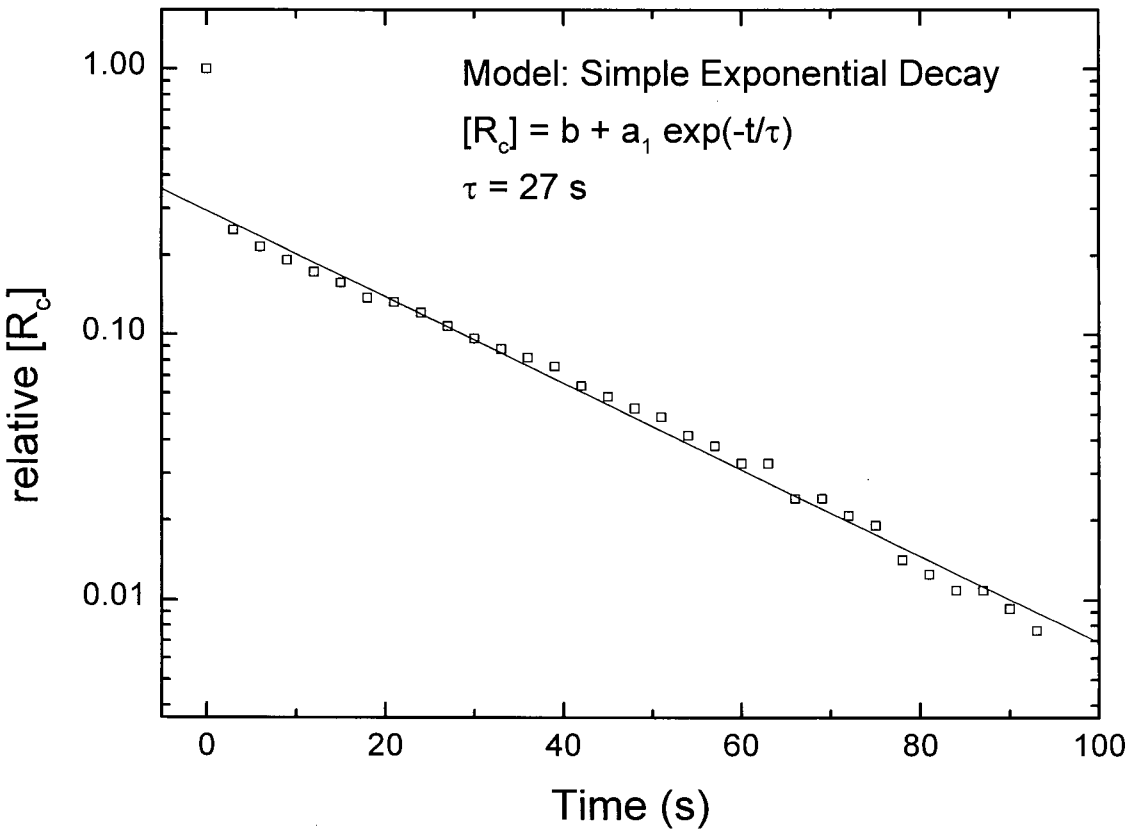

Figure 4.3 Plot of the relative recombination centre density as a function of time. Effect of H-atoms on an intrinsic (100) Si/SiO_2 interface, at 200°C. This effect was observed after exposure of a freshly washed surface to H-atoms and it represents the irreversible process. The solid line represents the least-squares fitting line for the simple exponential process.

$$R_c + H \rightarrow HR_c \qquad [4.1]$$

This process (a radical-radical reaction) would probably be very fast, occurring spontaneously with essentially no energy barrier.[57]

The much slower process that follows the initial drop in Figure 4.3, appears to obey an exponential rate law. As we can see, that portion of the curve in the semi-logarithmic plot is a straight line. Since the reactions of –Si≡ (P_b centres) or –OSi≡ (other possible recombination centres) with H-atoms would probably be too fast, the only likely reaction that could be slow enough is:

$$R_c + H_2 \rightarrow HR_c + H \qquad [4.2]$$

The recombination of H-atoms at the interface could be the source of the H_2 at the interface. For more details about this last process, i.e. reaction [4.2], see the next chapter.

A simple exponential decay fits the $[R_c]$ versus time curve. This was also true for the irreversible process in the H + GaAs reaction. The fitting done by Microcal Origin took the form

$$[R_c] = b + a_1 e^{-t/\tau} \qquad [4.3]$$

where $[R_c]$ is the recombination centre density, b is a baseline correction representing the recombination centre density at infinite reaction time, a_1 is a normalization constant, and τ represents the recombination centre lifetime (τ = 27 s at 200°C).

In the case of GaAs the initial improvement of the passivation level was attributed to the removal of As_2O_3 or to surface reconstruction. However, at the Si/SiO_2 interface such processes are not possible, so we must seek another explanation. As the kinetic analysis has shown, the

irreversible process for Si could involve the passivation of dangling bonds at the interface by both H and H_2.[50]

4.1.2 The Reversible Process

As in the reversible process which was observed for GaAs, the Si/SiO_2 interfacial recombination centre creation by H-atoms is too fast to be followed by our instrumentation. However, the disappearance of these sites, when the H-atoms were shut off, can be subjected to a kinetic analysis. Again we found that a single exponential could not describe this part of the reversible process. Figure 4.4, where the normalized recombination centre density is plotted as a function of time, illustrates the non-exponential decay of the process. However, this process can be fitted quite well with a triple exponential in the form:

$$[R_c] = b + a_1 e^{-t/\tau_1} + a_2 e^{-t/\tau_2} + a_3 e^{-t/\tau_3} \qquad [4.4]$$

where $[R_c]$ and b have the same significance as in equation [4.3], the normalization constants a_1, a_2, a_3 represent the contributions of each kind of recombination centre, while τ_1, τ_2, and τ_3 represent the recombination centre lifetimes (i.e. the inverse of the pseudo first order rate constants) governing their individual decay rates. The solid curve shown in Figure 4.4 represents the triple exponential fitted curve, and suggests that there are at least three kinds of recombination centres with lifetimes ranging from a few seconds (τ_1 = 6 s) to a few minutes (τ_3 = 400s) at 200°C.

In the case of GaAs we could not conduct our kinetic analysis any further, due to instrumental constraints. These include the difficulty of obtaining data either at low temperatures (no equipment to measure the PLI at low temperatures) or at high temperatures (where the PLI is

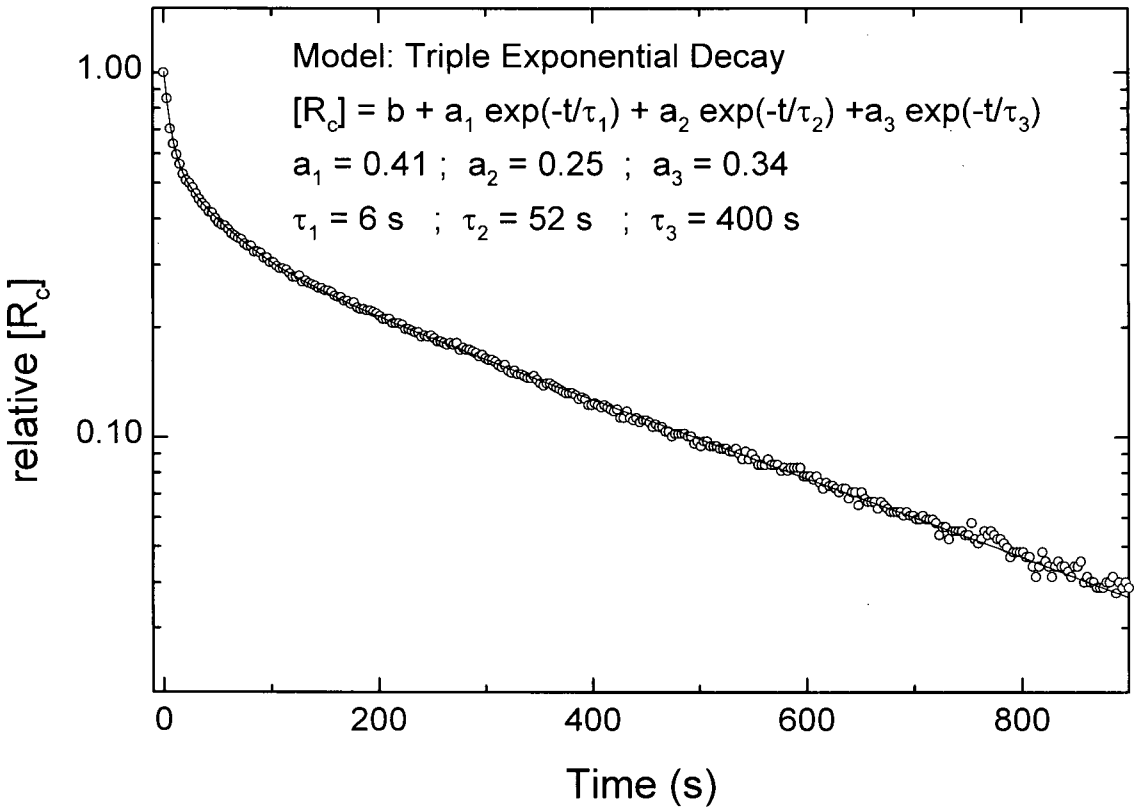

Figure 4.4 Plot of the relative recombination centre density as a function of time. Effect of H-atoms on an intrinsic (100) Si/SiO_2 interface, at 200°C. This effect was observed after repeated H-atom exposures and it represents the reversible process. The solid line is the triple exponential decay best fit.

very weak). However, in the case of Si, due to the fact that we are not measuring the PLI, we were not constrained to conduct our experiments at room temperature. In fact, the RF-probe signal, which essentially measures the sample photoconductivity, was higher as the temperature was raised.

Figure 4.5 illustrates the effect of atomic hydrogen on the relative recombination centre density of an i-(100) Si/SiO_2 interface, monitored as a function of time at 6 different temperatures. This effect was observed when the H-atoms were shut off after a long exposure (~10 minutes) to H-atoms at 23°, 83°C, 148°C, 173°C, 192°C, and 214°C. This data was collected by Zheng[107] for i-Si capped SiGe samples. However, the data manipulation (as described earlier) was performed in this thesis.

It can be seen that at all 6 temperatures, the removal of atomic hydrogen produced a decrease in the carrier recombination centre density. At room temperature, beside the fact that the signal was very noisy, there was very little decrease in the recombination centre density. However, as the temperature was raised, there was an increasing rate of decay of the recombination centre density when the H-atoms were switched off.

Since the plot in Figure 4.5 is on a logarithmic scale, it is clear, as we have seen previously (Figure 4.4), that these processes do not obey first order kinetics. We will again analyze the recombination centre removal process by a multiple-exponential decay. Table 4.1 lists the parameters (lifetimes, τ, and the rate constants, k) obtained by fitting all the curves in Figure 4.5 using a triple-exponential decay model described by equation [4.4]. The dashed lines in Figure 4.5 represent the "best fit" curves.

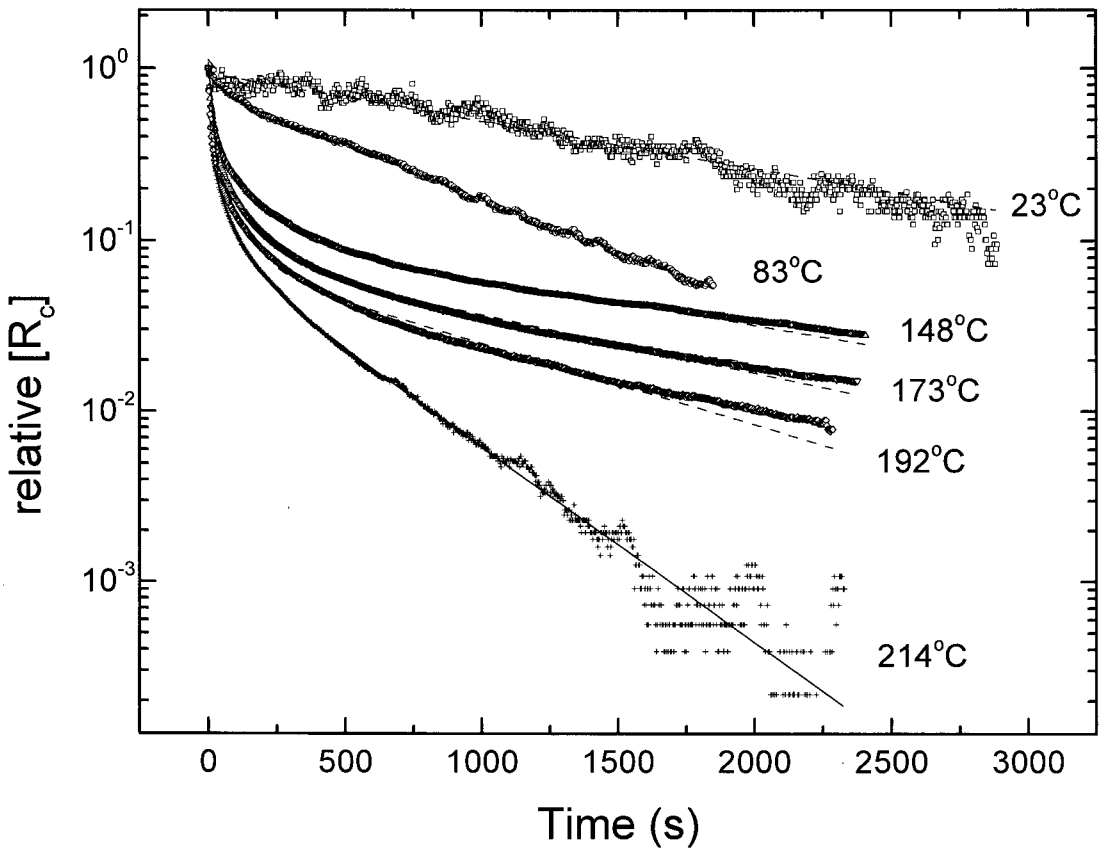

Figure 4.5 Plot of the relative recombination centre density as a function of time for an intrinsic (100) Si/SiO_2 interface at 23°, 83°C, 148°C, 173°C, 192°C, and 214°C. This effect was observed after long H-atom exposures and it represents the disappearance of recombination centres. The dashed lines represent the best fit obtained from a triple-exponential decay function.

Table 4.1 Lifetimes (τ_1, τ_2, τ_3) and rate constants (k_1, k_2, k_3) at different temperatures, when the H-atoms were shut off. These parameters[a] were obtained by fitting the data representing the H-atom interaction with an intrinsic (100) Si/SiO_2 interface.

T (°C)	τ_1 (s)	τ_2 (s)	τ_3 (s)	k_1 (s^{-1})	k_2 (s^{-1})	k_3 (s^{-1})
23	15[b]	3[b]	1580	$6.74x10^{-2}$	$3.64\ x10^{-1}$	$6.33x10^{-4}$
83	14	59	716	$7.23x10^{-2}$	$1.69x10^{-2}$	$1.40x10^{-3}$
148	10	115	1587	$1.03x10^{-1}$	$8.70x10^{-3}$	$6.30x10^{-4}$
173	11	111	1289	$9.29x10^{-2}$	$8.99x10^{-3}$	$7.76x10^{-4}$
192	6	86	917	$1.59x10^{-1}$	$1.17x10^{-2}$	$1.09x10^{-3}$
214	8	71	379	$1.26x10^{-1}$	$1.42x10^{-2}$	$2.64x10^{-3}$

[a] The values for the lifetimes were obtained directly from the fitting program (Microcal Origin)using equation [4.4] while the k's are calculated values.

[b] Note that the uncertainties for these two lifetimes at room temperature is huge, therefore the values are not very significant.

The activation energy can be calculated from the slope of the straight line of the Arrhenius type of plot:

$$k = Ae^{-E_a/k_BT} \qquad [4.5]$$

where k is the rate constant, A is the pre-exponential factor, E_a is the activation energy, k_B is the Boltzmann constant, and T is the absolute temperature.

Figure 4.6 illustrates the plot of the 3 rate constants from Table 4.1, as a function of inverse temperature. This figure shows clearly that the rate constants are quite scattered, especially k_2. Although the triple exponential decay model gives quite a good fit for the data, there is no discernible trend in the rate constants, and therefore the data does not yield any reliable activation energies.

4.2 Multiple-Trapping Model of Dispersive Transport

An alternative to the triple exponential decay model is the multiple-trapping model of dispersive transport well known in work on amorphous Si.[108,109] In this model electrons in localized sites must first be thermally excited above the mobility edge before they can move to other sites. We will give a short overview of this theory, and then show how it could be applied to our experiments.

In photoconductivity (time-of-flight) experiments, electrons are injected into the conduction band by a short flash of light. In a very short time (~ 1 ps), the electrons drop down to the bottom of the conduction band, where they are captured by the localized states of the band tail. It is assumed that each localized state has the same probability of capturing an electron.

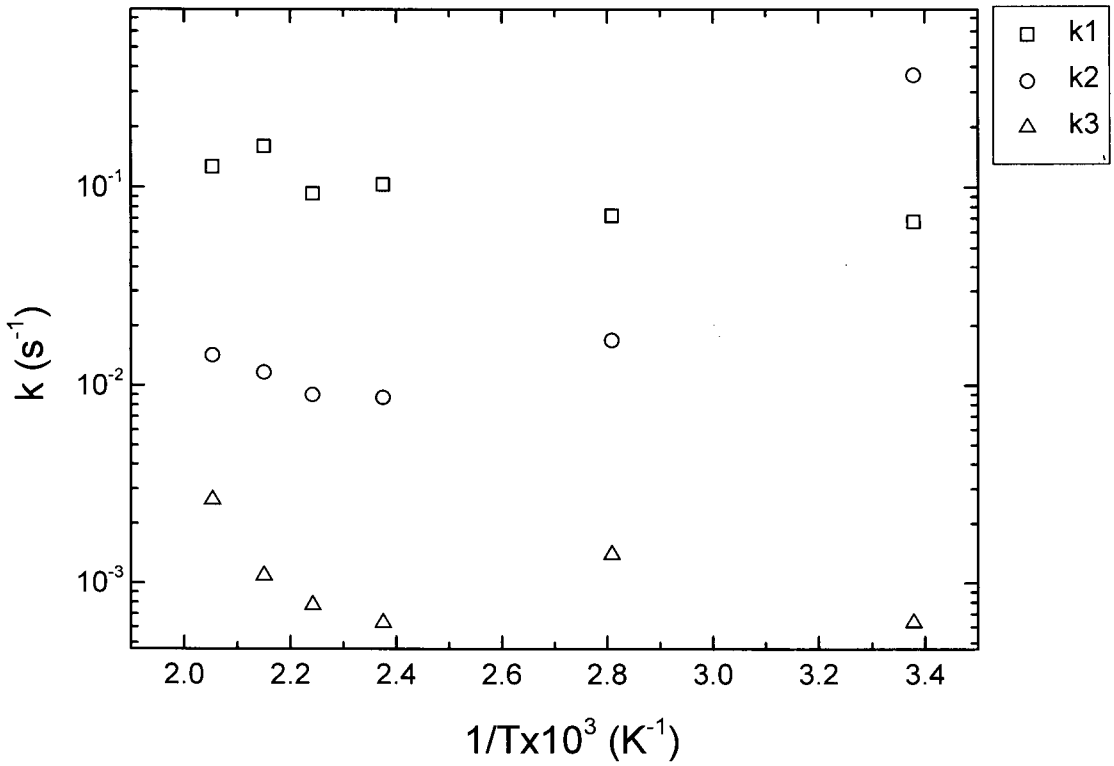

Figure 4.6 Arrhenius plot of the recombination centre decay rate constants for a triple exponential decay process, when the H-atoms were turned off.. Effect of atomic hydrogen on an intrinsic (100) Si/SiO_2 interface at 23°, 83°C, 148°C, 173°C, 192°C, and 214°C.

The following convention was adopted: the zero energy is at the mobility edge, and the positive energy points towards mid gap. The density of states, N(E), decreases exponentially from the zero energy level with the form:

$$N(E) = N_0 \, e^{-E/k_B T_c} \qquad [4.6]$$

where N_0 is the initial DOS, E is the energy, k_B is the Boltzmann constant, and T_c is a characteristic temperature ($k_B T_c$ is the characteristic width of the conduction band tail).

At some time ν^{-1} later, where ν, the attempt frequency, is of the order of a phonon frequency, the electrons in the shallow localized states are re-excited back into the band states above the mobility edge. The electrons that happened to fall into deep states (for which $E > k_B T$) must stay there for an exponentially longer time, of the order of τ:

$$\tau = \nu^{-1} e^{E/k_B T} \qquad [4.7]$$

before the probability of thermal emission is significant. The result is that the electrons tend to accumulate in the deep states.

In order to quantify this physical process some assumptions have been made. At some time t, all the deep states for which $E > E^*$, accumulate electrons without re-emitting them, since the mean time for thermal emission τ is much longer than t. E^* is given by:

$$E^* = k_B T \ln \nu t \qquad [4.8]$$

This shows that the distribution of the electrons in these states mirrors the DOS distribution as illustrated in Figure 4.7. The electrons in the shallow states for which $E<E^*$ have a Boltzmann distribution, $N(E) \, e^{E/k_B T}$.

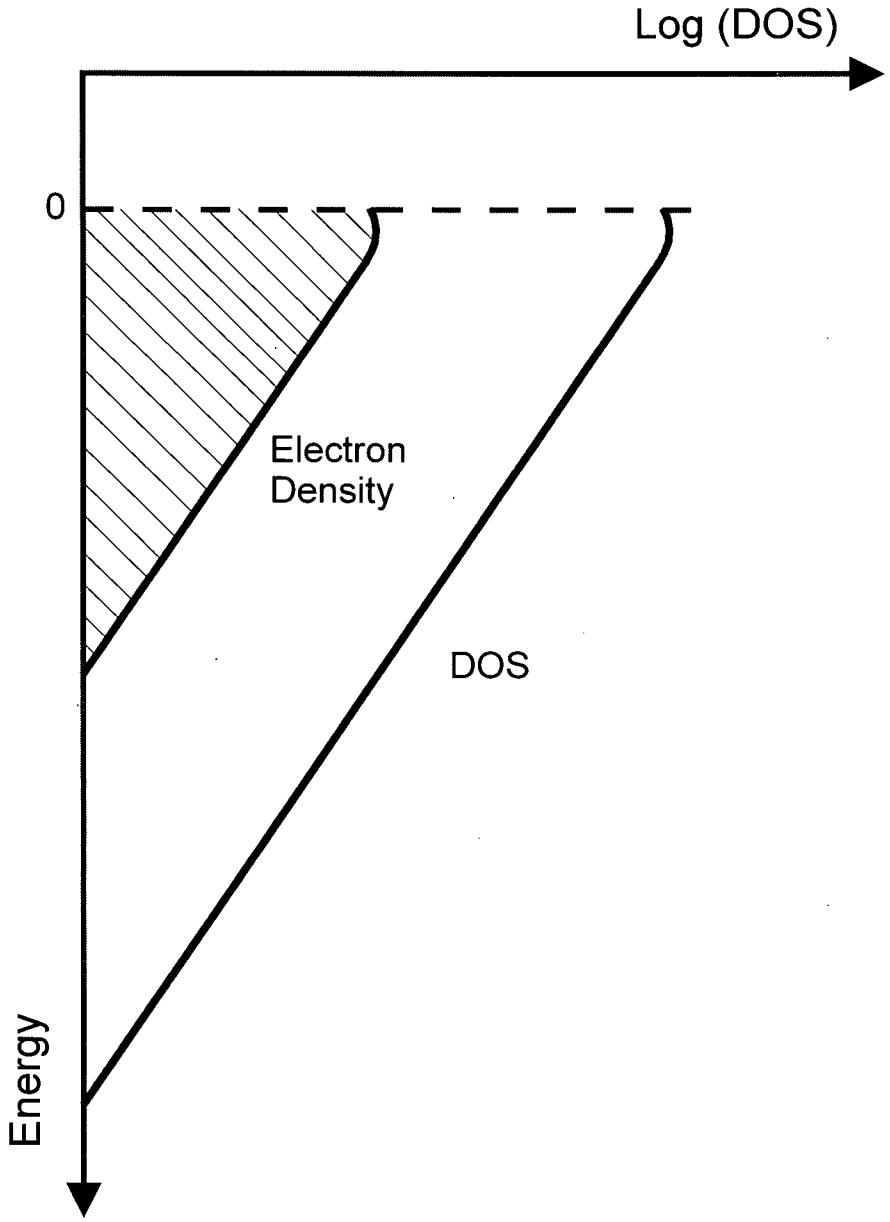

Figure 4.7 Distribution of trapped electrons (dashed area) and density of states (DOS), immediately after the photo-injected electrons have thermally excited to the bottom of the conduction band.

Experimentally this means that a power law governs the behaviour of the photocurrent as a function of time. If we try to apply this physical process to our own experiments in which H-atoms rather than electrons are being trapped, we will have to bear in mind that we are looking at very long times ($t >> 0$), where any escaping H-atom is lost at the boundary. Therefore, there is no re-trapping of H-atoms below E*. The total population of the states in our process is given by:

$$[R_c] = N_c \, e^{-E^*/k_B T_c} \qquad [4.9]$$

where $[R_c]$ is the hydrogen recombination centre (site) density equal to the DOS at time t, and N_c is an effective DOS. By substituting equation [4.8] in [4.9] we obtain the following equations:

$$[R_c] = N_c \, e^{-\frac{T}{T_c} \ln \nu t} \qquad [4.10]$$

$$[R_c] = N_c \, (\nu t)^{-T/T_c} \qquad [4.11]$$

$$[R_c] = N_c \, (\nu t)^{-\alpha} \qquad [4.12]$$

$$\alpha = \frac{T}{T_c} \qquad [4.13]$$

This yields the following expression for R_c:

$$[R_c] = c \, t^{-\alpha} \qquad [4.14]$$

where c is a constant, and α ($0<\alpha<1$) is a parameter which is determined by the disorder in the material.

Thus, a power law applies to the trapped H-atoms that are recombination centres at (or near) the surface or interface. In other words, H-atoms are assumed to be trapped in sites with dissociation energies that are distributed exponentially below the dissociation limit. However, as illustrated by the non-linearity of the plot in Figure 4.8 such a power law provides a somewhat unsatisfying fit for our data. In Figure 4.9, which illustrates the data from Figure 4.5, the fit is somewhat better, however, in no case is the plot linear, as predicted by the theory.

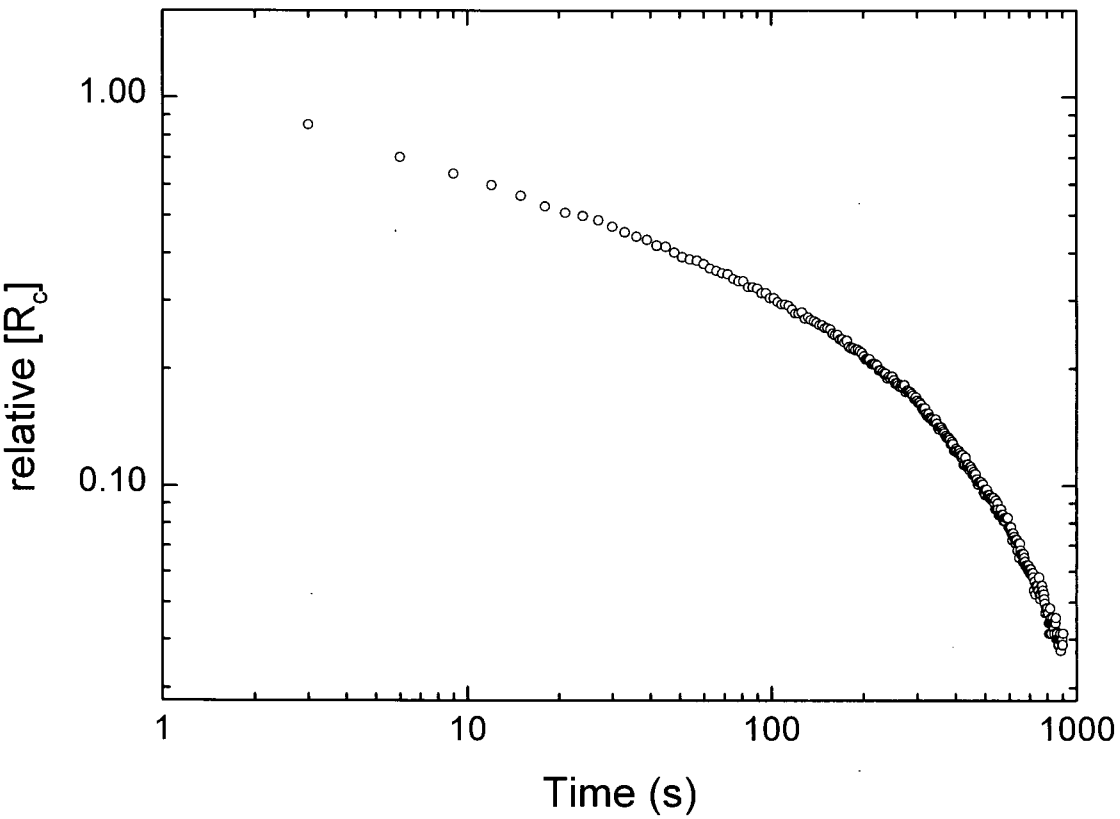

Figure 4.8 Power law plot of the relative recombination centre density as a function of time for an intrinsic (100) Si/SiO_2 interface, when the H-atoms were shut off and at 200°C.

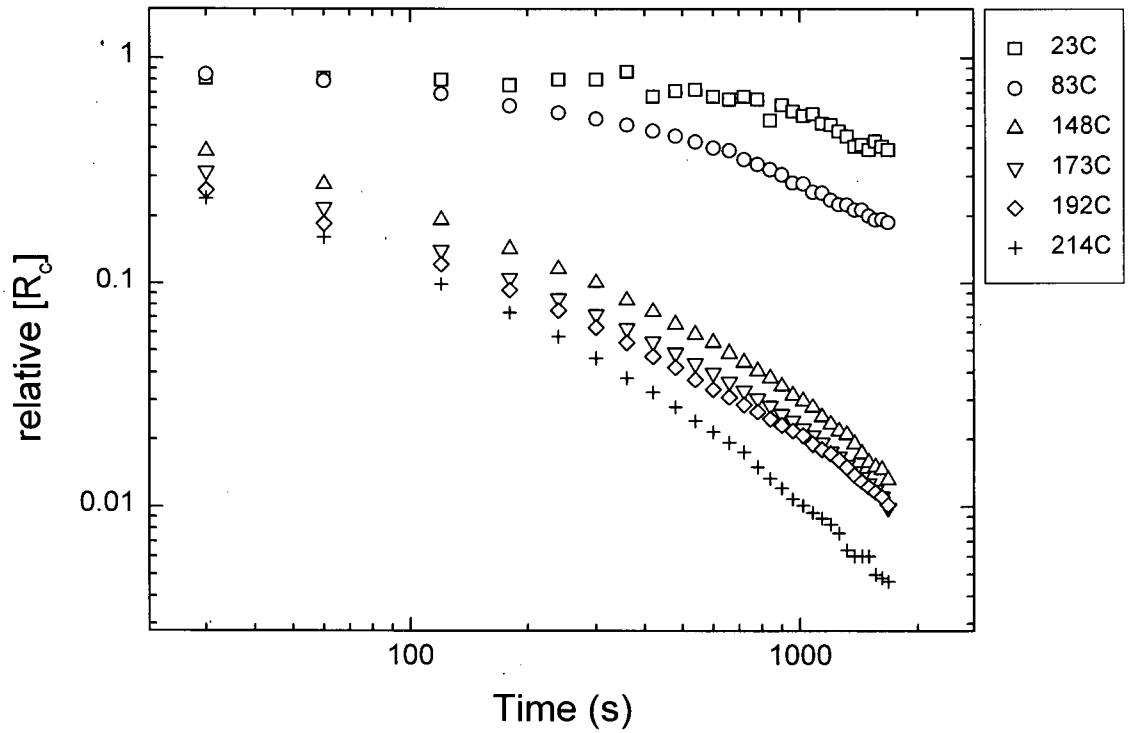

Figure 4.9 Power law plot of the relative recombination centre density as a function of time for an intrinsic (100) Si/SiO_2 interface, when the H-atoms were shut off and at 6 different temperatures.

4.3 Gaussian Distribution of Activation Energies Model

Since both the relatively simple triple-exponential decay model and the multiple trapping model provided unsatisfactory fits to our data, we tried to find a more complex model that might fit all our data more consistently. The Gaussian distribution of activation energies described by Stesmans[61] for the reaction of molecular hydrogen with P_b centres appeared to be one possibility.

For the kinetic analysis of our decay of recombination centres when H-atoms were shut off, we have assumed, as did Stesmans, that the activation energy for the process has a Gaussian distribution around a mean value E_a^o, with a spread σ:

$$\frac{[R_c]}{[R_c]_0} = \frac{1}{\sigma\sqrt{2\pi}} \int_{-\infty}^{\infty} e^{-(E_a - E_a^o)^2/2\sigma^2} \; e^{-t\,A\exp(-E_a/k_B T)} \; dE_a \qquad [4.15]$$

where $[R_c]$ is the recombination centre density, $[R_c]_0$ is the initial recombination centre density, E_a is the activation energy, A is the pre-exponential factor, t is the reaction time, k_B is the Boltzmann constant, and T is the absolute temperature.

A Gaussian distribution of activation energies, such as the one described by equation [4.15], produces a non-exponential rate process resulting from a distribution of rate constants centred around some average value at each temperature. In order to obtain the parameters E_a^o, σ, and A from equation [4.15] the decay curves have to be fitted simultaneously at all the temperatures. Since this presented a problem for our software (Microcal Origin) we approximated the integral in equation [4.15] with a sum of nine rate constants. We chose a step of ½ σ and summed from -2σ to $+2\sigma$:

$$\frac{[R_c]}{[R_c]_0} \approx \left(\frac{1}{2}\sigma\right)\frac{1}{\sigma\sqrt{2\pi}} \sum_{j=-4}^{j=+4} e^{-j^2/8}\, e^{-t\,A\exp\{-(E_a^o+\frac{j}{2}\sigma)/k_BT\}} \qquad [4.16]$$

Figure 4.10 illustrates the semi-logarithmic plot of the relative recombination centres as a function of time at different temperatures when the H-atoms were switched off. In this case, not all the collected data points from Figure 4.5 were plotted. The same number of data points was plotted on each curve. With the exception of the second point (after the first 30 s), only the data points at 60 s intervals were chosen. This data manipulation was done for the following reason: the number of data points was too great for the Gaussian fitting to be handled by our software (Microcal Origin). Moreover, the fitting parameters of the curves containing all the data points were found to be in good agreement with the fitting parameters obtained with fewer data points. We were thus satisfied that we are not missing any important information by using this approximation.

Equation [4.16] was used to fit the recombination centre decay curves shown in Figure 4.10. The spread around the mean activation energy (σ) is determined by the curvature of the R_c decay curves shown in Figure 4.10.

The decay curves do not determine unique values for E_a^o and A, at any given temperature. The solid lines in Figure 4.10 represent the fit that is obtained with these parameters. An average rate constant, which corresponds to a "family" of E_a^o and A values, is determined as given by equation [4.16]. The six rate constants, calculated in this manner and obtained from experimental results at the six different temperatures, are listed in Table 4.2. It will be appreciated that each such rate constant is just the magnitude of the central rate constant in a distribution of values that are determined by a Gaussian distribution of activation energies.

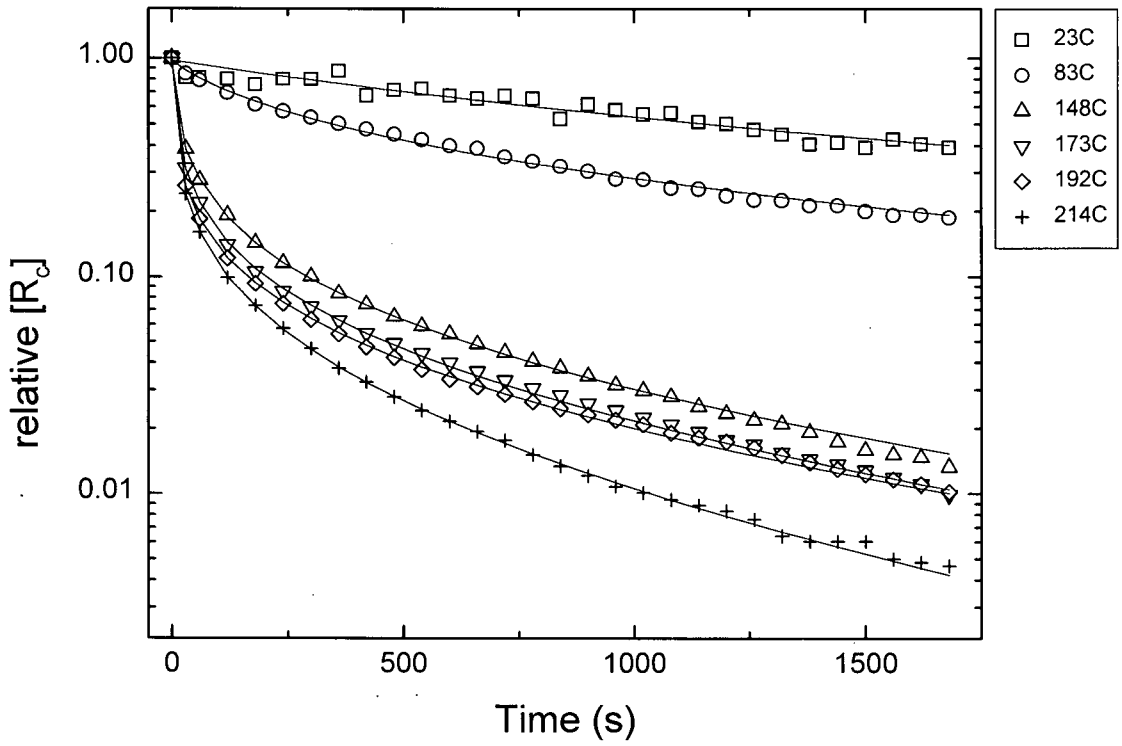

Figure 4.10 Plot of the relative recombination centre density as a function of time. Effect of H-atoms on an intrinsic (100) Si/SiO_2 interface at 23°, 83°C, 148°C, 173°C, 192°C, and 214°C. This effect was observed after long H-atom exposures and it represents the disappearance of recombination centres. The solid lines represent the best fit obtained from a triple-exponential decay function.

Table 4.2 Mean activation energies, spreads, pre-exponential factors, and rate constants measured when the H-atoms are shut off. These parameters (E_a^o, A, and σ) were obtained by fitting the data representing the H-atom interaction with an intrinsic (100) Si/SiO_2 interface with a Gaussian function. Note that the values of E_a^o and A are simply values that have been used to calculate k in the final column.

T (°C)	E_a^o (eV)	σ (eV)	A (s^{-1})	k (s^{-1})
23	0.753	0.024	2.30×10^{9}	3.55×10^{-4}
83	0.794	0.045	2.91×10^{8}	1.66×10^{-3}
148	0.812	0.076	1.92×10^{8}	3.71×10^{-2}
173	0.853	0.087	2.91×10^{8}	6.72×10^{-2}
192	0.813	0.102	6.76×10^{7}	1.06×10^{-1}
214	0.815	0.096	2.95×10^{7}	1.10×10^{-1}

Figure 4.11 illustrates the Arrhenius plot of the rate constants. An activation energy of ~0.41 eV is obtained from the slope of the straight line. An average pre-exponential factor of ~$2.3x10^3$ s^{-1} was obtained from the graph. The average value of the Gaussian spread was calculated to be ~0.07 eV. Thus the rate constant for the disappearance of traps from the intrinsic Si/SiO_2 interface is:

$$\mathbf{k = 2.3x10^3 e^{-0.41/k_B T}} \qquad [4.17]$$

The exponential decay of the recombination centre density is not a simple exponential process, as the kinetic analysis has already shown. The occurrence of this non-exponential decay at both the surface of GaAs and the Si/SiO_2 interface suggests that it can be attributed to H-atoms that are simply trapped in energetically shallow interstitial crystal sites near the GaAs or Si surface.

The following mechanisms could describe the reversible process that occurs when the Si/SiO_2 interface is exposed to H-atoms. The H-atoms (with their partially filled s-orbital) are rapidly trapped at certain sites in Si that are close to the interface, according to the reaction:

$$H + Site\bullet \rightarrow HSite\bullet \qquad [4.18]$$

and they reach a steady state concentration because of the reverse process:

$$HSite\bullet \rightarrow H + Site\bullet \qquad [4.19]$$

and the process:

$$H + HSite\bullet \rightarrow H_2 + Site\bullet \qquad [4.20]$$

When the H-atoms are turned off, reaction [4.19] continues to occur, and thus these particular recombination sites disappear.

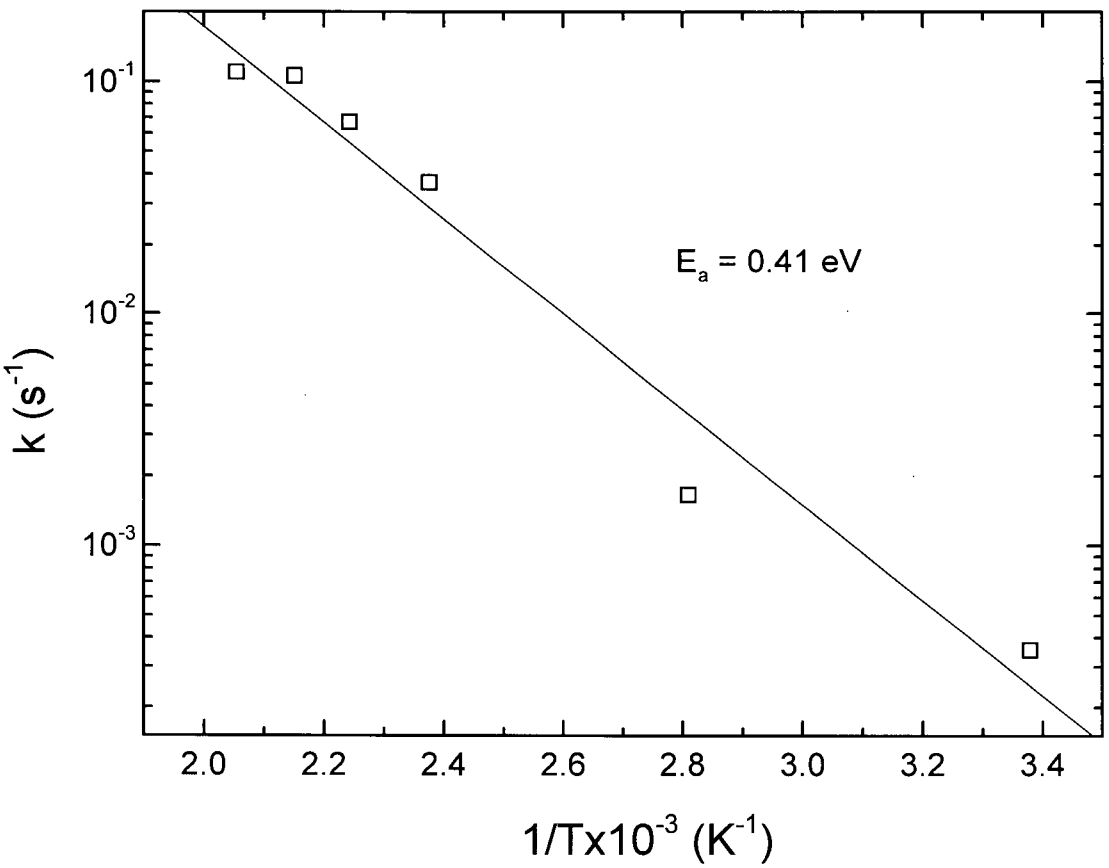

Figure 4.11 Arrhenius plot of the recombination centre decay rate constants when the H-atoms were turned off. Effect of H-atoms on an intrinsic (100) Si/SiO_2 interface at 23°C, 83°C, 148°C, 173°C, 192°C, and 214°C.

4.4 P-type Oxynitrided (100) Si/SiO_2 Interfaces

The oxynitrided Si/SiO_2 system has become of great interest to the semiconductor industry because of its superior interface properties, and enhanced device reliability.[110] We therefore considered it useful to conduct some experiments on these types of samples. At the same time this represented a good way to test our theory concerning the effect of atomic hydrogen on different Si/SiO_2 interfaces. We reasoned that if our theory regarding the irreversible process was correct, we could pre-passivate all the R_c sites with a high temperature H_2 annealing (see page 67 in the experimental chapter). The "irreversible process" should then be absent during an H-atom exposure.

4.4.1 Exposure of a Fresh Sample to Atomic Hydrogen

A fresh p-(100) Si/SiO_2 oxynitrided sample was introduced into the reactor at room temperature (RT), heated to 240°C and then to 330°C. A peak in the measured RF-probe signal was observed at about 330°C, therefore this was chosen as the working temperature. Figures 4.12 and 4.13 illustrate the carrier and the recombination centre density, respectively, plotted as a function of time. It can be seen that the behaviour resembles that previously recorded for GaAs and intrinsic Si/SiO_2. Here too, the irreversible and reversible processes are observed. The reversible process depicted in Figure 4.14 is consistent with the one observed in intrinsic Si samples and is a non-exponential process. The solid line represents the best fit obtained with a sum of 9 rate constants with a Gaussian distribution of activation energies around a mean value (see previous section).

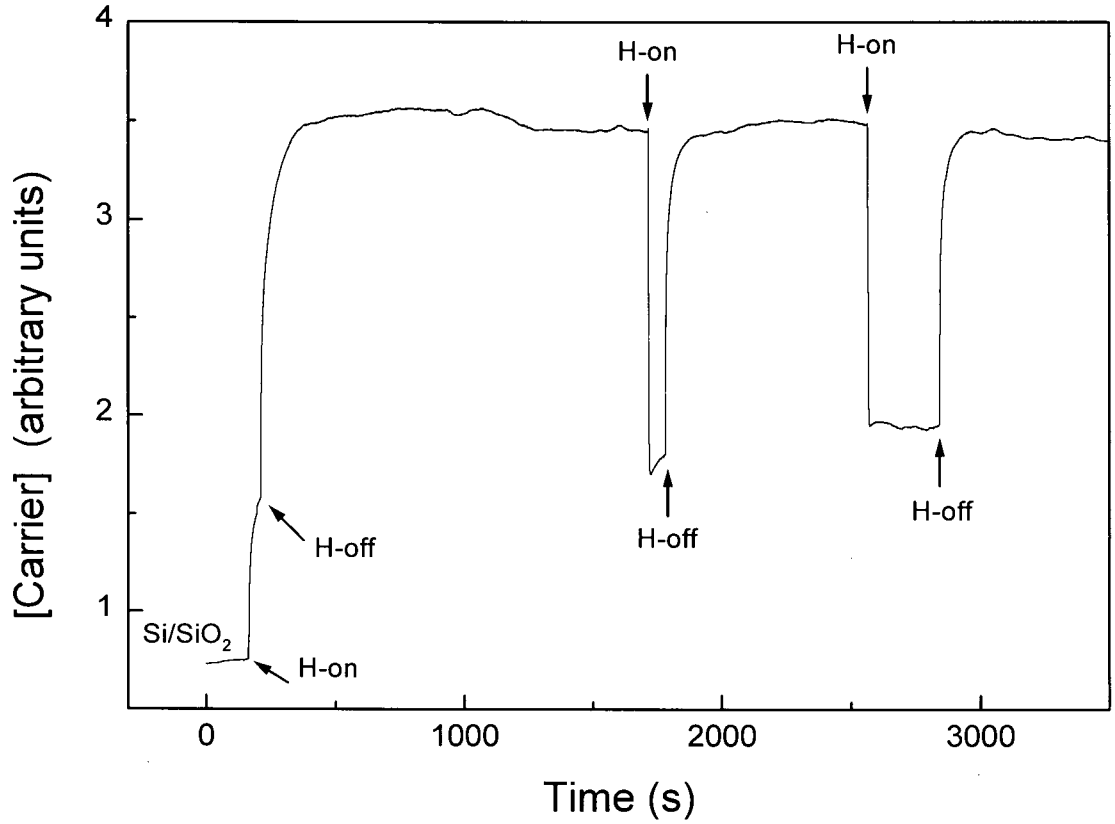

Figure 4.12 Plot of the carrier density as a function of time. Effect of exposure of a p-(100) Si/SiO_2 oxynitrided sample to H-atoms at 330°C.

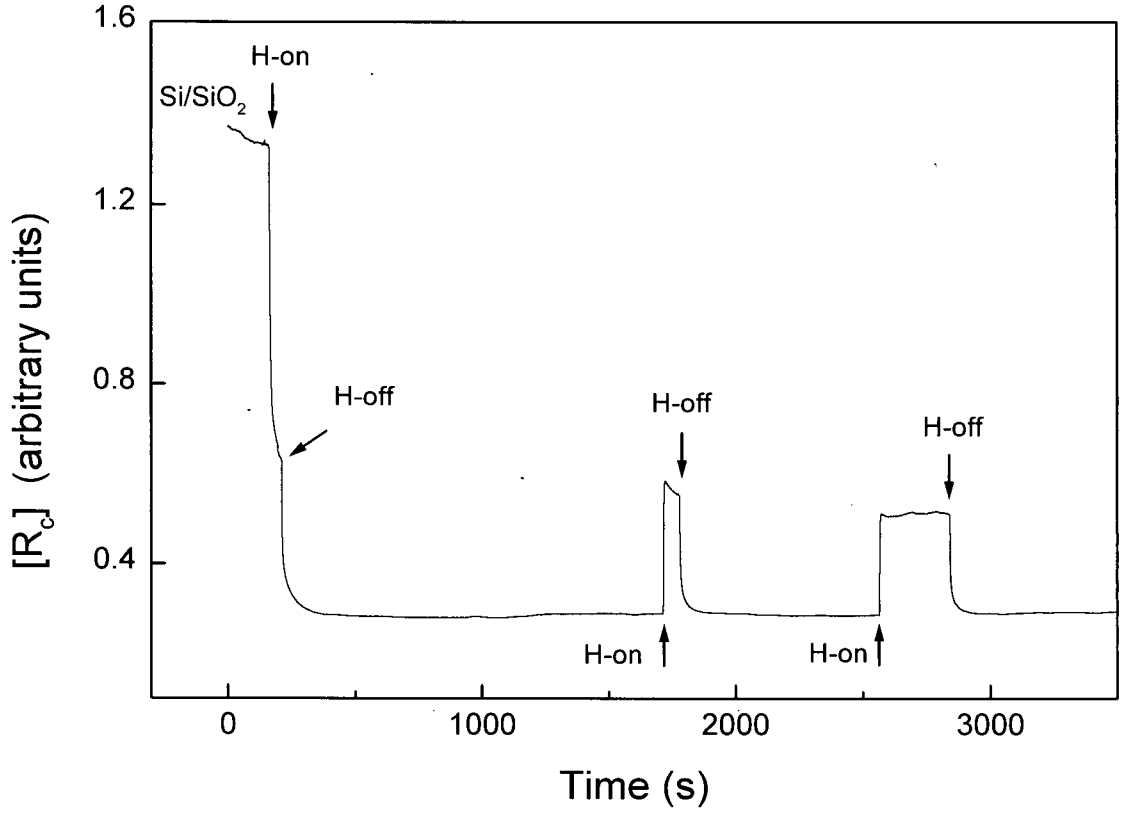

Figure 4.13 Plot of the recombination centre density as a function of time. Effect of exposure of a p-(100) Si/SiO_2 oxynitrided sample to H-atoms at 330°C.

4.4.2 Exposure of an H_2 Passivated Sample to Atomic Hydrogen

Figure 4.15 illustrates a comparison between an H_2 oxynitrided p-type (100) Si/SiO_2 sample that has been pre-passivated in H_2 at 450°C (solid line) and one that has not been thus passivated (dashed line). It can be seen that the change that occurs instantly for both samples brings them to approximately the same level (near 2 on that arbitrary scale). This is consistent with the H-atoms principally passivating the R_c sites in the unpassivated sample through the reaction:

$$R_c + H \rightarrow HR_c \qquad [4.1]$$

and principally depassivating the pre-passivated sample through the reaction[85]:

$$HR_c + H \rightarrow R_c + H_2 \qquad [4.21]$$

Then both samples are further passivated more slowly, by the accumulation of H_2 through the slower process:

$$R_c + H_2 \rightarrow HR_c + H \qquad [4.2]$$

From here on the two samples behave almost identically. In the presence of H-atoms, which occupy sites at the interface, the $[R_c]$ value is higher. When the H-atoms were switched off, both the treated and untreated samples exhibited a further decrease of the recombination centre density to the same level.

It may be noted that if H_2 accumulates slowly at the interface, the recombination centre density can go through a maximum. Li[111] also observed this process upon exposure of previously H_2 passivated p-type (100) Si/SiO_2 samples to H-atoms, and has studied it in detail so that we will not pursue this aspect of the phenomenon.

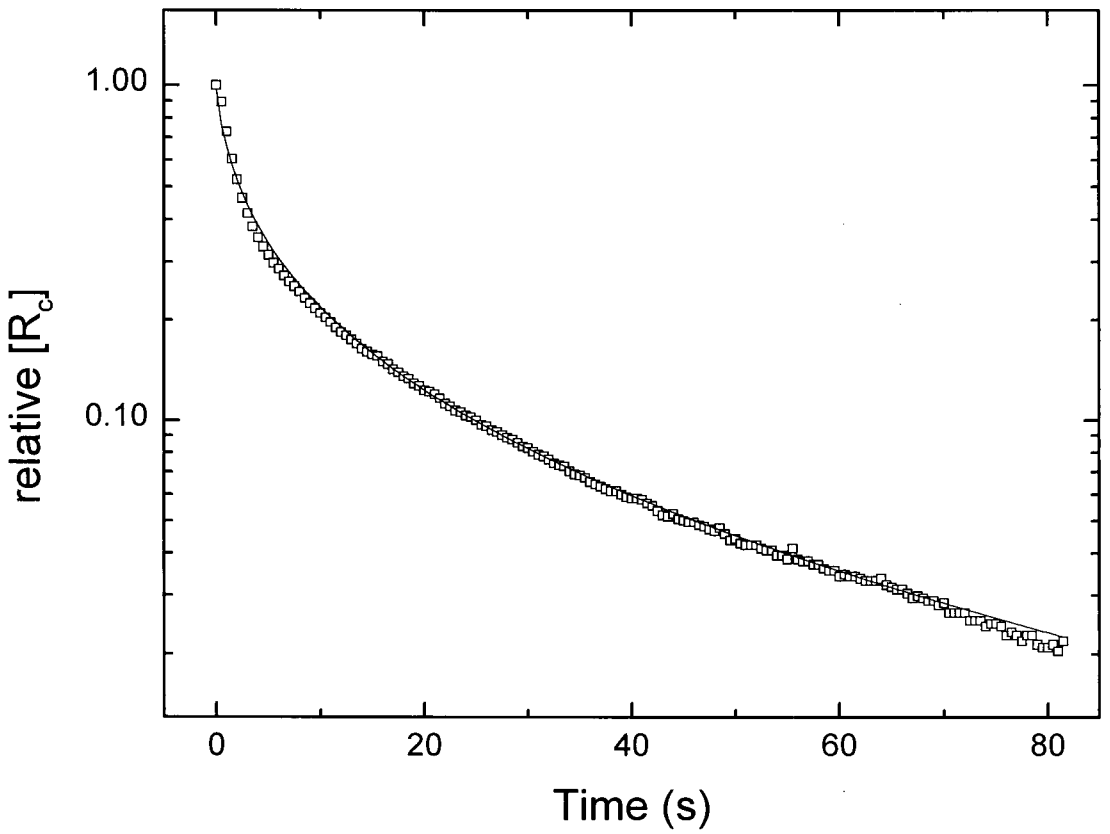

Figure 4.14 Logarithmic plot of the recombination centre density as a function of time. Reversible process: effect of the subsequent exposure of a p-(100) Si/SiO_2 oxynitrided sample to H-atoms at 330°C. The solid curve represents the best fit obtained with a sum of 9 rate constants with a Gaussian distribution of activation energies.

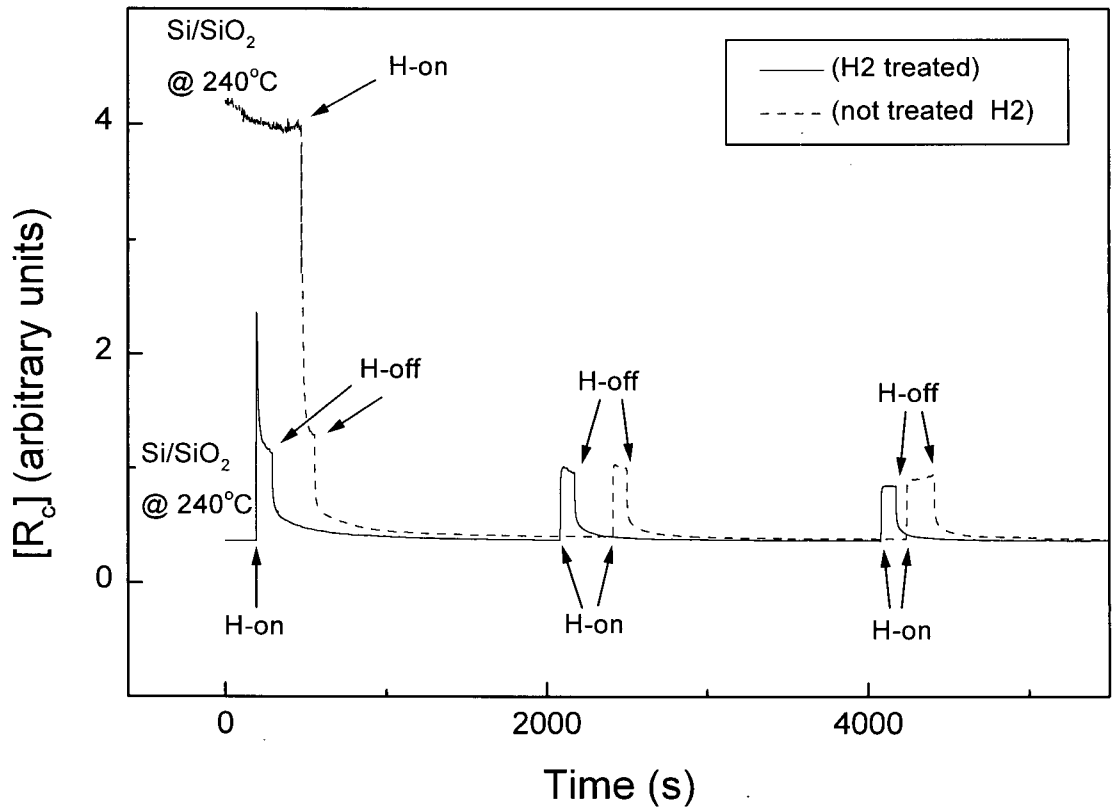

Figure 4.15 Plot of the recombination centre density as a function of time at 240°C. Effect of exposure of a p-(100) Si/SiO_2 oxynitrided sample to atomic hydrogen at 240°C. This sample had previously been passivated in H_2 at 450°C.

For the moment, it is worth noting that the industrial passivation of interfaces requires the "annealing in an H_2 ambient" for a period of at least two hours to passivate all the recombination centres. From our work it can be seen that much the same passivation level can be obtained with a few minutes exposure to H-atoms at much lower temperatures because of: (i) the presence of the more reactive atoms, and (ii) the apparently much larger concentration of interstitial H_2, both of which make the passivation process much faster.

Although our results indicate that at elevated temperatures H-atoms are trapped in sites near the Si/SiO_2 interface they are released quite rapidly. However, at room temperature the H-atoms are more permanently trapped in these sites. Their lifetimes in some of these traps exceed several hours at 25°C. This provides an explanation of Cartier's[19] observation that a large number of interfacial states are produced by exposure to a remote H-plasma. From our work it is clear that these recombination sites are simply atomic hydrogen.

5. RESULTS AND DISCUSSION (III): Interaction of Molecular Hydrogen with the Si/SiO_2 Interface

5.1 Passivation of Recombination Centres at the p-$Si(111)/SiO_2$ Interface by H_2

Samples of (111) Si which are coated with a 200 Å layer of SiO_2 were thermally annealed in vacuum (~ $5x10^{-6}$ Torr) for 1 h at ~700°C. This step was necessary in order to get rid of the H_2 that had unintentionally passivated any defects during the thermal oxidation. The samples were then introduced into the quartz passivation reactor and kept under a H_2 flow (760 Torr) at a constant temperature somewhere between 100 and 300°C, for periods of time up to 20 h while the RF-probe signal was continuously monitored. The data points were collected continually, at a rate of 1 data point/min. The RF probe signal, i.e. the carrier density, increased slowly with time. A similarly prepared sample, which was kept under a He flow (760 Torr), showed no change in the RF-probe signal with time. This behaviour, at 240°C, is illustrated in Figure 5.1, where the inset graph shows in more detail the initial part of the curve. The plot of the inverse RF-signal, as a function of time, is a measure of the recombination centre density (Figure 5.2).

The results of our RF-probe measurements for the H_2 exposures of p-$Si(111)/SiO_2$, are presented in Figure 5.3, where the normalized recombination centre densities at three different temperatures (223°C, 240°C, and 260°C) are plotted against the reaction time. The three temperatures illustrated were chosen for comparison with Brower's and Stesmans' data.

From Figure 5.3 (note the logarithmic scale for the recombination centre density) it is clear that the passivation of electrically active defects does not follow a simple exponential rate law. A simple exponential decay (i.e. a straight line on a semi-logarithmic plot) would be

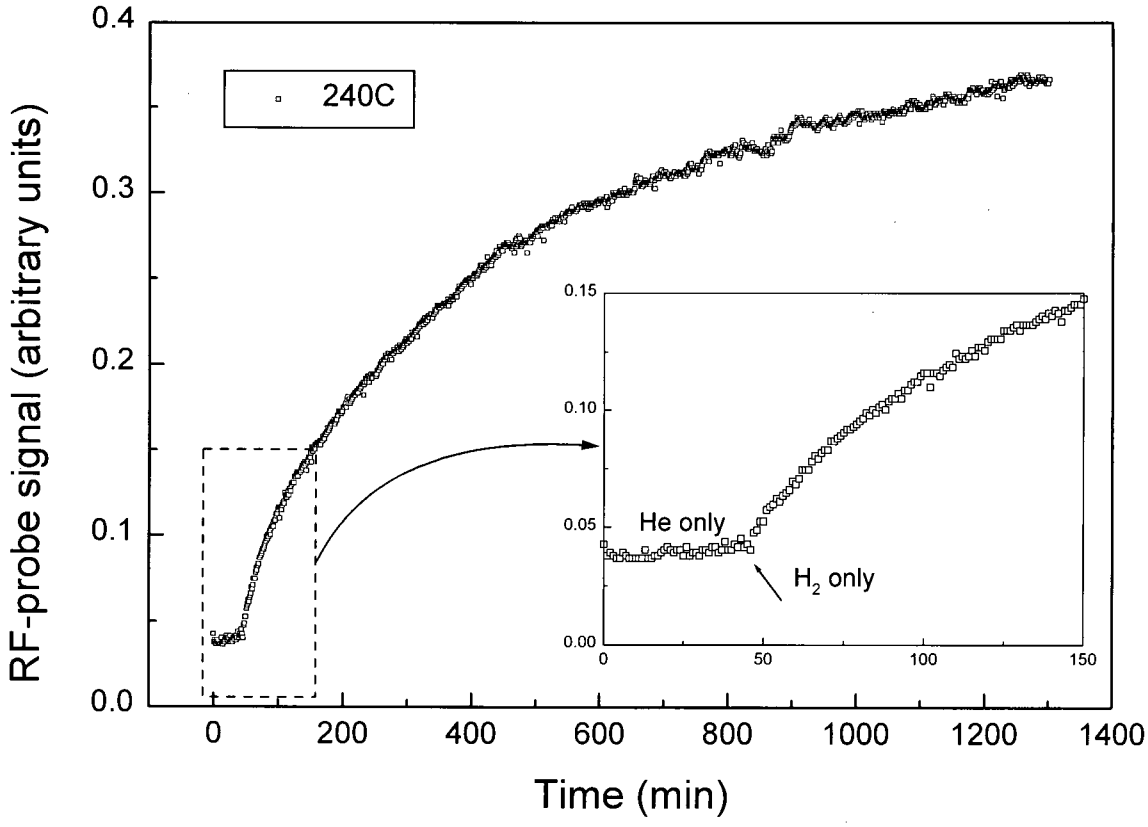

Figure 5.1 Plot of the RF-probe signal versus time, showing the effect of He and H_2 exposure on a p-Si(111)/SiO_2 sample. The inset graph shows the initial part of the curve in more detail.

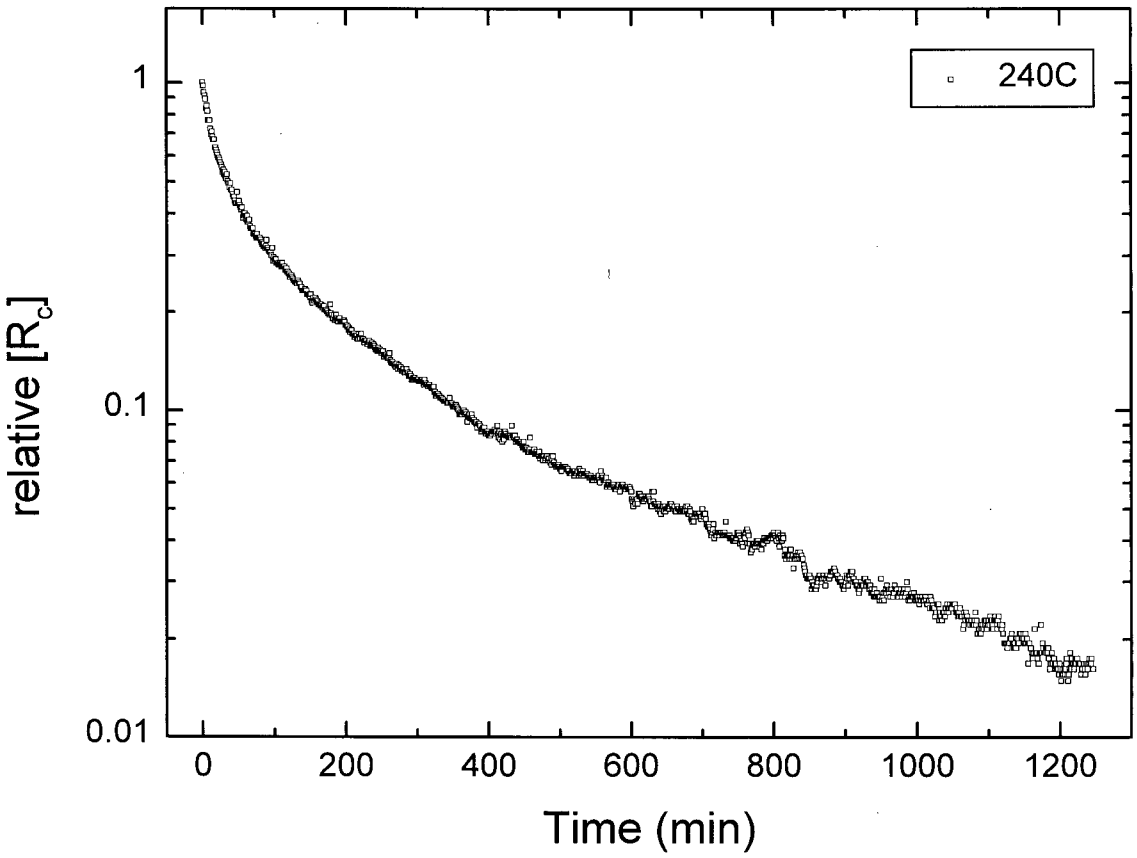

Figure 5.2 Plot of the inverse of the RF-probe signal (recombination centre density) versus reaction time at 240°C. All the data points (sampling rate of 1 data point/min) are shown.

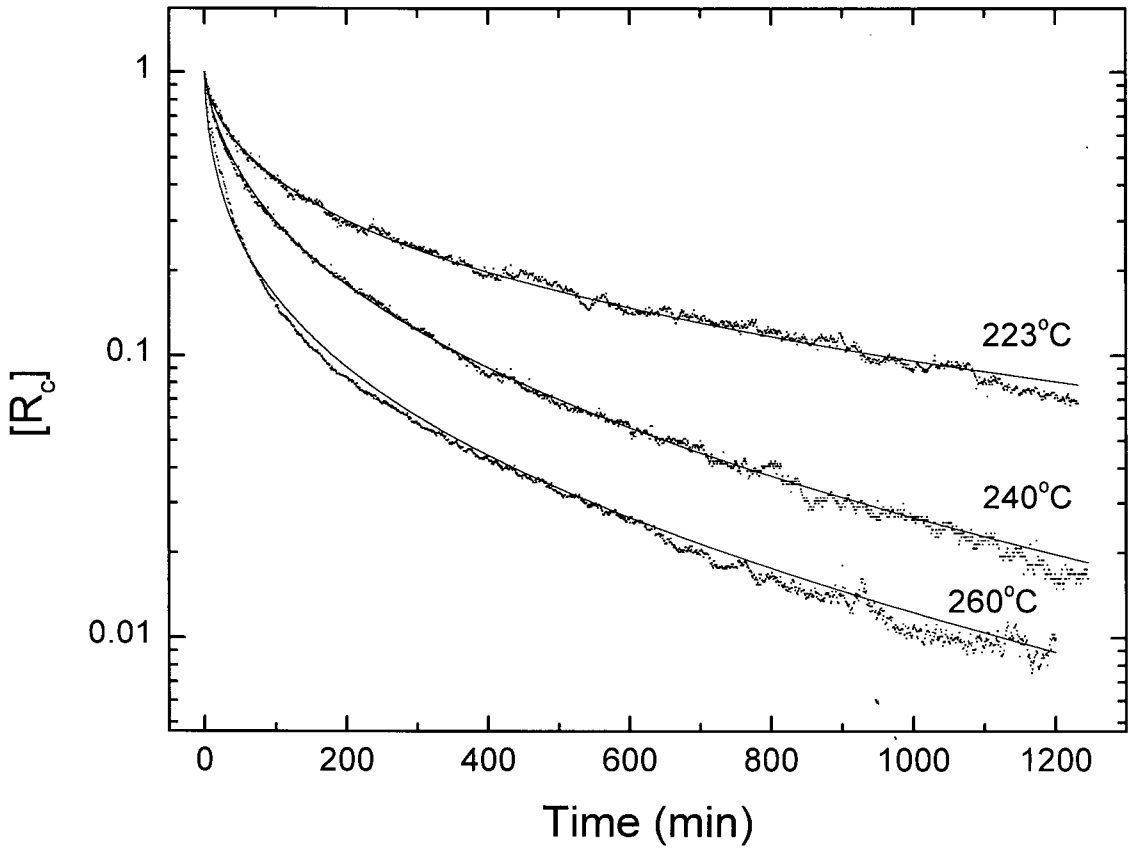

Figure 5.3 Plot of the relative recombination centre density of a p-Si(111)/SiO_2 sample as a function of time, in the presence of H_2 (760 Torr) at 223, 240, and 260°C (Brower and Stesmans temperature range).

characteristic of a simple pseudo first order reaction described by equation [1.26] and the rate equation [1.23], as first proposed by Brower (see page 33 of the introductory chapter). By measuring the P_b centres at the (111) Si/SiO_2 interface with EPR, Brower had found that H_2 passivated these defects at a measurable rate between 230°C and 260°C.[50] He reported that the passivation reaction that followed first order kinetics had an activation energy of 1.66 eV.

Stesmans repeated this study in the 225-265°C temperature range, and in contrast to Brower, found a non exponential removal of P_b defects by H_2, with an activation energy of 1.51 eV.[61] He suggested that the non-exponential process could be due to the existence of P_b sites in slightly different environments, resulting in a distribution of activation energies for the reaction.

The results at 223°C, 240°C, and 260°C (Brower and Stesmans temperature range) shown in Figure 5.3 are similar to those of Stesmans but differ from those first reported by Brower insofar as the passivation of the defects is not a simple exponential process. However, a careful inspection of Brower's results revealed that his samples were studied for shorter reaction times (i.e. 300-400 min) than the reaction times used by either Stesmans or by us. Therefore he could have been looking at a shorter initial period in the reaction, which is almost linear.

For the kinetic analysis of this P_b passivation process, we have assumed (as did Stesmans), that the activation energy has a Gaussian distribution around a mean value E_a^o, with a spread σ:

$$\frac{[R_c]}{[R_c]_0} = \frac{1}{\sigma\sqrt{2\pi}} \int_{-\infty}^{\infty} e^{-(E_a - E_a^o)^2/2\sigma^2} \; e^{-t\,[H_2]\,A\,\exp(-E_a/k_B T)} \, dE_a \qquad [5.1]$$

where $[R_c]$ is the recombination centre density, $[R_c]_0$ is the initial recombination centre density, E_a is the activation energy, A is the pre-exponential factor, t is the reaction time, $[H_2]$ is the

concentration of H_2 at the Si/SiO_2 interface, k_B is the Boltzmann constant, and T is the absolute temperature.

The hydrogen in our experiments has reached the interface by the diffusion of H_2 through the thermal oxide. Shelby has shown that H_2 diffusion through a relatively thick (200-500 Å) thermal oxide is very rapid.[63] At room temperature, the H_2 concentration at the interface reaches 84% of the dissolved H_2 concentration at the surface in approximately 1 s. At about 250°C, the H_2 concentration equilibrates within about 1 ms.

The chemical (dissociative) solubility of H_2 in vitreous silica dominates only above 600°C. Therefore, the value for $[H_2]$ used in equation [5.1] corresponds to the physical solubility of H_2. For low pressures the solubility of H_2 in vitreous silica, $[H_2]$, is proportional to the gaseous H_2 pressure, p, at the surface and is given by Shelby[63] as:

$$[H_2] = K(T)\, p\, V^{-1} \qquad [5.2]$$

where $V^{-1} = 1.27 \times 10^{21}$ sites/cm^3 is the concentration of sites in which molecular hydrogen dissolves in vitreous silica.

The exact experimental values for the hydrogen solubility under 300°C have not been reported in the literature. However, the solubilities determined for D_2 in the 0-700°C temperature range[63] and for H_2 in the 300-500°C temperature range[62] indicate that the solubility varies linearly with inverse temperature. The temperature dependence of the solubility has been shown to be adequately described by a statistical-mechanics model, which treats gas solubility as an equilibrium between the dissolved gas molecules and those in the gas phase. Schackelford *et al.*[62] derived the following expression for the equilibrium constant, K(T):

$$K(T) = \left(\frac{h^2}{2\pi m k_B T}\right)^{3/2} \left(\frac{1}{k_B T}\right) \left(\frac{e^{-h\nu/2k_B T}}{1 - e^{-h\nu/k_B T}}\right)^3 e^{-\varepsilon/k_B T} \qquad [5.3]$$

Here h and k_B are the Planck and the Boltzmann constants, respectively. T is the absolute temperature, while $\nu = 4.1 \times 10^{12}$ is the vibrational frequency for H_2 in vitreous silica. The binding energy is $\varepsilon = -0.105$ eV, for a molecule of hydrogen of mass $m = 3.35 \times 10^{-27}$ kg, and corresponds to the heat of adsorption at the surface. We have therefore used this model to calculate the molecular hydrogen concentration at the Si/SiO_2 interface, $[H_2]$, at various working temperatures (see Table 5.1 on page 124) and used these values in equation [5.1].

At any given temperature a Gaussian distribution of activation energies, such as the one described by equation [5.1], produces a non-exponential rate process by resulting in a distribution of rate constants centred around some average value. In order to obtain the parameters E_a^o, σ, and A from equation [5.1] the decay curves have to be fitted simultaneously at all the temperatures. Since this presented a problem for our software (Microcal Origin) we approximated the integral in equation [5.1] with a sum of nine rate constants. We chose a step of $\frac{1}{2}\sigma$ and summed from -2σ to $+2\sigma$:

$$\frac{[R_c]}{[R_c]_0} \approx \left(\frac{1}{2}\sigma\right) \frac{1}{\sigma\sqrt{2\pi}} \sum_{j=-4}^{j=+4} e^{-j^2/8} \, e^{-t\,[H_2]\,A \exp\{-(E_a^o + \frac{j}{2}\sigma)/k_B T\}} \qquad [5.4]$$

Equation [5.4] was used to fit the recombination centre decay curves shown in Figure 5.3. The final recombination centre density after the reaction with H_2 was subtracted from all recombination centre density values, and then all the values obtained were normalized. The

spread around the mean activation energy (σ) is determined by the curvature of the R_c decay curves shown in Figure 5.3.

The decay curves do not determine unique values for E_a^o and A, at any given temperature. The solid lines in Figure 5.3 represent the fit that is obtained with these parameters. An average rate constant, which corresponds to a "family" of E_a^o and A values, is determined as given by equation [5.4].

Figure 5.4 illustrates the Arrhenius plots of the rate constants in the 220-260°C temperature range, while the values obtained for k are listed in Table 5.1. Inspecting the plot of the rate constants obtained in this temperature range (220-260°C) which was used earlier by Stesmans and Brower, we can see that not only are our rate constants larger, but we would obtain a significantly lower activation energy than Stesmans and Brower. It was possible for us to extend our reaction temperature range outside the Brower and Stesmans range, i.e. down to 135°C and up to 300°C, because the reaction rates were still measurable at the two extremes. Measurements beyond this range are not possible with our system due to two factors: (i) the samples we used give a very noisy signal below 135°C, and (ii) the passivation process is too fast above 300°C. The results at some of these temperatures are presented in Figure 5.5. The non-exponential decay is again evident in this data and the solid lines represent the fitted curves obtained by using equation [5.4].

As in the previous chapter, not all the collected data points were plotted in Figure 5.5. The same number of data points was plotted on each curve. With the exception of the second point (after the first 30 min), only points at 100 min intervals were chosen. This data manipulation was done because the number of data points was too great for the Gaussian fitting

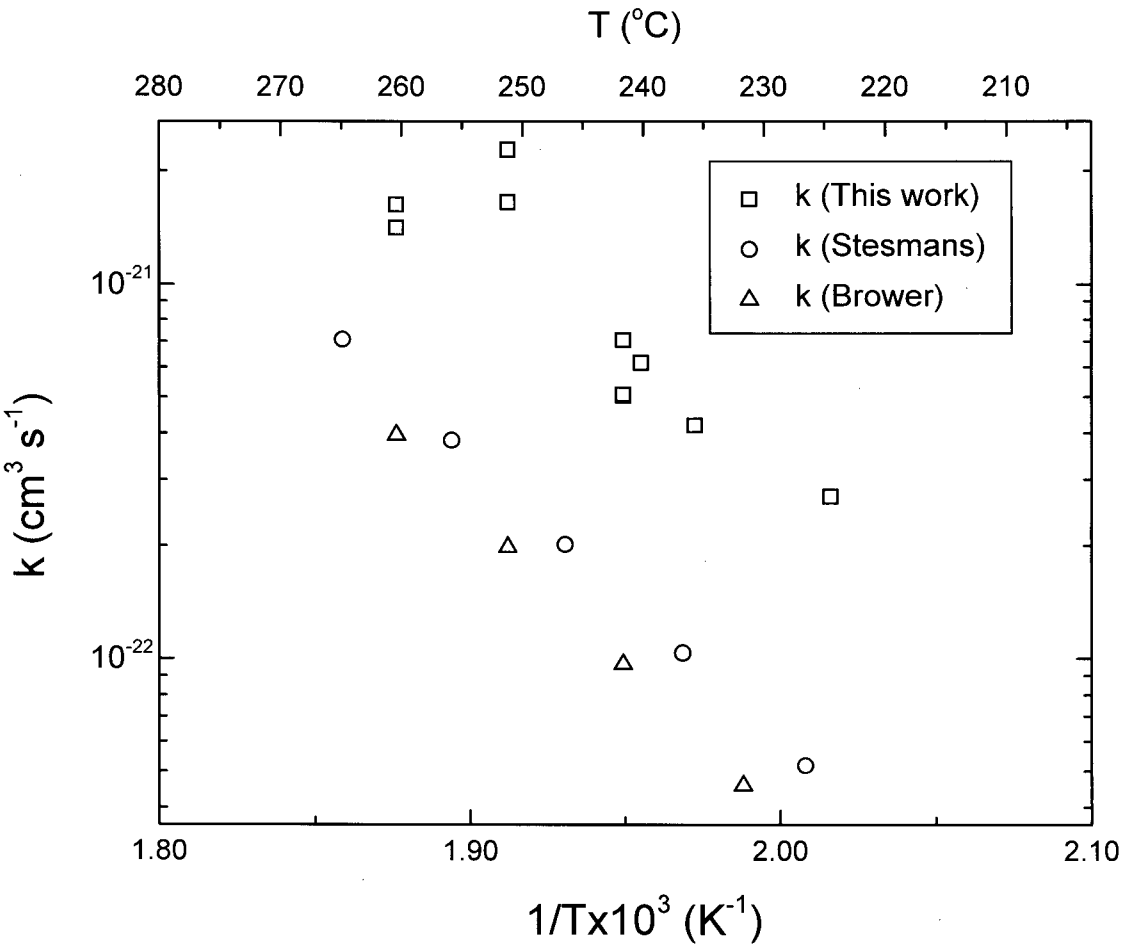

Figure 5.4 Plot of the reaction rate constants, k, obtained by Stesmans, Brower and the present author, as a function of the reciprocal of the temperature in the range from 220°C to 265°C.

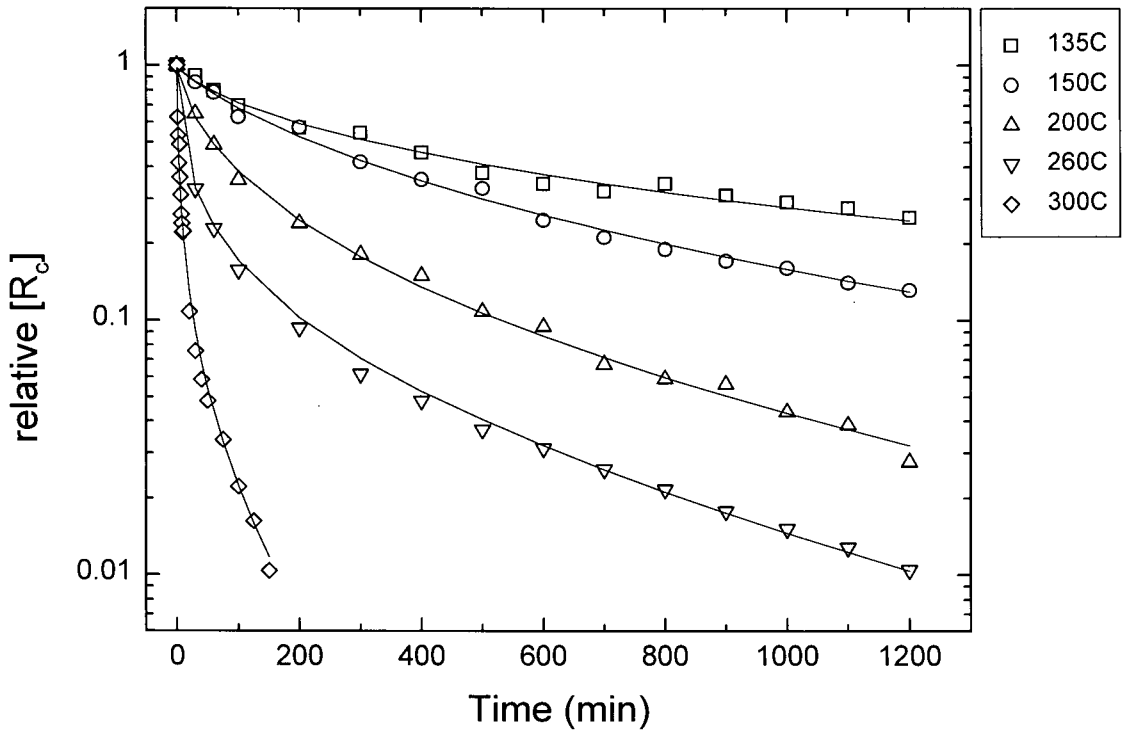

Figure 5.5 Plot of the relative recombination centre density of a p-Si(111)/SiO_2 sample as a function of time, in the presence of H_2 (760 Torr) H_2 in the 135-300°C temperature range.

to be handled by our software (Microcal Origin). Here too, the fitting parameters of the curves containing all the data points were found to be in good agreement with the fitting parameters obtained with fewer data points. We were thus satisfied that important information was not being discarded by eliminating some of the data points.

Several rate constants, evaluated in the manner described above and obtained from experimental results in the temperature range of 135-300°C, are listed in Table 5.1. The Arrhenius plot of these rate constants is illustrated in Figure 5.6.

When we extended our temperature range to both higher and lower temperatures, it immediately became apparent that our rate constants approach those of Stesmans and Brower at high temperatures. Furthermore, at very low temperatures, where the rate of passivation of P_b defects would be insignificant, a new passivation process, which is measured by our probe, but not by EPR, takes over. That new passivation reaction, which takes over at temperatures below 200°C, has an activation energy and pre-exponential value that are both lower than the reaction involving the species studied by EPR. The values of the parameters E_a^o, σ, and A, as well as the values obtained by Stesmans and Brower are listed in Table 5.2.

We will continue to refer to the defect studied by EPR as the P_b defect, and will now refer to the recombination centre seen for the first time in this work, as the R centre. The inverse of the signal measured by our RF-probe, $[R_c]$ is therefore given by:

$$[R_c] = [P_b] + [R] \qquad [5.5]$$

In the 220-260°C temperature range our rate constants represent a sum of the k's (solid curve in the middle temperature range of Figure 5.6) obtained for the recombination centres we measured at lower temperatures and the P_b defects measured by Stesmans and Brower

Table 5.1 Solubilities of H_2 in vitreous silica, mean activation energies, Gaussian spread, pre-exponential factors, and rate constants for the H_2 passivation reaction of p-Si(111)/SiO_2 at different temperatures. Note that the values of E_a^o and A, obtained by fitting the data with a Gaussian function, are simply values that have been used to calculate k in the final column.

T (°C)	$p(H_2)$ (Torr)	$[H_2]$ (cm^{-3})	E_a^o (eV)	σ (eV)	A (cm^3s^{-1})	k (cm^3s^{-1})
135	760	$8.83x10^{17}$	0.781	0.055	$1.50x10^{-13}$	$3.37x10^{-23}$
150	760	$8.11x10^{17}$	0.879	0.040	$1.66x10^{-12}$	$5.59x10^{-23}$
180	760	$6.96x10^{17}$	0.903	0.038	$1.60x10^{-12}$	$1.45x10^{-22}$
200	760	$6.36x10^{17}$	1.366	0.061	$8.03x10^{-8}$	$2.26x10^{-22}$
223	760	$5.79x10^{17}$	1.112	0.073	$5.33x10^{-11}$	$2.7x10^{-22}$
234	760	$5.55x10^{17}$	1.306	0.095	$3.99x10^{-9}$	$4.2x10^{-22}$
240	760	$5.43x10^{17}$	1.086	0.091	$3.27x10^{-11}$	$7.06x10^{-22}$
250	760	$5.25x10^{17}$	1.304	0.099	$6.04x10^{-9}$	$1.32x10^{-22}$
260	760	$5.07x10^{17}$	1.539	0.104	$5.75x10^{-7}$	$1.63x10^{-21}$
287	760	$4.66x10^{17}$	0.957	0.077	$1.12x10^{-12}$	$2.75x10^{-21}$
300	760	$4.49x10^{17}$	1.245	0.089	$7.34x10^{-10}$	$8.29x10^{-21}$

Table 5.2 Parameters for the reaction of H_2 with recombination centres at the (111) Si/SiO_2 interface. The temperature range, ΔT, where these values are obtained is also listed.

Average Activation Energy E_a^o (eV)	Gaussian Spread σ (eV)	Pre-exponential Factor A (cm^3s^{-1})	ΔT (°C)
[a]0.51±0.05	0.049±0.012	$6.7x10^{-17}$($\pm6x10^{-17}$)	135-200
[b]1.51±0.04	0.060±0.004	$9.8x10^{-8}$(+8/-$5x10^{-8}$)	225-265
[c]1.66±0.06	0	$1.94x10^{-6}$ (+2/-$1x10^{-6}$)	230-260

[a] This work.
[b] Stesmans.[61]
[c] Brower.[50]

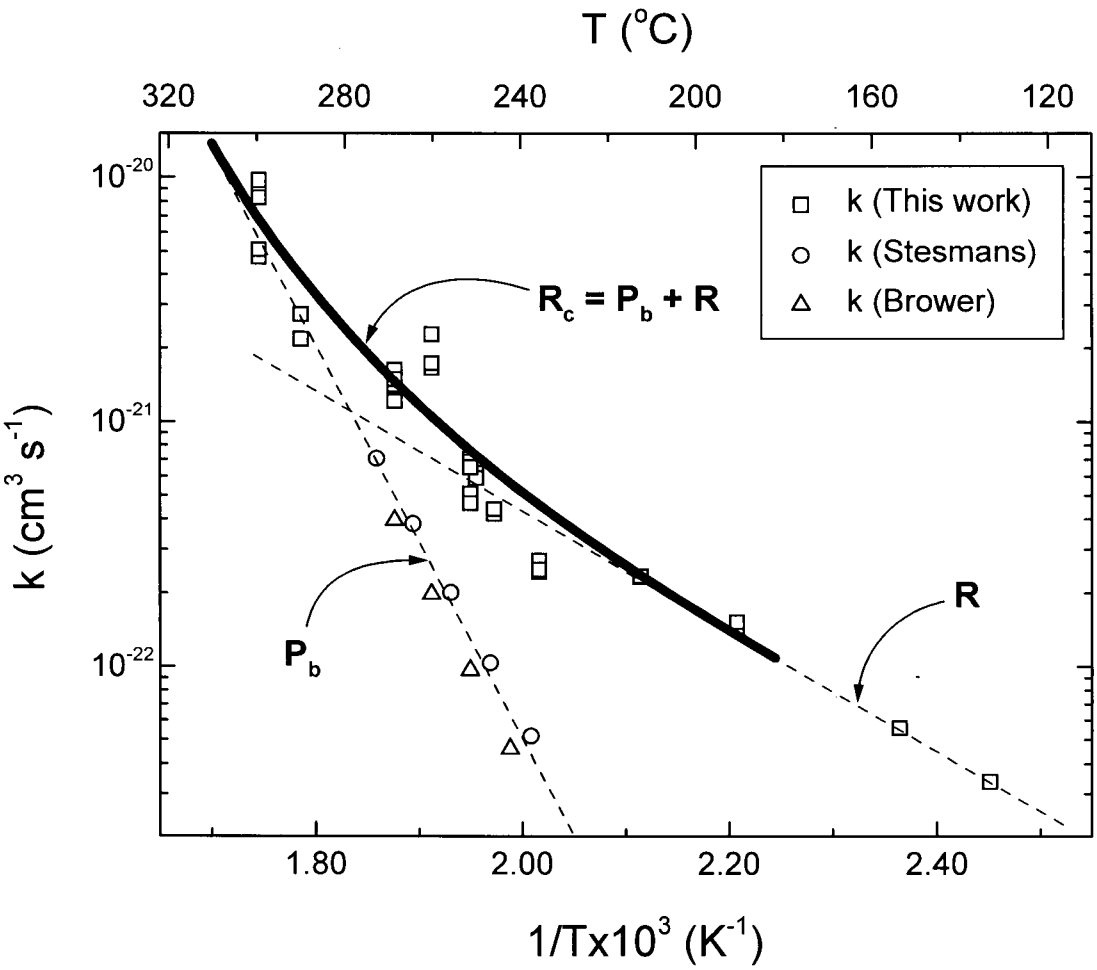

Figure 5.6 Plot of the reaction rate constants, k, obtained by Stesmans, Brower and the present author, as a function of the reciprocal of the temperature in the extended range from 135°C to 300°C.

in this range. Above 265°C, where EPR could not measure the passivation rate, the P_b centres dominate the loss rate. In other words, Stesmans, Brower and we are measuring the passivation rate for P_b centres with an activation energy of ~ 1.5 eV (dashed line on the L.H.S. of Figure 5.6).

From the slope of the line in the low temperature region (dashed line on the R.H.S. of Figure 5.6) we obtained a pre-exponential factor, of ~ $6.7\text{x}10^{-17}$ cm^3s^{-1}, a Gaussian spread of ~ 0.05 eV (average value) around an activation energy of only ~ 0.51 eV, i.e. the rate constant is:

$$\mathbf{k = 6.7x10^{-17} e^{-0.51/k_BT}} \qquad [5.6]$$

The spread in this temperature range is lower than in the 220-260°C range. At these lower temperatures the new recombination centres (R) take over because the lower activation energy for this process makes their decay-rates faster than those of the P_b centres. The passivation of P_b centres is a very slow process, not measurable by EPR, below ~ 220C.

Our analysis of this data proceeded along the following lines. We assume that the passivation of all recombination centres is always governed by the reaction:

$$R_c + H_2 \xrightarrow{k} HR_c + H \qquad [5.7]$$

The rate equation for reaction [5.6] is

$$\frac{d[R_c]}{dt} = -k[H_2][R_c] = k'[R_c] \qquad [5.8]$$

where k is and k' represent the reaction rate constant and the pseudo first order rate constant, respectively.

It can be seen that the pre-exponential factor for R_c is many orders of magnitude smaller than that obtained for P_b centres. Let us look again (see introductory chapter) at the significance

of the pre-exponential factor for reaction [5.6], as Brower[50] did in his study. We assume that the H_2 molecule can diffuse to recombination centres as easily as any other accessible sites in the SiO_2. Thus the fraction of time that H_2 spends on average at the R_c site is about the same as the time it spends at the other sites. The passivation reaction [5.6] occurs only when H_2 is in the vacant site (i.e. reaction site), adjacent to the recombination centre. The pre-exponential factor is approximated by the expression

$$A \approx \frac{\nu_s f}{[H_2]} \qquad [5.9]$$

where ν_s represents the attempt frequency for the reaction, and is of the order of magnitude of the vibrational frequency for H_2, 1.24×10^{14} Hz,[112] while f represents the fraction of time that H_2 spends next to R_c (or P_b). Equation [5.9] reduces to a strictly geometric term

$$A \approx \frac{\nu_s}{V^{-1}} \qquad [5.10]$$

where $V^{-1} \approx 1.27 \times 10^{21}$ interstices cm^{-3} is the density of accessible sites in vitreous SiO_2.[62,63] This model predicts that $A \approx 9.8 \times 10^{-8}$ $cm^3 s^{-1}$. As can be seen from Table 5.2, Stesmans obtained precisely this value for the pre-exponential factor in the $H_2 + P_b$ reaction. However, the pre-exponential factor for the defect R, which we have observed for the first time in this work, is only 6.7×10^{-17} $cm^3 s^{-1}$. How could one rationalize a pre-exponential factor which is about 10^9 lower than that found for P_b centres, coupled with an activation energy that is 1/3 of that found for the reaction of H_2 with P_b centres? Let us first consider possible reasons for a much lower activation energy.

We know that the H_2 passivation of P_b centres involves the formation of a hydrogen-silicon bond (H–Si≡) in an endothermic reaction (Table 5.3), which has an activation energy of ~1.5 eV. Let us consider the possibility that the recombination centre (R) is an O–Si≡ site. The reaction in question then becomes:

$$H_2 + -OSi\equiv \rightarrow H-OSi\equiv +H \qquad [5.11]$$

We can obtain an estimate of the exothermicity of this reaction if we assume that the H–OSi bond energy is similar to the to that in $H-OSiH_3$. Estimates from theoretical calculations[113,114] yield a value for this bond energy of ~ 5.1 eV, making reaction [5.11] exothermic by about 0.6 eV. The equivalent reaction with P_b defects:

$$H_2 + -Si\equiv \rightarrow H-Si\equiv +H \qquad [5.12]$$

is endothermic by 0.5 eV. With this in mind we have sketched the potential energy curves for the reaction of H_2 with P_b and R in Figure 5.7, using the activation energies obtained in this work.

The difference in the activation energies for the reactions of H_2 with P_b (–Si) and R (–OSi) centres may then be explained by the fact that the reaction with the oxygen species forms a much stronger bond. Such a correlation between exothermicity and activation energies has been observed in other systems.[115]

Table 5.3 Bond dissociation energies for different compounds or radicals containing hydrogen.[116]

	BOND ENERGY (eV)[a]
H–H	4.5
Si–H	4.0
SiH_3O–H	5.1[113]
HO–H	5.2
O–H	4.4
CH_3O–H	4.5
CH_3CH_2O–H	4.4
H_3C–H	4.5
H_5C_2–H	4.2

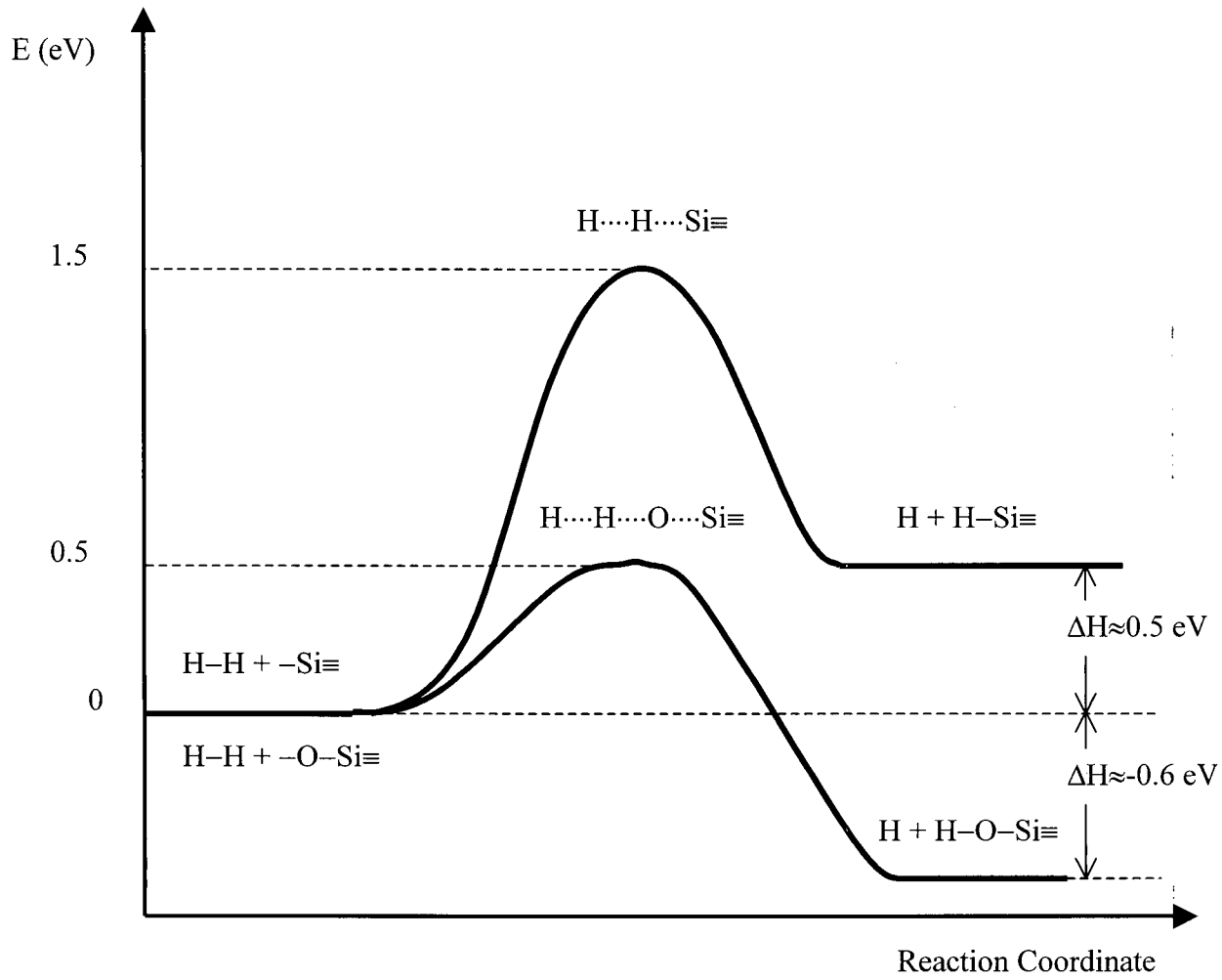

Figure 5.7 Potential energy diagrams for the possible reactions of molecular hydrogen with recombination centres at the Si/SiO_2 interface.

Regarding the magnitude of the pre-exponential factor, we have to look at the significance of the steric factor involved. For a bimolecular reaction, in the general form:[117]

$$A + B \leftrightarrow [AB]^* \rightarrow \text{products} \qquad [5.13]$$

where [AB]* is the transition state complex, the rate constant is given by the approximate expression:[117]

$$k \approx e^{\Delta S^*/R} e^{-\Delta H^*/RT} \qquad [5.14]$$

where ΔS^* is the entropy change for the complex, and ΔH^* is the enthalpy change. If we use the Arrhenius equation:

$$k = Ae^{-E/RT} \qquad [5.15]$$

then the pre-exponential factor can be identified as:

$$A \propto e^{\Delta S^*/R} \qquad [5.16]$$

An abnormally small A indicates that the entropy of activation, ΔS^* is smaller than normal for such a process, i.e. the transition state is very "tight" or "restricted" in its dimensions. We have no data which would indicate why this might be true, and can only assume that for some reason the position of the –OSi species is such that the H-atom can only approach it at a very restricted angle.

5.2 Calculation of the Relative Number of the Defects at the (111) Si/SiO_2 Interface

It is possible to calculate the relative number of the three types of defects that occur at the Si/SiO_2 interface. These are P_b defects, R defects and the remaining defects (X) that cannot be passivated by molecular hydrogen. This can be done by comparing the recombination centre densities, $[R_c]$, after the reaction with H_2 at low temperatures (135°C), and at high temperatures (near 280°C). At low temperatures only the R centres are removed, while at high temperatures only the P_b centres are passivated. We obtained the following relative concentration for the defects: $[P_b] = 0.54$, $[R] = 0.27$, and $[X] = 0.19$ for the (111) Si/SiO_2 interface.

5.3 Effect of H_2 Pressure on the H_2-Recombination Centre Reaction at the p-Si(111)/SiO_2 Interface

Brower[50] has reported that the passivation of P_b centres that occurs when the Si/SiO_2 interface is annealed in H_2, is first order in the pressure of H_2. In view of our conclusion that the RF-probe monitors both P_b and R centres, we considered it prudent to check this relationship.

The plot of the relative recombination centre density, $[R_c]$ as a function of time is shown in Figure 5.8, at 240°C and at three different pressures (0.3, 0.7, and 1 atm). As in the earlier analysis, we obtained the rate constant k by fitting our curves with equation [5.4]. The plot of these rate constants as a function of H_2 pressure is illustrated in Figure 5.9. It can be seen that, within experimental error, the reaction is first order in $[H_2]$, in agreement with the results of Brower.

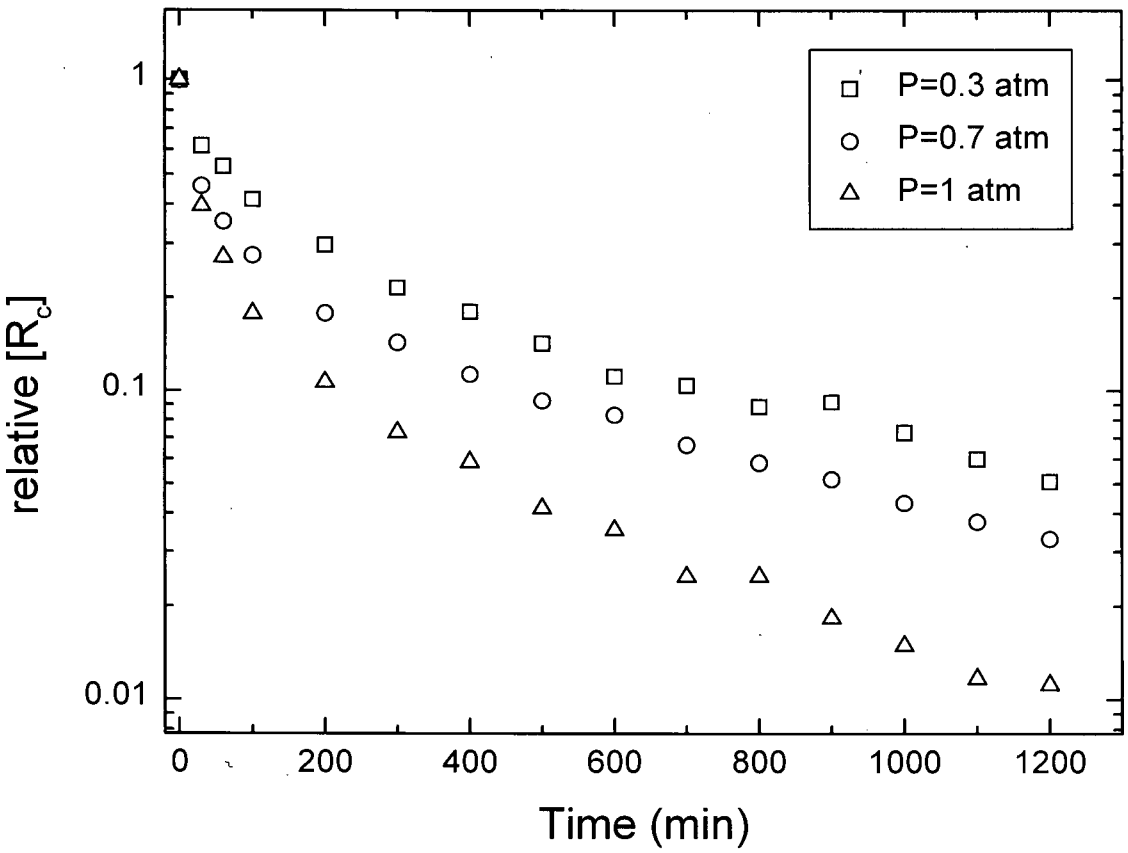

Figure 5.8 Plot of the recombination centre density as function of time. The data points at 240°C correspond to H_2 pressures of 0.3, 0.7, and 1 atm.

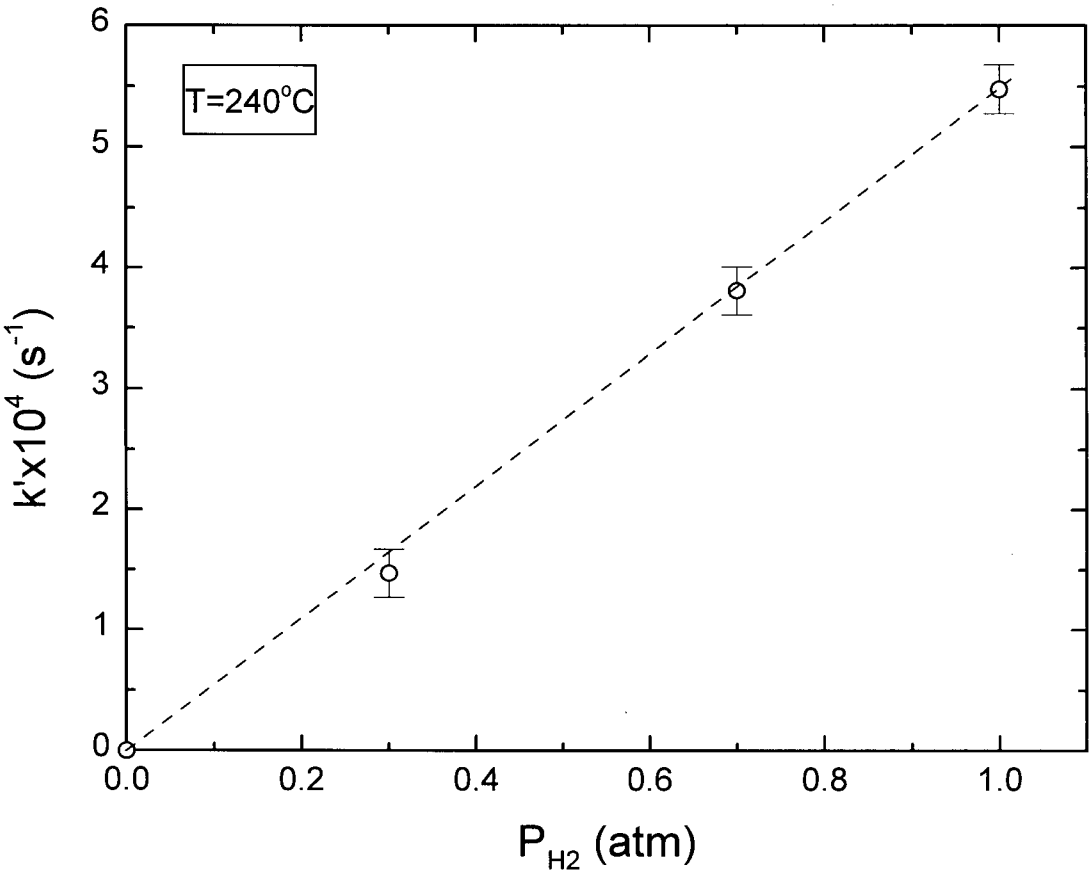

Figure 5.9 Plot of the pseudo first order reaction rate constant as a function of the H_2 pressure. The data points at 240°C correspond to H_2 pressures of 0.3, 0.7, and 1 atm.

5.4 Passivation of Recombination Centres at the Intrinsic (100) Si/SiO_2 Interface by H_2

Samples of intrinsic (100) Si (i-Si) coated with a 200 Å layer of SiO_2 were thermally annealed in vacuum (~ $5x10^{-6}$ Torr) for 1 h at ~700°C. As in the case of (111) Si/SiO_2 samples, the i-Si(100)/SiO_2 samples were then introduced into the quartz passivation reactor and kept under an H_2 flow (760 Torr) at a constant temperature somewhere between 100 and 300°C, for periods of time up to 20 h while the RF-probe signal was continuously monitored. The experimental conditions were similar to those used in the case of (111) Si/SiO_2 samples.

Figure 5.10 illustrates the plot of the recombination centre density as a function of time for an SiO_2 covered i-Si(100) sample exposed to H_2 at 5 temperatures (150, 180, 200, 220, and 240°C). As in the case of (111) Si/SiO_2 the non-exponential decays have been fitted using a Gaussian distribution of activation energies around a mean value E_a^o, according to equation [5.4]. The solid lines in the figure represent these best fits.

The parameters (E_a^o, A, and σ) determined by the Gaussian distribution were used to calculate the reaction rate constants. These values, as well as the H_2 concentrations at the working temperatures are listed in Table 5.4. We exposed the i-Si(100)/SiO_2 sample to H_2 at various other temperatures and the calculated rate constants are also listed in Table 5.4. Figure 5.11 illustrates the Arrhenius plot of all the rate constants in the 135-270°C temperature range. The rate constants that Stesmans[18] obtained for the H_2 passivation of P_{b0} and P_{b1} centres at 213, 229, and 234°C are also shown for comparison. It is clear that our rate constants show the same trend as in the case of p-Si(111)/SiO_2 although it has a lot more scatter than in the (111) Si/SiO_2

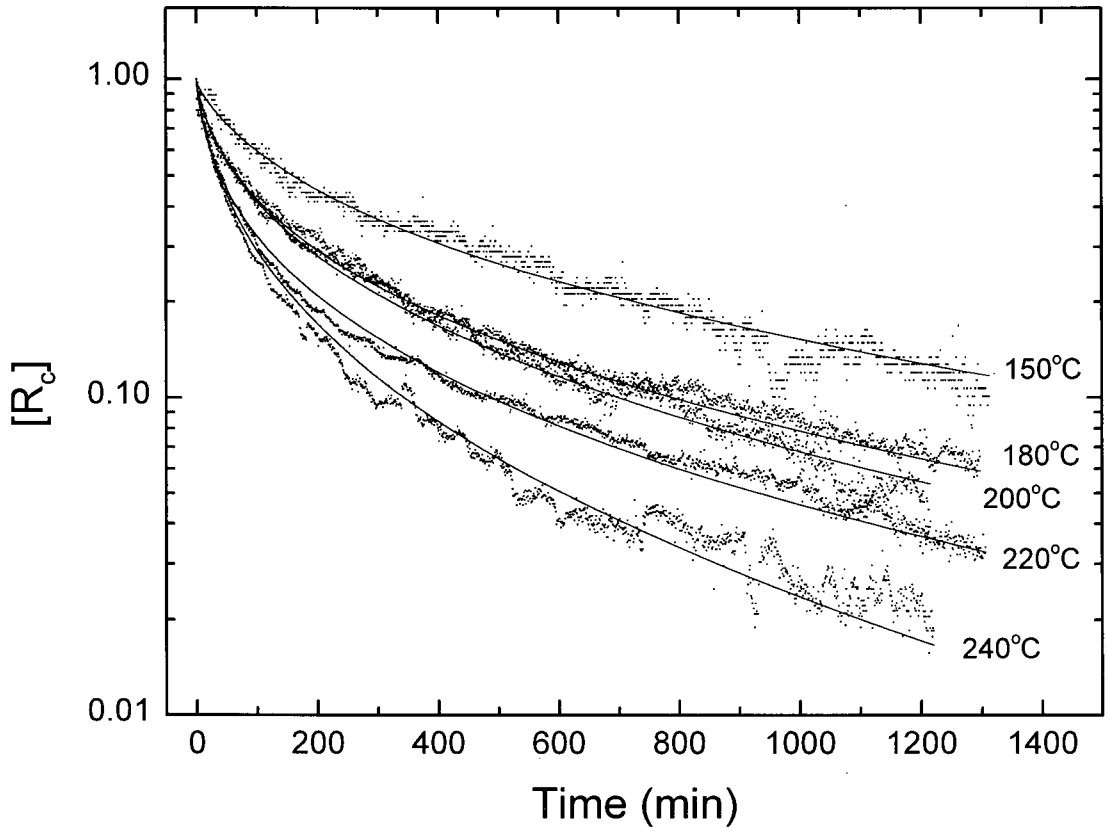

Figure 5.10 Plot of the relative recombination centre density of an intrinsic Si(100)/SiO_2 sample as a function of time, in the presence of H_2 (760 Torr) at 150, 180, 200, 220, and 240°C.

Table 5.4 Solubilities of H_2 in vitreous silica, mean activation energies, Gaussian spread, pre-exponential factors, and rate constants for the H_2 passivation reaction of p-Si(111)/SiO_2 at different temperatures. Note that the values of E_a^o and A, obtained by fitting the data with a Gaussian function, are simply values that have been used to calculate k in the final column.

T (°C)	$p(H_2)$ (Torr)	$[H_2]$ (cm^{-3})	E_a^o (eV)	σ (eV)	A (cm^3s^{-1})	k (cm^3s^{-1})
135	760	$8.83x10^{17}$	0.9409	0.039	$8.87x10^{-12}$	$2.13x10^{-23}$
150	760	$8.11x10^{17}$	1.083	0.057	$8.23x10^{-11}$	$1.04x10^{-23}$
160	760	$7.68x10^{17}$	0.9466	0.047	$7.49x10^{-12}$	$7.25x10^{-23}$
180	760	$6.96x10^{17}$	1.086	0.063	$7.65x10^{-11}$	$6.42x10^{-22}$
200	760	$6.36x10^{17}$	0.972	0.072	$1.81x10^{-12}$	$8.06x10^{-22}$
220	760	$5.86x10^{17}$	1.001	0.072	$6.80x10^{-12}$	$4.09x10^{-22}$
230	760	$5.64x10^{17}$	1.122	0.098	$4.69x10^{-11}$	$2.69x10^{-22}$
240	760	$5.43x10^{17}$	1.109	0.063	$3.74x10^{-11}$	$4.81x10^{-22}$
250	760	$5.25x10^{17}$	1.059	0.087	$1.25x10^{-11}$	$7.89x10^{-22}$
260	760	$5.07 x10^{17}$	1.013	0.082	$1.27x10^{-11}$	$3.41x10^{-21}$
270	760	$4.91x10^{17}$	0.988	0.088	$1.10x10^{-11}$	$7.44x10^{-21}$

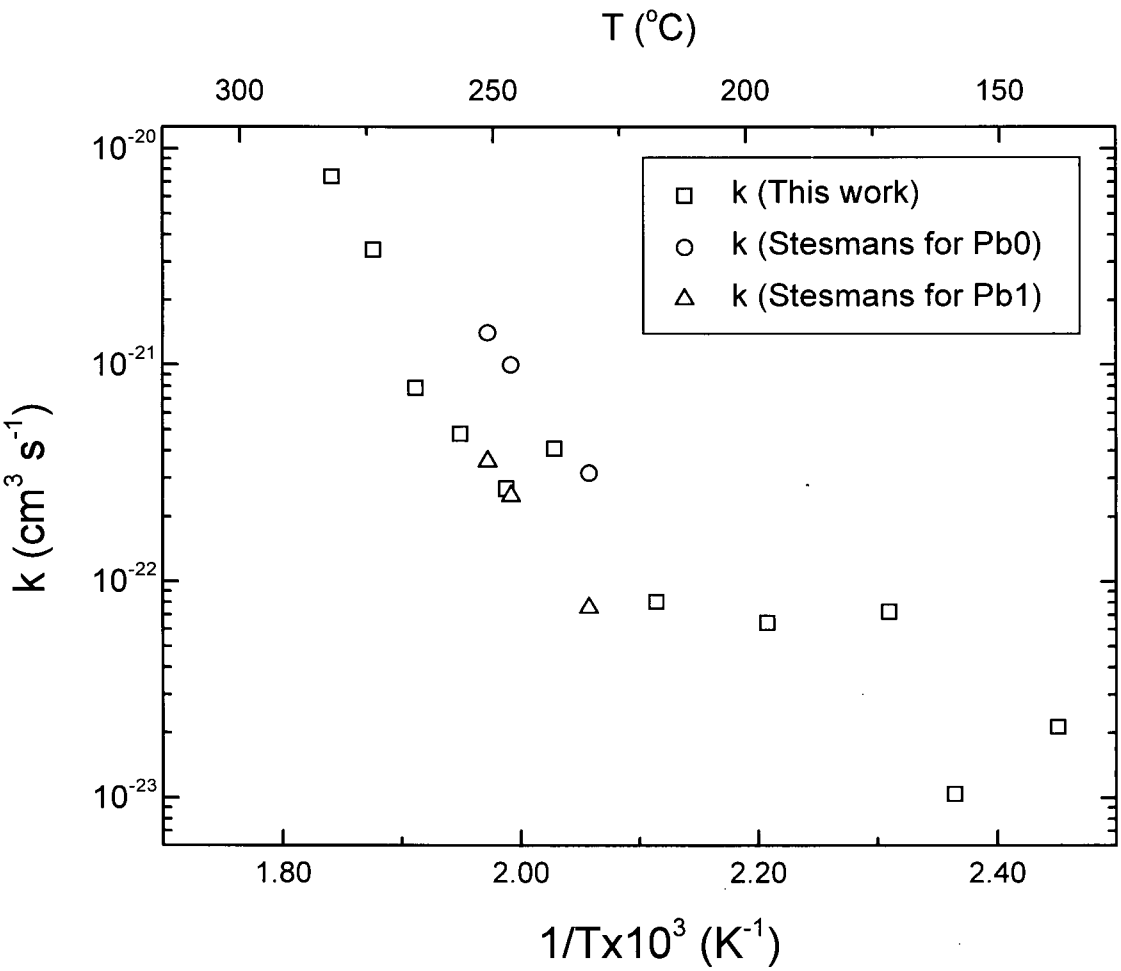

Figure 5.11 Arrhenius plot of reaction rate constants obtained for an intrinsic Si(100)/SiO_2 sample in the presence of 760 Torr of H_2. Comparison with Stesmans' rate constants, for the reaction of P_{b0} and P_{b1} centres and H_2 in the 213-234°C temperature range.

case. Firstly, at lower temperatures (R.H.S. of Figure 5.11) where we are passivating recombination centres other than P_b's the rate constants are quite high, have a very small temperature dependence. Secondly, in the Stesmans temperature range (middle range), where we observe the passivation of all the recombination centres (including P_b's), our rate constants are about the same order of magnitude as Stesmans. Thirdly, in the high temperature range (L.H.S. of Figure 5.11), where the P_b passivation process takes over, our rate constants fall on approximately the same line as Stesmans'.

In a recent paper[74] Stesmans presents evidence that the P_{b1} centres are not electrically active. Consequently, in our measurements we are dealing with only two kinds of electrically active defects, the P_{b0} and R centres, just as in the case of the (111) Si/SiO_2 interface (see section 5.1).

The activation energy calculated from the slope of reaction rate constants for the passivation of recombination centres in the 135-200°C temperature range is 0.44 eV. The pre-exponential factor determined from the graph is $4.5x10^{-18}$ cm^3s^{-1}, while the Gaussian spread is about 0.056 eV. Considering the large scatter of our rate constants in this case, these values compare well with the values previously obtained for the reaction of H_2 and p-type (111) Si/SiO_2.

We have thus shown that a similar multiple-exponential process occurs at both the p-type (111) Si/SiO_2 and the intrinsic (100) Si/SiO_2 interfaces when they are exposed to H_2. We have also observed the same effect on p-type oxynitrided Si/SiO_2 interface, as well as in samples with low temperature and oxygen-plasma oxides. However at this point we do not have enough data to determine the activation energy for these materials.

The significance of our observations that qualitatively as well as quantitatively the same results are obtained both with and without dopants, and with nitrided interfaces lies in the support they provide for our earlier assumption that the RF-probe accurately measures all of the electrically active defects (carrier recombination sites). At the same time measurements with this device are not significantly affected by any form of band bending in the presence of molecular or atomic hydrogen (see previous chapter).

6. CONCLUSION AND RECOMMENDATIONS FOR FUTURE WORK

The room temperature interaction of atomic hydrogen with (100) GaAs surfaces has been studied. The atoms were produced in a remote microwave plasma and their effects on carrier recombination centres were continuously monitored *in situ* by the change in photoluminescence intensity (PLI). It was found that the initial exposure to H-atoms passivated the recombination centres. A further improvement in the passivation level was observed when the H-atoms were switched off. Only this latter change was found to be reversible. A kinetic analysis indicates that this latter process does not obey a simple first order rate law.

A remote radio frequency (RF) probe was used to continuously monitor the changes in the steady state charge-carrier densities at Si/SiO_2 interfaces. When H-atoms were allowed to interact with these interfaces at ~200°C, the behaviour of the recombination centres was found to be similar to that observed with GaAs. The reversible changes in the recombination centre concentrations were successfully described by a model in which atoms are trapped in sites in which their binding energies (centred near 0.41 eV) have a Gaussian distribution (with a spread of ~ 0.07 eV). For both GaAs and Si the initial irreversible decrease in recombination centres is attributed to the removal of some unsaturated valencies (dangling bonds). This study indicates that atomic hydrogen could provide a very rapid passivation technique at relatively low temperatures (~ 200°C), compared to the standard industrial H_2 annealing (for a few hours) at higher temperatures (~ 450°C).

Our study of the reaction of molecular hydrogen with carrier recombination centres at the Si/SiO_2 interface yielded rate constants over a large temperature range. This data indicates that

more electrically active defects than just the well known P_b centre, measured by electron paramagnetic resonance (EPR), exist at the Si/SiO_2 interface. We conclude that more than half of the electrically active defects are P_b centres, about a quarter are the R centres first reported in this thesis, while just under one fifth of the defects cannot be passivated by molecular hydrogen. Our data confirms the non-exponential nature of the reaction reported by the EPR work. These other defects that we measure, which we refer to as recombination centres R, have a lower activation energy for the passivation process than do the P_b defects. We suggest that, whereas the passivation of P_b centres involves the formation of an H–Si≡ bond by an endothermic reaction with a higher activation energy (1.5 eV), the passivation of R centres involves the formation of an H–OSi≡ bond, by an exothermic reaction with a lower activation energy (0.5 eV).

It is possible that the multiple-exponential rate laws that we have observed in this work, but were first reported by Stesmans[61], are characteristic of many reactions that occur at the surfaces of solids and the interface between two solids. It will therefore be interesting to see whether other examples of this type of behaviour appear in the literature in the next few years. In contrast to gases and liquids, where molecules can orient themselves freely, so that simple exponential rate laws prevail, interfaces of crystalline solids with amorphous materials may always create a distribution of environments for reactive sites. Such a distribution of sites would then yield rate constants that are different for each orientation of the reactive site, thus producing non-exponential rate laws.

The results obtained in this work provide a further test of the remote radio frequency (RF) probe developed earlier in this laboratory. Our study of the rate of removal of all the electrically active defects at the Si/SiO_2 interface yielded data for intrinsic and p-doped materials that was

indistinguishable, confirming the absence of any complication from band bending, and supporting the view that the RF-probe is an effective technique for monitoring the concentration of dangling bonds at surfaces and interfaces.

Some questions that stem directly from this work, and will require further studies include:

(i) The reason for the very low pre-exponential factor in the reaction of H_2 with "R" defects. It is possible that this results from a tunnelling process. In that case a study with D_2 might be useful.

(ii) The nature and properties of the defects in low temperature oxides. It will be interesting to see if the defects are somewhat different at interfaces that are grown at much lower temperatures.

(iii) This work has barely scratched the surface of the number of systems that can be studied with the RF probe. The SiO_2 interface was chosen for this study because only hydrogen atoms and molecules can diffuse to the interface. However, now that the nature of these interactions has been established, it will be interesting to study the interactions of bare (100) and (111) silicon surfaces with atomic and molecular hydrogen, oxygen, fluorine, chlorine, bromine, iodine, etc. Since some of these species etch silicon, it will be interesting to monitor the dangling bond concentration during the etching process. Very little is known about the surface during these technologically important processes.

References

[1] James F. Shackelford, *Introduction to Materials Science for Engineers*, 3rd Ed., Macmillan, New York, 1992, pp 13-15.

[2] J.W. Mayer and S.S. Lau, *Electronic Materials Science: For Integrated Circuits in Si and GaAs*, Macmillan, New York, 1990.

[3] James F. Shackelford, *Introduction to Materials Science for Engineers*, 3rd Ed., Macmillan, New York, 1992, pp 527-572, pp-573-616.

[4] S.M. Sze, *Semiconductor Devices, Physics and Technology*, John Wiley & Sons, New York, 1985, p 14.

[5] B.G. Streetman, *Solid State Electronic Devices*, 4th Ed., Prentice Hall, New Jersey, 1995, pp 240-302.

[6] R.K. Ahrenkiel, *Minority-Carrier Lifetime in III-V Semiconductors*, edited by R.K. Ahrenkiel and M.S. Lundstrom, Academic Press, New York, 1993, pp 39-150.

[7] E.A. Ogryzlo, *Physical Chemistry of the Solid State*, Course Material, University of British Columbia, Vancouver, 1999.

[8] W. Shockley and W.T. Read, Phys. Rev. **87**, 835 (1952).

[9] R.N. Hall, Phys Rev. **87**, 387 (1952).

[10] A. Rose, *Concepts in Photoconductivity and Allied Problems*, Robert Krieger Publishing, Huntington, NY, 1978, p 11.

[11] T. Tiedje, J.J. Haberman, R.W. Francis, and A.K. Gosh, J. Appl. Phys. **54**, 2499 (1983).

[12] H. Li, *Studies of the Interactions of Silicon with H, H_2 and O using a Novel RF Probe Technique*, PhD Thesis, 1997, University of British Columbia, Vancouver, Canada, pp 36-56.

[13] J. Linnros, J. Appl. Phys. **84**, 284 (1998).

[14] D.K. Schroder, *Semiconductor Material and Device Characterization*, John Wiley, New York, 1990, pp 244-296.

[15] P.M. Lenahan and J.F. Conley Jr., J. Vac. Sci. Technol. B **16**, 2134 (1998).

[16] E.H. Poindexter, Semicond. Sci. Technol. **4**, 961 (1989).
[17] K.L. Brower and T.J. Headley, Phys. Rev. B **34**, 3610 (1986).

[18] A. Stesmans, Appl. Phys. Lett. **68**, 2076 (1996).

[19] E. Cartier and J.H. Stathis, Microelectronic Engineering **28**, 3 (1995).

[20] I. Tamm, Z. Phys. **76**, 849 (1932).

[21] W. Shockley, Phys. Rev. **56**, 317 (1939).

[22] R.J. Hamers, R.M. Tromp, and J.E. Demuth, Surf. Sci. **181**, 346 (1987).

[23] B.E. Deal, J. Electrochem. Soc. **121**, C198 (1974).

[24] Y. Nishi, Jpn. J. Appl. Phys. **10**, 52 (1971).

[25] E.H. Poindexter, P.J. Caplan, B.E. Deal, and R.R. Razouk, J. Appl. Phys. **52**, 879 (1981).

[26] P.J. Caplan, J.N. Helbert, B.E. Wagner, and E.H. Poindexter, Surf. Sci. **54**, 33 (1976).

[27] E.H. Poindexter, E.R. Ahlstrom, and P.J. Caplan, *The Physics of SiO_2 and Its Interfaces*, edited by S.T. Pantelides, Pergamon, New York, 1978, p 227.

[28] A. Stesmans, Appl. Phys. Lett. **48**, 177 (1986).

[29] J.F. Conley Jr., P.M. Lenahan, H.L. Evans, R.K. Lowry, and T.J. Morthorst, J. Appl. Phys. **76**, 2872 (1994).

[30] P.J. Caplan, E.H. Poindexter, B.E. Deal, and R.R. Razouk, J. Appl. Phys. **50**, 5847 (1979).

[31] E.H. Poindexter and P.J. Caplan, *Insulating Films on Semiconductors*, edited by M. Schultz and G. Pensl, Springer, Berlin 1981, p 150.

[32] A. Stesmans and G. Van Gorp, Phys. Rev. B **39**, 2864 (1986).

[33] A.H. Edwards, *The Physics and Chemistry of SiO_2 and the Si-SiO_2 Interface*, edited by C.R. Helms and B.E. Deal, Plenum, New York, 1988, p 271.

[34] A.H. Edwards, Phys. Rev. B **36**, 9638 (1987).

[35] J.H. Stathis and L. Dori, Appl. Phys. Lett. **58**, 1641 (1991),

[36] E.H. Poindexter, P.J. Caplan, J.J. Finegan, N.M. Johnson, D.K. Biegelsen, and M.D. Moyer, *The Physics and Technology of MOS Insulators*, edited by G. Lukovsky, S.T. Pantelides, and F.L. Galeener, Pergamon, New York, 1980, p 326.

[37] C. Brunstrom and C.V. Svensson, Solid State Commun. **37**, 339 (1981).

[38] P.M. Lenahan and P.V. Dressendorfer, Appl. Phys. Lett. **41**, 542 (1982).

[39] P.M. Lenahan and P.V. Dressendorfer, J. Appl. Phys. **55**, 3495 (1984).

[40] E.H. Poindexter, G.J. Gerardi, M.-E. Rueckel, P.J. Caplan, N.M. Johnson, and D.K. Biegelsen, J.Appl. Phys. **56**, 2844 (1984).

[41] S.T. Chang, J.K. Wu, and S.A. Lyon, Appl. Phys. Lett. **48**, 662 (1986).

[42] G.J. Gerardi, E.H. Poindexter, P.J. Caplan, and N.M. Johnson, Appl. Phys Lett. **49**, 348 (1986).

[43] P.M. Lenahan and P.V. Dressendorfer, Appl. Phys Lett. **44**, 96 (1984).

[44] M.J. Uren, J.H. Stathis, and E. Cartier, J. Appl. Phys. **80**, 3915 (1996).

[45] N.M. Johnson, D.K. Biegelsen, M.D. Moyer, S.T. Chang, E.H. Poindexter, and P.J. Caplan, Appl. Phys Lett. **43**, 563 (1983).

[46] N.M. Johnson, W. Shan, and P.Y. Yu, Phys. Rev. B **39**, 3431 (1989).

[47] H.G. Grimmeis, W.R. Buchwald, E.H. Poindexter, P.J. Caplan, M. Harmatz, G.J. Gerardi, D.J. Keeble, and N.M. Johnson, Phys. Rev. B **39**, 5175 (1989).

[48] B. Deal, J. Electrochem. Soc. **127**, 979 (1980).

[49] E.H. Nicollian, C.N. Berglund, P.F. Schmidt, and J.M. Andrews, J. Appl. Phys. **42**, 5654 (1971).

[50] K.L. Brower, Phys. Rev. B **38**, 9657 (1988).

[51] K.L Brower, Appl. Phys. Lett. **53**, 508 (1988).

[52] K.L. Brower, Semicond. Sci. Technol. **4**, 970 (1989).

[53] K.L. Brower, Phys. Rev. B **42**, 3444 (1990).

[54] J. Stathis, J. Appl. Phys. **77**, 6205 (1995).

[55] J. Stathis, J. Appl. Phys. **78**, 5215 (1995).

[56] S.M. Myers and P.M. Richards, J. Appl. Phys. **67**, 4064 (1990).

[57] K.L. Brower and S.M. Myers, Appl. Phys. Lett. **57**, 162 (1990).

[58] CRC *Handbook of Chemistry and Physics*, edited by R.C. Weast, CRC, Boca Raton, FL, 1980, F-225.

[59] K.L. Brower, P.M. Lenahan, and P.V. Dressendorfer, Appl. Phys. Lett. **41**, 251 (1982).

[60] A. Stesmans, Solid State Commun. **97**, 255 (1996).

[61] A. Stesmans, Appl. Phys. Lett. **68**, 2723 (1996).

[62] J.F. Shackelford, P.L. Studt, and R.M. Fulrath, J. Appl. Phys. **43**, 1619 (1972).

[63] J.E. Shelby, J. Appl. Phys. **48**, 3387 (1977).

[64] A. Stesmans and V.V. Afanas'ev, J. Phys. Condens. Matter **8**, L505 (1996).

[65] A. Stesmans and V.V. Afanas'ev, Phys. Rev. B **54**, R11129 (1996).

[66] A. Stesmans, V.V. Afanas'ev, and A.G. Revesz, J. Phys. Condens. Matter **10**, L367 (1998).

[67] A. Stesmans, V.V. Afanas'ev, Appl. Phys. Lett., **74**, 1009 (1999).

[68] A. Stesmans, V.V. Afanas'ev, Appl. Phys. Lett., **74**, 1466 (1999).

[69] J.H. Stathis, J. Phys. Condens. Matter **9**, 3297 (1997).

[70] A. Stesmans and V.V. Afanas'ev, J. Phys. Condens. Matter **9**, 3299 (1997).

[71] A. Stesmans and V.V. Afanas'ev, Appl. Phys. Lett. **72**, 2271 (1998).

[72] A. Stesmans, B. Nouwen, and V.V. Afanas'ev, J. Phys. Condens. Matter **10**, L465 (1998).

[73] A. Stesmans and V.V. Afanas'ev, Phys. Rev. B **57**, 10030 (1998).

[74] A. Stesmans and V.V. Afanas'ev, J. Phys. Condens. Matter **10**, L19 (1998).

[75] V.V. Afanas'ev and A. Stesmans, J. Phys. Condens. Matter **10**, 89 (1998).

[76] V.V. Afanas'ev and A. Stesmans, Appl. Phys. Lett. **72**, 79 (1998).

[77] V.V. Afanas'ev and A. Stesmans, Phys. Rev. Lett. **80**, 5176 (1998).

[78] R.E. Stahlbush and E. Cartier, IEEE Trans. Nucl. Sci. **41**, 1844 (1994).

[79] E. Cartier and J.H. Stathis, Appl. Phys. Lett. **69**, 103 (1996).

[80] E. Cartier, D.A. Buchanan, J.H. Stathis, and D.J. DiMaria, J. Non-Crystalline Solids, **187**, 244 (1995).

[81] R.E. Stahlbush, E. Cartier, and D.A. Buchanan, Microelectronic Engineering **28**, 15 (1995).

[82] T.E. Tsai, D.L. Griscom, and E.J. Friebele, Phys. Rev. B **40**, 6374 (1989).

[83] P.S. Winokur and H.E. Boesch Jr., IEEE Trans. Nucl. Sci. **NS-28**, 4088 (1981).

[84] N.M. Johnson, in *Hydrogen in Semiconductors*, edited by J. Pankove and N.M. Johnson, Academic Press, San Diego, 1991, p 113.

[85] E. Cartier, J.H. Stathis, and D.A. Buchanan, Appl. Phys. Lett. **63**, 1510 (1993).

[86] N.S. Saks, M.G. Ancona, and J.A. Modolo, IEEE Trans. Nucl Sci. **NS-33**, 1185 (1986).

[87] G.J. Dunn, Appl. Phys. Lett. **53**, 1650 (1988).

[88] M. Dutoit, P. Latourneau, J. Mi, N. Novkovski, J. Manthey, and J.S. de Zaldivar, J. Electrochem Soc. **41**, 549 (1993).

[89] E. Cartier, D.A. Buchanan, and G.J. Dunn, Appl. Phys. Lett. **64**, 901 (1994).

[90] J.W. Lyding, K. Hess, and I.C. Kizilyalli, Appl. Phys. Lett. **68**, 2526 (1996).

[91] I.P. Ipatova, O.P. Chikalova-Luzina, and K. Hess, J. Appl. Phys. **83**, 814 (1998).

[92] P. Viktorovitch, F. Benyahia, C. Santinelli, R. Blanchet, P. Leyral, and M. Garrigues, Appl. Surf. Sci. **31**, 317 (1988).

[93] C. Wilmsen, J. Vac. Sci. Technol. **19**, 279 (1982).

[94] R.A. Gottscho, B.L. Preppernau, S.J. Pearton, A.B. Emerson, and K.P. Giapis, J. Appl. Phys. **68**, 440 (1990).

[95] A. Mitchell, R.A. Gottscho, S.J. Pearton, and G.R. Scheller, Appl. Phys. Lett. **56**, 821 (1990).

[96] E. Yoon, R.A. Gottscho, V.M. Donnelly, and H.S. Luftman, Appl. Phys. Lett. **60**, 2681 (1992).

[97] E. Yoon, R.A. Gottscho, V.M. Donnelly, and W.S. Hobson, J. Vac. Sci. Technol. **10**, 2197 (1992).

[98] H. Li, E.A. Ogryzlo, T. Tiedje, and J.G. Cook, Proceedings of the 22nd International Conference on the Physics of Semiconductors, **1**, 541 (1995).

[99] H. Li and E.A. Ogryzlo, Can. J. Phys. **74**, S233 (1996).

[100] M.C. Chuang and J.W. Coburn, J.Appl. Phys. **67**, 4372 (1990).

[101] R.W. Fair and B.A. Thrush, Trans. Faraday Soc. **65**, 1208 (1969).

[102] H. Li, *Studies of the Interactions of Silicon with H, H_2 and O using a Novel RF Probe Technique*, PhD Thesis, 1997, University of British Columbia, Vancouver, Canada, pp 76-79.

[103] L. Zheng, *Growth and Characterization of Thin Oxide Films on SiGe*, M.Sc. Thesis, 1997, University of British Columbia, Vancouver, BC, Canada, pp 53-70.

[104] E.S. Aydil, Z. Zhou, K.P. Giapis, Y.Chabal, J.A. Gregus, and R.A. Gottscho, Appl. Phys. Lett. **62**, 3156 (1993).

[105] G. Gu, H. Li, and E. Ogryzlo, J. Chem. Soc. Faraday Trans. **91**, 3021 (1995).

[106] A. Stesmans, Phys. Rev. B **48**, 2418 (1993).

[107] L. Zheng, *Growth and Characterization of Thin Oxide Films on SiGe*, M.Sc. Thesis, University of British Columbia, Vancouver, Canada, 1997, pp 75-76.

[108] T. Tiedje, in *The Physics of Hydrogenated Amorphous Silicon*, edited by J.D. Joannopoulos and G. Lucovsky, Springer-Verlag, Heidelberg, 1984, pp 267-281.

[109] T. Tiedje, in *Semiconductors and Semimetals*, vol. 21, Part C, edited by R.K. Willardson and A.C. Beer, Academic Press, San Diego, 1984, pp 207-239.

[110] Z.H. Lu, in *Fundamental Aspects of Ultrathin Dielectrics on Si-based Devices*, edited by E. Garfunkel, E. Gusev, and A. Vul, Kluwer Academic Publishers, Boston, 1998, p 49.

[111] H. Li, *Studies of the Interactions of Silicon with H, H_2, and O Using a Novel Probe Technique*, Ph.D. Thesis, 1997, University of British Columbia, Vancouver, BC, Canada, pp 97-154.

[112] J. Vitko, C.M. Hartwig, and P.L. Mattern, in *The Physics of SiO_2 and Its Interfaces*, edited by S.T. Pantelides, Pergamon, New York, 1978, p 215.

[113] D.J. Lucas, L.A. Curtiss, and J.A. Pople, J. Chem. Phys. **99**, 6697 (1993).

[114] R. Becerra and R. Walsh, in *The Chemistry of Organic Silicon Compounds*, Vol.2, edited by Z. Rappoport and Y. Apeloig, John Wiley & Sons, New York, 1998, pp 153-180.

[115] S. Glasstone, K.J. Laidler, and H. Eyring, *The Theory of Rate Processes*, McGraw-Hill, New York, 1941, p 145.

[116] S.W. Benson, *Thermochemical Kinetics*, John Wiley & Sons, New York, 1968, p 215.

[117] S.W. Benson, *Thermochemical Kinetics*, John Wiley & Sons, New York, 1968, p 66.